HISTOMORPHOMETRIC EFFECTS OF ANTIRETROVIRAL TREATMENT AND OBESITY ON THE PANCREAS, LIVER, KIDNEY AND PERIVASCULAR ADIPOSE TISSUE IN A RAT MODEL

by

Simoné Nel

Thesis presented in fulfilment of the requirements for the degree of Masters of Science in the Faculty of Medicine and Health Sciences at Stellenbosch University

Supervisor: Prof S.H. Kotzé

Co-supervisor: Dr. N. Chellan

December 2017

The financial assistance of the National Research Foundation (NRF) towards this research is hereby acknowledged. Opinions expressed and conclusions arrived at, are of the author and are not necessarily to be attributed to the NRF.

Stellenbosch University https://scholar.sun.ac.za

DECLARATION

By submitting this thesis electronically, I declare that the entirety of the work contained therein is my own, original work, that I am the sole author thereof (save to the extent explicitly otherwise stated), that reproduction and publication thereof by Stellenbosch University will not infringe any third party rights and that I have not previously in its entirety or in part submitted it for obtaining any qualification.

December 2017

Copyright @ 2017 Stellenbosch University

All Rights Reserved

Stellenbosch University https://scholar.sun.ac.za

ABSTRACT

Human immunodeficiency virus (HIV)-infected patients receiving antiretroviral treatment (ART) may develop metabolic syndrome and lipodystrophy, leading to obesity rather than wasting. Obesity is associated with metabolic homeostasis disruptions leading to pancreatic toxicity, diabetes, renal vasodilation and compression as well as liver steatosis. In addition, patients on long-term combination antiretroviral treatment (cART) can develop pancreatitis, nephrotoxicity, hepatic steatosis, and diabetes. This study aims to investigate the effects of cART combined with a high-calorie diet (HCD) on the histomorphometry of the pancreas, kidney, liver, and aortic perivascular adipose tissue (PVAT) leptin expression in the rat. Male Wistar rats (N=40) were divided into four groups (n=10); C/ART- (lean control), C/ART+ (ART control), HCD/ART- (HCD control) and HCD/ART+ (HCD and ART). The aorta with surrounding PVAT, pancreas, liver and kidney were harvested and processed to wax. Pancreas sections underwent a double immunohistochemistry (IHC) labelling for insulin and glucagon and reactive cell areas were measured. Aortic PVAT was labelled with anti-leptin and the staining intensity classified accordingly. Kidney sections underwent haematoxylin and eosin (H&E) stain measuring the areas of the renal corpuscles, glomeruli, renal spaces as well as the renal arcuate arteries lumen diameter and artery wall thickness. Pancreatic, kidney and liver sections underwent H&E staining which were used for pathology assessment.

The HCD/ART+ had a significant body mass increase compared to the C/ART-, suggesting ART combined with a HCD causes body mass increase. Unilocular and differentiating adipocytes in the C/ART+ had intense leptin staining, suggesting ART may lead to increased leptin expression in aortic PVAT. Unilocular and differentiating adipocytes in the HCD/ART- and HCD/ART+ had weak to no leptin intensity, suggesting possible leptin deficiency with a HCD. The C/ART+ showed a trend in smaller total pancreatic islet area compared to the C/ART-, suggesting that islets underwent possible hypotrophy with ART. Based on the average values, alpha-cells were increased in the HCD/ART-, whereas beta-cells decreased in the ART and HCD. This suggests that a HCD potentially increases glucagon secreting area, whereas ART and a HCD leads to β-cell mass loss. The HCD/ART- and HCD/ART+ showed a trend in increased number of islets per section compared to the C/ART-, suggesting that HCD leads to new forming islets. Based on the average values, the renal corpuscle, glomeruli and renal space sizes were increased in the HCD/ART- compared to the other groups, although not significantly. A trend in the HCD/ART+ showed increased arcuate artery lumen diameter and tunica media thickness, whereas the C/ART+ had increased tunica adventitia compared to the

Stellenbosch University https://scholar.sun.ac.za

C/ART-. This suggests that ART combined with a HCD causes hypertrophic remodelling in the tunica media and hypotrophic remodelling in the tunica adventitia. All groups had mild vacuolisation and swelling of the proximal convoluted tubules in the kidney and granular appearance, vacuolisation, and fatty change in the liver. The six week cART and HCD used in the present study caused no significant morphometric or pathological changes within the pancreas, kidney, and liver, apart from significant leptin intensity staining with ART.

Stellenbosch University https://scholar.sun.ac.za

OPSOMMING

Pasiënte wat met die menslike immuniteitsgebreksvirus (MIV) besmet is en antiretrovirale behandeling (ARB) ontvang, kan metaboliese sindroom en lipodistrofie ontwikkel, wat tot obesiteit eerder as uittering lei. Obesiteit word geassosieer met metaboliese homeostase-versteurings, wat lei tot pankreas-toksisiteit, diabetes, renale vasodilatasie en kompressie asook lewersteatose. Hierbenewens kan pasiënte wat langtermyn-kombinasie- antiretrovirale behandeling (kARB) ontvang pankreatitis, nier-toksisiteit, hepatiese steatose en diabetes ontwikkel. Hierdie studie was daarop gemik om die histomorfometriese effekte van kARB gekombineer met ’n hoëkalorie-dieet (HKD) op die pankreas, niere, lewer en leptienuitdrukking van die aorta-perivaskulêre adiposisweefsel (PVAW) in ’n rotmodel te ondersoek.

Manlike Wistar-rotte (N=40) is in vier groepe verdeel (n=10); K/ARB- (vetvrye beheergroep), K/ARB+ (ARB-beheergroep), HKD/ARB- (HKD-beheergroep) en HKD/ARB+ (HKD en ARB). Die aorta met omliggende PVAW, pankreas, lewer en niere is geoes en histologies voorberei. Pankreasdele het ’n dubbele immunohistochemie- (IHC-)merking vir insulien en glukagon ondergaan en reaktiewe seldele is gemeet. Aorta-PVAW is gemerk met antileptien en die kleuringintensiteit is dienooreenkomstig geklassifiseer. Nierdele is gekleur met hematoksilien- en eosien (H&E-) en die renale liggaampies, glomeruli, renale ruimtes asook die renale arkuate arterielumendeursnee en arteriewanddikte is gemeet. Pankreas-, nier- en lewerdele word met H&E gekleur, wat vir patologie-assessering gebruik is.

Die HKD/ARB+ het ’n aanmerklike liggaamsmassatoename getoon in vergelyking met die K/ARB-, wat aan die hand doen dat ARB gekombineer met ’n HKD liggaamsmassatoename veroorsaak. Unilokulêre en differensiërende adiposiete in die K/ARB+ het intense leptienkleuring getoon, wat aan dui dat ARB tot verhoogde leptienuitdrukking in aorta-PVAW kan lei. Unilokulêre en differensiërende adiposiete in die HKD/ARB- en HKD/ARB+ het swak tot geen leptienintensiteit getoon, wat op moontlike leptientekort met HKD kan dui. Die K/ARB+ het ’n neiging tot kleiner totale pankreas-eilandoppervlakte in vergelyking met die K/ARB- getoon, wat aan dui dat eilande moontlike hipotrofie met ARB ondergaan het. Alfa-selle het in die HKD/ARB- toegeneem, terwyl beta-selle in die ARB en HKD afgeneem het. Dit dui daarop dat ’n HKD moontlik verhoogde alfa-sel area veroorsaak, terwyl ARB en ’n HKD tot β-sel-massaverlies lei. Die HKD/ARB- en HKD/ARB+ het ’n neiging getoon tot verhoogde aantal eilande per deel in vergelyking met die K/ARB-, wat aan die hand doen dat HKD tot die vorming van nuwe eilande lei. Renale liggaampies, glomeruli en renale ruimtegroottes is

Stellenbosch University https://scholar.sun.ac.za

verhoog in die HKD/ARB- in vergelyking met die ander groepe, dog nie beduidend nie. ’n Neiging in die HKD/ARB+ het verhoogde arkuate arterielumendeursnee en tunica mediadikte getoon, terwyl die K/ARB+ verhoogde tunica adventitia in vergelyking met die K/ARB- getoon het. Dit doen aan die hand dat ARB gekombineer met ’n HKD hipertrofiese hermodellering in die tunica media en hipotrofiese hermodellering in die tunica adventitia veroorsaak. Alle groepe het matige vakuolisering en swelling van die proksimale kronkelbuise in die nier en granulêre voorkoms, vakuolisering en vetverandering in die lewer getoon. Die sesweek-kARB en HKD wat in die huidige studie gebruik is, het geen aanmerklike morfometriese of patologiese veranderinge in die pankreas, nier en lewer veroorsaak nie, buiten beduidende leptienintensiteitkleuring met ARB.

Stellenbosch University https://scholar.sun.ac.za

PUBLISHED ARTICLES

Nel, S., Strijdom, H., Genis, A., Everson, F., Van Wijk, R., Kotzé, S.H. 2017. A histomorphometric study on the effects of antiretroviral therapy (ART) combined with a high-calorie diet (HCD) on aortic perivascular adipose tissue (PVAT). Acta Histochemica. 119, 555-562. (**Appendix N**)

Stellenbosch University https://scholar.sun.ac.za

ACKNOWLEDGMENTS

I would like to thank Prof S.H Kotzé, my supervisor, for the guidance and support during the two years working on this study. A special thank you to Dr. N Chellan, my co-supervisor, for her guidance and support. I would also like to thank my parents and sister for their love and support throughout my studies.

I acknowledge the National Research Foundation (NRF) for financial assistance during this time.

Thank you to Prof M Kidd from the Statistical Centre of Stellenbosch University for assistance with the statistical analysis.

Thank you to the Anatomy and Histology department of Stellenbosch University and the South African Medical Research Council (SAMRC) for their assistance.

Stellenbosch University https://scholar.sun.ac.za

CONTENTS

Stellenbosch University https://scholar.sun.ac.za

Stellenbosch University https://scholar.sun.ac.za

FIGURES

Stellenbosch University https://scholar.sun.ac.za

Stellenbosch University https://scholar.sun.ac.za

TABLES

Stellenbosch University https://scholar.sun.ac.za

APPENDICES

Stellenbosch University https://scholar.sun.ac.za

ACRONYMS AND ABBREVIATIONS

ADR	Adverse drug reaction
AIDS	Acquired immune deficiency syndrome
ART	Antiretroviral treatment
BAT	Brown adipose tissue
BMI	Body mass index
cART	Combination antiretroviral treatment
CD4	Cluster of differentiation four (T–lymphocyte cell bearing CD4 receptor)
CVD	Cardiovascular disease
DAB	Diaminobenzidine
DNA	Deoxyribonucleic acid
EFV	Efavirenz
FTC	Emtricitabine
H&E	Haematoxylin and Eosin
HAART	Highly active antiretroviral therapy
HCD	High-calorie diet
HDL	High density lipoproteins
HIV	Human immunodeficiency virus
HIVAN	HIV-associated nephropathy
IHC	Immunohistochemistry
NAFLD	Non-alcoholic fatty liver disease
NASH	Non-alcoholic steatohepatitis
NGS	Normal goat serum
NHS	Normal horse serum
NNRTIs	Non-nucleoside reverse transcriptase inhibitors
NRTIs	Nucleoside reverse transcriptase inhibitors
PBS	Phosphate buffered saline
PFA	Paraformaldehyde
PIs	Protease inhibitors
PVAT	Perivascular adipose tissue
SAMRC	South African Medical Research Council

Stellenbosch University https://scholar.sun.ac.za

SANS	South African National Standards
SEM	Standard error mean
SOP	Standard operating procedure
T2DM	Type 2 diabetes mellitus
TBM	Total body mass
TBS	Tris buffered saline
TDF	Tenofovir
UNAIDS	Joint united nations programme on HIV/AIDS
VEPAC	Variance Estimation, Precision and Comparison
VLDL	Very low density lipoproteins
VSMC	Vascular smooth muscle cell
WAT	White adipose tissue
WHO	World health organization

Stellenbosch University https://scholar.sun.ac.za

1. INTRODUCTION

Implementation of combination antiretroviral treatment (cART) has been successful in reducing morbidity and mortality rates in human immunodeficiency virus (HIV) infected individuals, however treatment may lead to drug related toxicity. Currently obesity is often associated with HIV patients on antiretroviral treatment (ART) (Amorosa *et al*. 2005). In turn, obesity is associated with pancreatic toxicity (Slavin *et al*. 2010), liver fibrosis and steatosis (Goodman 2016), renal vasodilation and compression (Hall 2003), and altered adipocytokine expression from perivascular adipose tissue (PVAT) (Tsiodras and Mantzoros, 2006). In addition, ART shows increased toxicity within various organs and may cause diseases such as pancreatitis, nephrotoxicity, lactic acidosis, and hepatic steatosis (Cornejo-juárez *et al*. 2003).

Pancreatic toxicity is a side effect of ART which may lead to pancreatitis, steatosis, islet alpha (α)- and beta (β)-cells dysfunction (Elfane *et al*. 2016; Adler *et al*. 1987). Furthermore, obesity is associated with pancreatic islet alterations such as increased islet number, size, and insulin secretion (Slavin *et al*. 2010).

In the kidney glomerular enlargement and renal toxicity which causes kidney injury is seen in HIV-patients on ART (Fabian *et al*. 2013; Jao & Wyatt 2016), while in obese patients renal vasodilation and renal medullary compression have been reported histologically (Hall 2003).

The most common liver diseases seen with the onset of obesity and ART are chronic hepatitis, liver steatosis and the development of liver cirrhosis from liver fibrosis (Yamauchi & Michitaka 1998; Grinspoon & Carr 2005; Neuman *et al*. 2012).

Adequate adipocytokine levels, such as leptin, are required to maintain normal metabolic homeostasis in the body (Lago *et al*. 2009). In obesity, leptin expression is up regulated in perivascular adipose tissue (PVAT) which in turn may cause elevated arterial pressure and hypertension (Shek *et al*. 1998). Furthermore, ART causes increased circulating leptin (Jan *et al*. 2004; Lagathu *et al*. 2005).

The present study aims to investigate the histomorphological effects of the first line cART (Odimune) used in South Africa in conjunction with a high-calorie diet (HCD) on the pancreatic islets, kidney renal corpuscle and arcuate artery, liver tissue and aortic PVAT leptin stain intensity in a rat model. The Wistar rat strain is a suitable model used in the present study and is one of the most popular rats used in laboratory research. This strain is bred for biological and medical research, whereas Zucker rats are bred to be a genetic model on obesity and

Stellenbosch University https://scholar.sun.ac.za

hypertension. As the aim of the present study was to determine the effects of a high-calorie diet (HCD) and ART on various organs, a wild type train was needed. The results of the study will provide information on the histological changes with the use of this specific cART (Odimune) in combination with a high-calorie diet, as is suggested by observational studies and case reports. Therefore this study may provide a basis for future research and development into obesity caused by ART increasing research output in South Africa.

Stellenbosch University https://scholar.sun.ac.za

2. LITERATURE REVIEW

2.1. Human immunodeficiency virus (HIV), antiretroviral treatment (ART) and obesity

In 2016, the United Nations Programme on human immunodeficiency (HIV)/ acquired immunodeficiency syndrome (UNAIDS) estimated worldwide 36.7 million individuals (adults and children) are HIV-infected (*UNAIDS* 2017). Currently in South Africa there are 7.1 million HIV-infected individuals (*UNAIDS* 2017). HIV targets a host cell, which the virus uses to multiply by fusing with the CD4 receptors and then enters the RNA strands to convert to DNA. The virus binds to various types of cells, such as CD4 lymphocytes (T cells), monocytes, macrophages and other white blood cells (Arts *et al.* 2012). Antiretroviral treatment (ART) disrupts the reproduction cycle of the virus, by inhibiting the viral enzyme. There are five commonly used antiretroviral treatments (ART) namely; Nucleoside reverse transcriptase inhibitors (NRTIs), Non-nucleoside reverse transcriptase inhibitors (NNRTIs), Protease inhibitors (PIs), Entry inhibitors and Integrase inhibitors. Different combinations of these treatments are known as highly active anti-retroviral treatment (HAART) (Arts *et al*. 2012). The NRTIs prevent viral reproduction and DNA elongation, their presence inhibits viral DNA replication. However, the NRTIs can function as substrates for other enzymes which are capable of DNA formation, such as mitochondrial DNA replication, which in turn could lead to mitochondrial disruption (Montessori *et al*. 2004).

HIV-infected individuals in South Africa receive a first line regimen of cART, called Odimune a generic version of Atripla®, consisting of a combination of Tenofovir Disoproxil Fumarate or TDF (a nucleoside reverse transcriptase inhibitor), Emtricitabine or FTC (nucleoside reverse transcriptase inhibitor) and Efavirenz or EFV (non-nucleoside reverse transcriptase inhibitors) (South African National Department of Health 2015). Odimune is administered orally, one tablet on a daily basis. Efavirenz is mostly bound to human plasma proteins, whereas Emtricitabine and Tenofovir are minimally bound (Frampton & Croom 2006). With the use of ART the mortality and morbidity has declined among HIV-infected patients, cART are more beneficial to the HIV-infected patients than single treatment (Palella *et al.* 1998).

Stellenbosch University https://scholar.sun.ac.za

Disorders associated with HIV/AIDS are the wasting syndrome and peripheral lipoatrophy, which both decrease with the use of ART, however in some HIV-infected patients receiving ART both the wasting syndrome and peripheral lipoatrophy can still occur (Longenecker *et al*., 2013; Wanke *et al*., 2015). Different combinations of ART and ART on its own can lead to a wide variety of adverse effects in the human body such as, gastrointestinal effects (nausea, diarrhoea, and bloating), fatigue, headaches, anaemia, hyperglycaemia, fat maldistribution, and hyperlipidaemia (Montessori *et al.* 2004; Dando & Wagstaff 2004). Combination ART can lead to various types of cellular adverse drug reactions (ADR), which include hepatocytotoxicity, lipodystrophy, type 2 diabetes mellitus (T2DM), hyperlipidaemia, nephrotoxicity (Carr *et al.* 2000; Neuman *et al*. 2012; Jain *et al.* 2001; Hawkins 2010). High levels of high-density lipoprotein (HDL) and triglycerides are seen in HIV-infected patients, with the use of ART the HDL and triglyceride levels increase even more (Pinto Neto *et al*. 2013). Crum-cianflone *et al*. (2008) described the prevalence of obesity associated with HIV-infected individuals before the use of ART and an increase in obesity with the use of ART. This suggested that the weight gained were associated with the general population and were unrelated to HIV or ART.

Individuals are classified as being obese when their body mass index (BMI) is greater than 30kg/m² (Achike *et al.* 2011; Balistreri *et al.* 2010). Obesity can be defined as imbalances between energy being stored and used and is associated with metabolic syndrome (Ogden *et al.* 2007). Obesity it is associated with metabolic homeostasis disruptions, over-nutrition and stress which links to visceral obesity (Karalis *et al*. 2009). Metabolic homeostasis disruptions caused by obesity often lead to lipodystrophy, hyperlipidaemia, hypertension, cardiovascular diseases (CVD), diabetes mellitus and non-alcoholic fatty liver disease (NAFLD) (Guzik *et al*. 2006; Pi-Sunyer 2002; Van der Merwe & Pepper 2006; Shah, P. Alio, *et al.* 2012; Achike *et al*. 2011). Both ART and obesity causes metabolic syndrome, leading to obesity-induced hypertension and development of T2DM, adipose tissue distribution, increased triglycerides (dyslipidaemia), insulin resistance and impaired glucose tolerance, NAFLD, hepatic steatosis, renal diseases (Ogden *et al*. 2007; Rea *et al*. 2006; John *et al*. 1998; Lagathu *et al*. 2005)

Stellenbosch University https://scholar.sun.ac.za

2.2. Leptin expression in aortic perivascular adipose tissue (PVAT), with antiretroviral treatment and obesity

Adipose tissue surrounding large arteries, such as the aorta, is known as perivascular adipose tissue (PVAT) (Schlett *et al*. 2009). PVAT is located on the outside of the tunica adventitia to which it adheres. It consist of mainly brown adipose tissue (BAT), while white adipose tissue (WAT) is found on the periphery and mixture of BAT and WAT, known as intermingled adipose tissue (Szasz *et al*. 2013). White adipose tissue is considered to be a source of free fatty acids (FFA) which are used as an energy substrate for the generation of adenosine triphosphate (ATP), providing energy for the organism during periods of fasting (Fain, Madan, Hiler, Cheema & Bahouth. 2015). Brown adipose tissue makes use of FFA to produce heat, which gives it a non-shivering thermogenesis function that assists in cold adaptions (Cannon & Nedergaard 2004; Raucci *et al*. 2013). Intermingled adipose tissue can also be described as differentiating adipocytes, due to the ability of WAT and BAT to transdifferentiate into one another, allowing the cells to participate in different energy demands (Cinti 1999). Adipose transformation is brought on by a physiological stimuli, such as growth of the rodent or human or with cold and heat exposure (Cousin *et al*. 1992). With cold exposure the WAT phenotype will differentiate into a BAT phenotype, whereas with warm exposure the BAT will change into WAT. This leads to the theory that newly formed brown adipocytes may be derived from stem cells migrating, or from differentiated white cells or a combination of the two (Cinti 2009). In genetic and diet-induced obese animals the white adipocytes develops within brown adipose tissue areas (Cinti 1999).

PVAT not only supports the arteries, but is considered to be metabolically active by secreting a variety of adipocytokines, such as adiponectin and leptin (Guzik *et al*. 2006; Szasz *et al*. 2013). Therefore PVAT can be classified as an endocrine organ, which effects the arteries it adheres to (Halberg *et al*. 2009; Szasz *et al*. 2013). Adiponectin is an adipocyte specific hormone and decreases with the onset of obesity (Arita *et al*. 1999; Guzik *et al*. 2006). Leptin regulates appetite via hypothalamic leptin-receptor signalling (Raucci *et al*. 2013). Leptin secretion is controversial as some studies suggest that it is expressed in both WAT and BAT (Moinat *et al*. 1995; Maffei *et al*. 1995), while other researchers maintain that leptin is expressed by WAT only and that the expression in BAT may be due to the presence of white adipocytes intermingled with BAT (Cancello *et al.* 1998; Cinti *et al*. 1997). A study done by Cinti *et al*. (1997) suggested that adipocytes at the multilocular stage of differentiation within

Stellenbosch University https://scholar.sun.ac.za

WAT depots were leptin-positive, suggesting that leptin is secreted by all lipid-containing cells found in adipose tissue. Leptin expression has been seen to decrease endothelium-dependant vasodilation, suggesting it plays a role in vascular dilation changes which causes blood pressure changes (Nakagawa *et al*. 2002; Payne *et al*. 2010; Rahmouni & Haynes 2005).

Adequate adipose tissue and adipocytokine levels are required to maintain normal metabolic homeostasis in the body (Lago *et al*. 2009). Increased calorie intake causes adipose tissue mass increase which alters adipocytokine secretion from adipocytes in adipose tissue (Halberg *et al*. 2009; Weisberg *et al*. 2003). Adipocytokines are increased with obesity which influence vasculature by endothelial dysfunction, vascular stiffness and smooth muscle migration (Payne *et al*. 2010; Montani *et al*. 2004). Altered adipocytokine levels, such as decreasing adiponectin and increasing leptin, are associated with both obesity and HIV-infected individuals receiving ART (Vlasova *et al*. 2010; Tsiodras & Mantzoros 2006). Circulating leptin levels are proportional to adipose tissue, therefore hyperleptinemia is associated with obesity (Giovannucci & Michaud 2007; Szasz *et al*. 2013). As previously mentioned leptin has a vasodilatory effect and is therefore associated with leptin resistance in obesity. Long term exposure to leptin secretion, due to a chronic obese state, leads hypertension and endothelial dysfunction (Shek *et al*. 1998). It has been suggested that adipocytokines are the molecular link between obesity and cardiovascular disease. The exact relationship between the two is not fully understood and there is still uncertainty concerning this association (Payne *et al*. 2010).

2.3. Pancreas structure, antiretroviral treatment toxicity and obesity

Observational studies have indicated that with obesity and the introduction of ART patients are insulin sensitive and glucose tolerant (Jain *et al*. 2001; Donath *et al*. 2013)

The pancreas in both humans and rodents is a large gland consisting of endocrine and exocrine pancreas (Kierszenbaum 2007). The exocrine pancreas consist of acinar cells, duct cells, vessels and nerves and its main function is to secrete digestive enzymes. The endocrine pancreas represents approximately 2% of the total pancreas organ, consisting of pancreatic islets (islets of Langerhans) which regulates glucose metabolism via insulin-, glucagon-, somatostatin-, and pancreatic polypeptide secreting cells (Motta *et al.* 1997). In rats, the pancreas is divided into a splenic and duodenal region (Dolensek *et al.* 2015). The exocrine pancreas is covered by a thin layer of connective tissue, which extends into septa which divides the gland into lobules (Motta *et al.* 1997). The functional component of the exocrine pancreas

Stellenbosch University https://scholar.sun.ac.za

is the acinus which are commonly labelled as centroacinar cells (Kierszenbaum 2007). The acinar cells are arranged to form convoluted tubuloacinar network within the lobules (Haschek *et al*. 2010). Haematoxylin and Eosin (H&E) stain the acinar cells blue at their base due to high concentrations of RNA and nuclei, whereas the apex will stain pink due to high concentrations of zymogen proteins (Longnecker 2014).

The endocrine pancreas, as mentioned previously, consist of pancreatic islets of varying sizes, ranging from 50-250 µm in diameter (Hellman 1959). Each islet is made up different cells and secretes peptide specific hormones, such as beta (β)-cells (insulin), alpha (α)-cells (glucagon), PP-cells (pancreatic polypeptide), and delta (δ)-cells (somatostatin) **(Figure 2.1)** (Longnecker 2014; Dolensek *et al*. 2015)

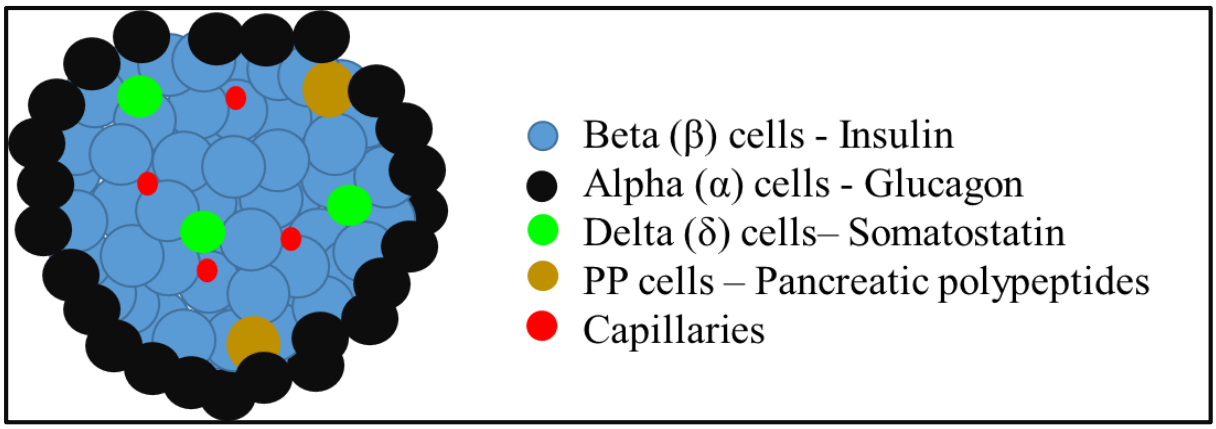

(Adapted from Dolensek *et al*. 2015)

Figure 2.1 Pancreatic islet, with alpha (α) cells (pink), beta (β) cells (orange), delta cells (beige) and capillaries (red) in a rat. Peptide hormones secreted from each pancreatic islet include glucagon (α-cells, 15% of islet), insulin (β-cells, 75-80% of islet), pancreatic polypeptides (PP-cells, less than 5% of islet), and somatostatin (δ, 5% of islet)-cells.

The endocrine cell arrangement in human islets are different compared to that of rodent islets (Dolensek *et al*. 2015). In rodents the β-cells make up the core of each islet, whereas the other cells (α-cells, δ-cells, and PP-cells) are on the mantle of the islets (**Figure 2.1**) (Dolensek *et al*. 2015). The human islet structure is more complicated compared to rodents, where the islet cells are organized into a trilaminar plate. This plate consist of one layer of β-cells which are covered by two layers of α-cells (**Figure 2.2**) (Bosco *et al*. 2010). When comparing the human islet to that of other species, such as the rodent islets, the human islets generally have smaller fraction of β-cells (Steiner *et al*. 2010).

Stellenbosch University https://scholar.sun.ac.za

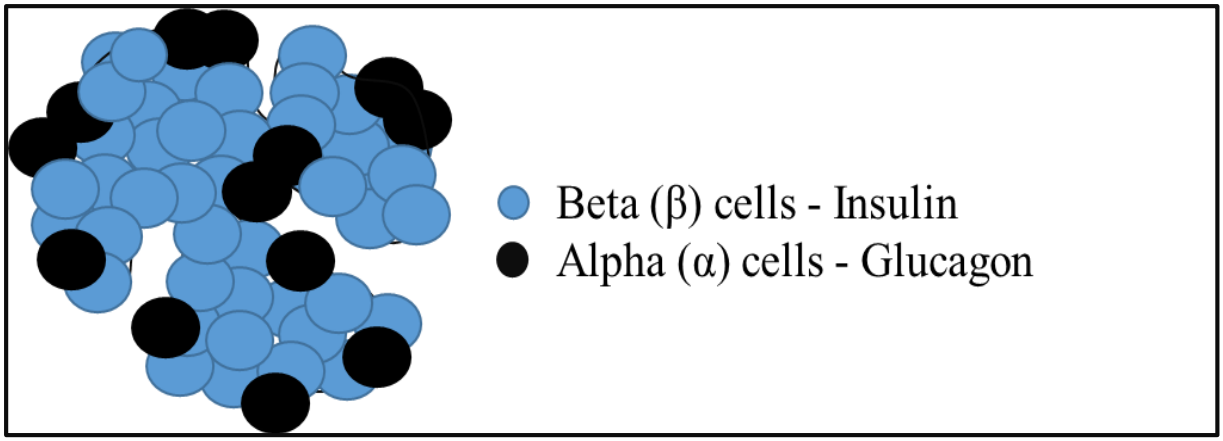

(Adapted from Bosco *et al*. 2010)

Figure 2.2 Pancreatic islet structure in a human islet. The black cells represent the α-cell (glucagon) layer and the blue cells are the β-cell (insulin) layer, forming the trilaminar plate.

Glucagon is secreted from the islet when blood glucose levels are decreased. Glucagon targets the liver which increases hepatic glucose production and therfore stimulates glycogenolysis and gluconeogenesis (Sherwood 2010). When the blood glucose levels are increased after a meal, the islet secretes insulin, which will allows glucose to be absorbed by insulin dependant tissue (Matschinsky & Ellerman 1967). Insulin is the main anabolic hormone in the body and regulates the metabolism of carbohydrates, fats and protein by promoting the absorption of glucose, forming a feedback system between insulin and glucagon, which maintains normal blood glucose levels in the body (Sherwood 2010).

It is suggested that alterations in the pancreas in HIV-infected patients may be due to causes unrelated to the virus. These causes include; alcoholism, hyperlipidaemia, hypercalcaemia, adenocarcinoma, opportunistic infections, and ART (Cappell 1997). Antiretroviral treatment causes pancreatic toxicity in humans which leads to pancreatitis, steatosis (fat infiltration), islet hypertrophy and α- and β-cells dysfunction (changes in cell mass, phenotype and function), therefore causing insulin resistance and diabetes mellitus (Barbosa *et al*., 2013). Protease inhibitors induce insulin resistance by reducing glucose transportation (Grinspoon & Carr 2005). Nucleoside reverse transcriptase inhibitors causes an increase in serum pancreatic enzymes, which leads to acute pancreatitis (Manfredi & Calza 2008). ART leads to acute pancreatitis, which is an inflammatory condition of the pancreas and is characterised by increased levels of pancreatic enzymes, acute inflammation and necrosis of pancreas parenchyma (Neuman *et al*. 2012).

Stellenbosch University https://scholar.sun.ac.za

Furthermore, the metabolic disruptions associated with obesity may lead to pancreas tissue inflammation, such as insulin resistance and type 2 diabetes mellitus (Donath *et al*. 2013; Savini *et al*. 2013). Obese individuals consume large amounts of carbohydrates causing elevated glucose levels which can be defined as impaired glucose tolerance, which in turn leads to hyperglycaemia (Donath *et al*. 2013). Type 2 diabetes mellitus is characterised by hyperglycaemia and dyslipidaemia (abnormal amount of lipids in the blood), causing islet dysfunction and insulin resistance (Nolan *et al*. 2011; Slavin *et al*. 2010). Hyperglycaemia induces beta-cell apoptosis thus causing an inflammatory process (Donath *et al*. 1999). The β-cells in the pancreatic islets still produce insulin, although the peripheral body tissue becomes resistant to the insulin (Tushuizen *et al*. 2007). The decline in β-cell mass and apoptosis is due to various mechanisms of which a few include toxic metabolites and increased oxidative stress (Shimabukuro *et al*. 1998; Bryan *et al*. 2013). Obesity in both human and rodents are associated with pancreatic islet morphology alterations such as increased islet number, size, and insulin secretion (Slavin *et al*. 2010).

2.4. Kidney structure, antiretroviral treatment toxicity and obesity

Both obesity and ART may cause renal diseases, such as nephrotoxicity and glomerular sclerosis (Kasiske & Napier 1985; Karras *et al*. 2003).

Each kidney in the human and rodent body consists of a cortex (outside) and a medulla (inside). The medulla (divided into the outer medulla and inner medulla) has pyramid structures, which are separated from each other by the cortex (**Figure 2.3**).

Stellenbosch University https://scholar.sun.ac.za

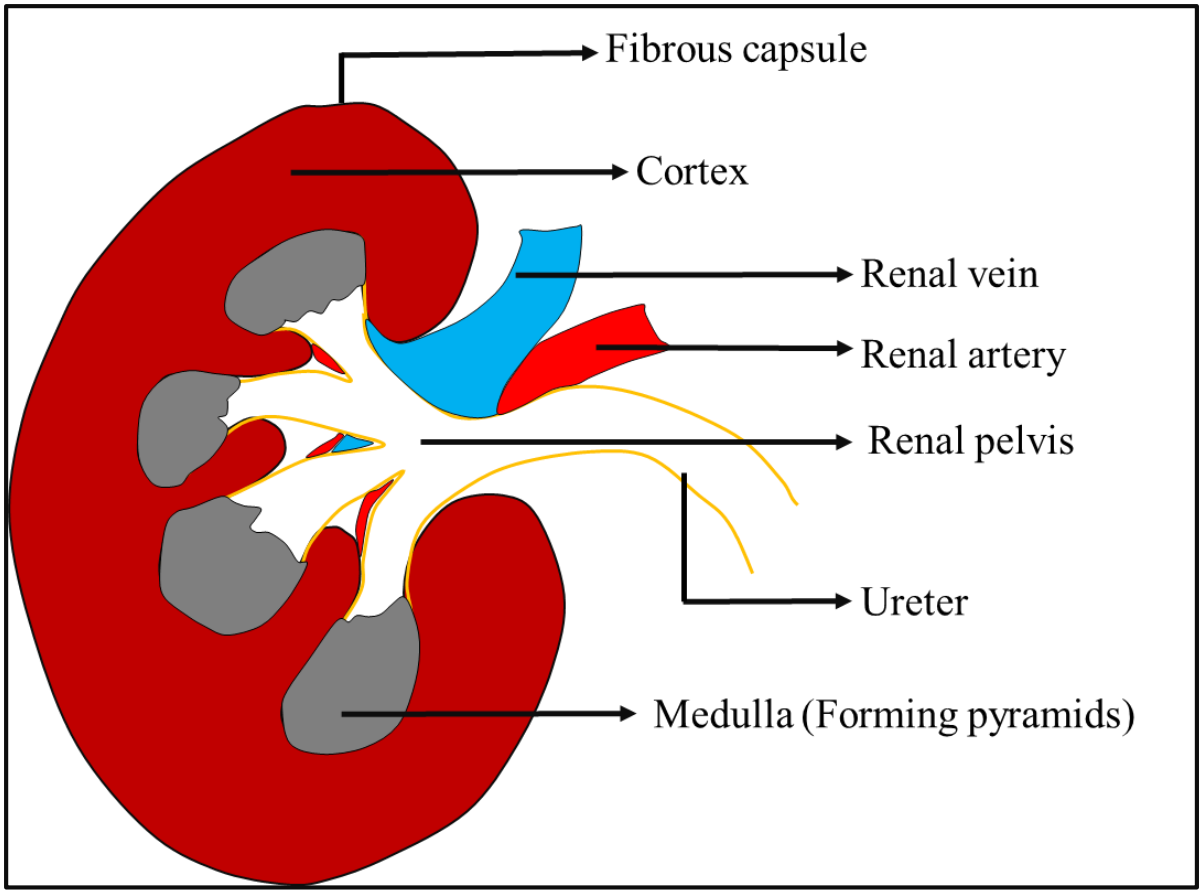

Figure 2.3 Annotated sketch indicating the kidney cut longitudinally, showing the cortex and medulla.

The base of the medullary pyramids are located in the corticomedullary junction, and forms the renal lobe. The renal lobe base is the renal capsule, with the renal lobes' lateral borders forming the renal columns (Kierszenbaum 2007; Young *et al*. 2006). The cortex (divided into the outer cortex and juxtamedullary cortex) forms a smooth outer layer and extends between the pyramids of the medulla, which contains the renal corpuscles. The glomerulus along with the capsule of Bowman forms the renal corpuscle (Silverthorn 2013; Kierszenbaum 2007). The function of the renal portal system is to filter fluids from the blood and into the glomerular capillaries to produce urine, which is composed of waste and extra fluid (Silverthorn 2013). Blood to the kidneys are supplied by the renal arteries, which branch into the interlobar arteries. The blood flows from the interlobar arteries into the arcuate arteries (located on the border of the cortex and medulla), which give off the interlobular arteries which penetrate the cortex to supply blood to the glomerular capillaries to be filtered (Kierszenbaum 2007; Young *et al*. 2006). The glomerular capillary network is formed from the afferent arterioles and is encased by the capsule of Bowman, which leads to the efferent glomerular arterioles. This network of arterioles and capillaries are called the glomerulus (**Figure 2.4**). Another function of the

Stellenbosch University https://scholar.sun.ac.za

kidneys are to regulate blood pressure via the renin-angiotensinogen system, which is activated with an increase and decrease in blood pressure (Marieb & Hoehn 2006).

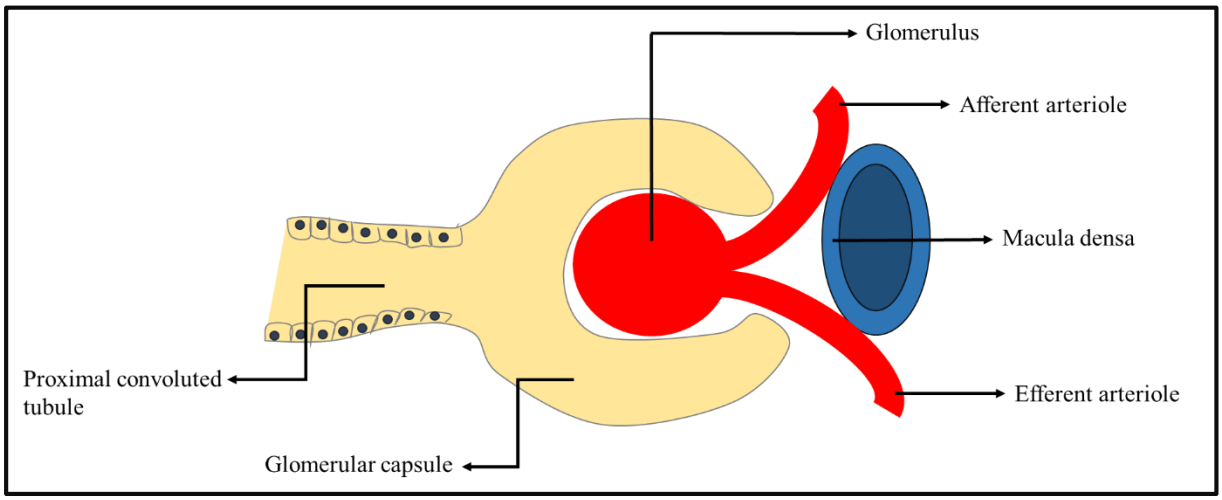

(Adapted from Kierszenbaum 2007)

Figure 2.4 Renal corpuscle which consist of the glomerular capsule. The glomerular capillary network is formed by the afferent and efferent arterioles (pink), filtering small molecules from the blood plasma.

Long term exposure to ART is associated with significant renal toxicity (nephrotoxicity), which may cause kidney injury (Jao and Wyatt, 2016; Menezes *et al*., 2011). High doses of Tenofovir had histopathological effects such as kidney disease (nephropathy) and/or tubular dysfunction (Karras *et al.*, 2003). Emtricitabine causes no nephrotoxicity, whereas Efavirenz causes minimal acute renal disease (Jao & Wyatt 2016). A recent study by Fabian *et al*. (2013) on the effects of pre-ART, seven month ART and 25 months ART on the histology of the kidney indicated that at seven months ART caused mild glomerular enlargement, dilated tubules and mesangial hyperplasia. Although at 25 months ART no glomerular enlargement and no mesangial alterations were observed in humans.

A review article by Hall (2003) described that in obese individuals increased adipose tissue encapsulates the kidneys, which penetrates the medulla and causes compression, increased arterial pressures and renal-pressure natriuresis. Excessive weight gain increases renal tubular reabsorption and impairs natriuresis (Excretion of sodium in the urine via the kidneys). This can happen via the renin-angiotensin system and compression of the kidneys (**Figure 2.5**) (Hall 2003). Changes occurring in the kidney due to obesity may cause compensatory mechanisms which leads to increased glomerular wall tension and glomerular hypertrophy. These

Stellenbosch University https://scholar.sun.ac.za

glomerular changes reduce the filtration surface area which in turn leads to increased blood pressure (Hall *et al*. 2014).

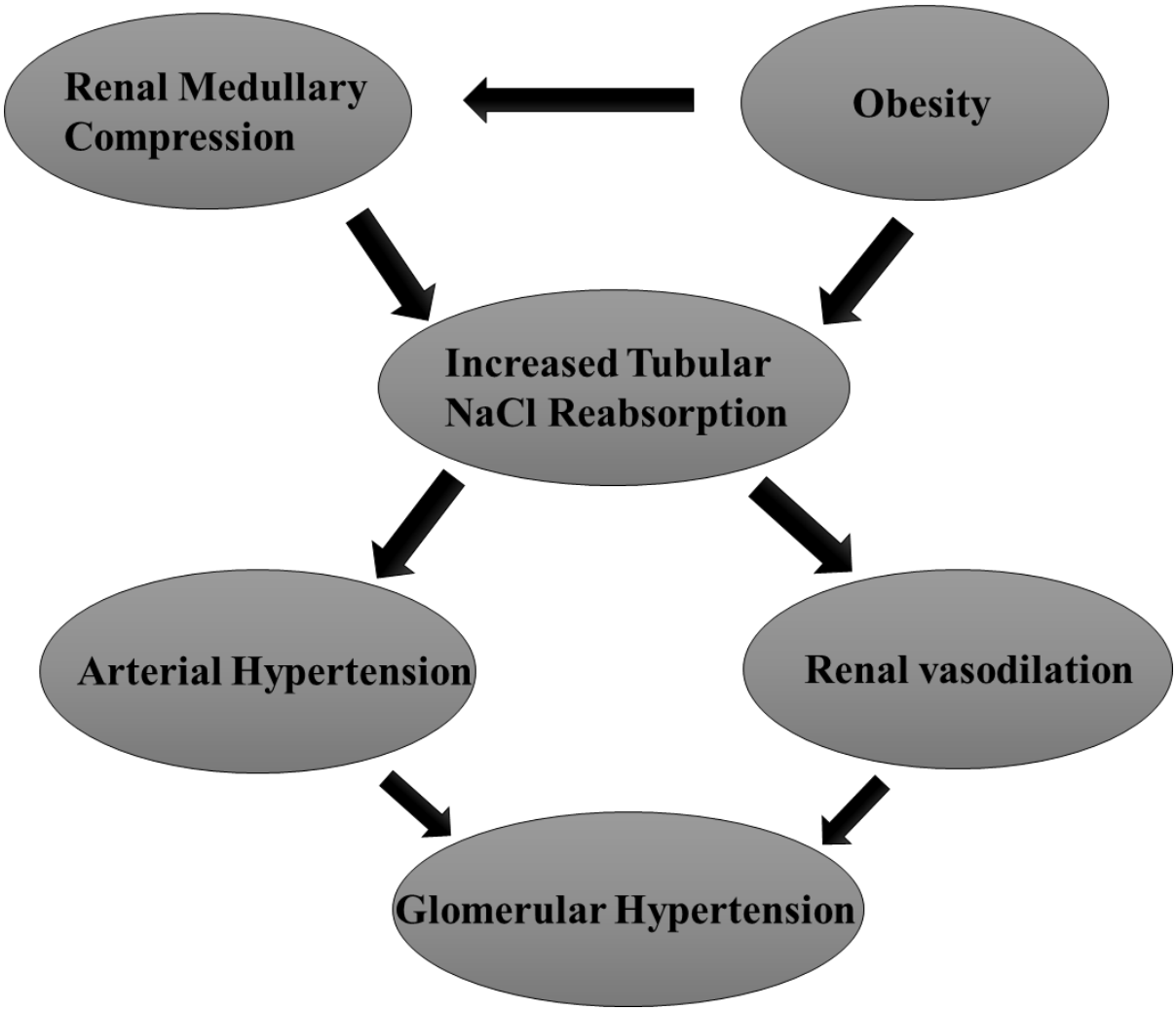

(Adapted from Hall 2003)

Figure 2.5 Obesity causes renal medullary compression, which leads to tubular reabsorption which in turn causes renal vasodilation and arterial hypertension.

Increased glomerular filtration rate is seen with diabetes, which is caused by a reduction in the renal vascular resistance and glomerular capillary hypertension (Hostetter *et al.* 1981). In a study by De Vriese *et al.* (2001), diabetic rats indicated vasodilation in all pre-glomerular and post-glomerular arterial vessels. Renal compression could explain the relationship between abdominal obesity and hypertension (Hall 2003). With hypertension, arteries undergo eutrophic and/or hypertrophic remodelling. Eutrophic remodelling is the decrease of the luminal space without changes to the vessel wall (Jacobsen & Holstein-Rathlou 2010). Hypertrophic remodelling is seen when the vascular wall thickens due to hyperplasia which in

Stellenbosch University https://scholar.sun.ac.za

turn increases the wall-to-lumen ration (Mulvany *et al.* 1996). Other causes of vascular thickening are intimal hyperplasia, vascular smooth muscle cells (VSMC) migration and proliferation (Safar *et al*. 1998). Some factors that have contributed to arterial remodelling includes; inflammation, apoptosis, fibrosis, and growth (Lu *et al*. 2011). Inflammatory cells increase in the tunica adventitia with hypertension (Intengan & Schiffrin 1993).

2.5. Liver structure, antiretroviral treatment toxicity and obesity

Hepatic steatosis and fibrosis is seen in obese individuals (Ratziu *et al.* 2000), whereas ART leads to hepatocytotoxicity effects, such as hepatitis, steatosis, and hepatocellular damage (Zimmerman 1978). The liver plays a role in fat, carbohydrates, and protein metabolism by storing metabolites, protein synthesis, and detoxify and secrete bile (Akiyoshi & Inoue 2012; Young *et al.* 2006). The liver is surrounded by a capsule containing collagen-elastic fibre (Kierszenbaum 2007). The functional unit of the liver is the hepatic lobules, consisting of hepatocytes and sinusoids, where the hepatocytes are arranged into irregular columns between the sinusoids (Akiyoshi & Inoue 2012). Each hepatocyte contains one round nucleus or sometimes two round nuclei (Silverthorn 2013). A distinctive component of the hepatic lobules are the portal triads, found in the portal spaces between the hepatic lobules and contains the portal vein, hepatic artery, bile duct, and lymph vessels (Young *et al.* 2006). The portal vein transports blood from other organs such as the spleen, pancreas and digestive tract, whereas the hepatic artery is branched from the celiac trunk and supplies the liver through the interlobar and interlobular artery (Kierszenbaum 2007).

The most common liver diseases with the onset of obesity and ART are chronic hepatitis, liver steatosis which leads to the development of liver cirrhosis from liver fibrosis (Yamauchi & Michitaka 1998). Most obese or diabetic individuals have liver disease, which is not due to alcohol consumption (Adler & Schaffner 1979). This led to the term non-alcoholic fatty liver disease (NAFLD), previously non-alcoholic steatohepatitis (NASH), being used to define liver steatosis in obese or diabetic individuals. Although obesity plays an important role in NAFLD, the metabolic syndrome and insulin resistance are very important in the pathology of the liver (Day 2002). With the role of lipid metabolism in the liver, it is possible that lipids may accumulate in the liver, specifically in the hepatocytes, when there is an imbalance between the fat delivery into the liver and the transfer out of fat as very-low-density lipoproteins (VLDL) (Goodman 2016). In conditions such as metabolic imbalances, stress, and cellular

Stellenbosch University https://scholar.sun.ac.za

injury, lipid droplets become larger and therefore be visible under a light microscope. These lipid droplets are seen as vacuoles in the cytoplasm of the hepatocytes (Goodman 2016).

ART interferes with liver mitochondrial metabolism, which may lead to lipid accumulation, because of oxidizing fatty acids. Therefore, hepatic steatosis in patients receiving ART, can be a sign of early mitochondrial dysfunction (Cornejo-juárez *et al*., 2003). ART has been reported to cause chronic hepatitis and portal hypertension (Neuman *et al.* 2012). In addition, NRTIs used in ART is seen to be associated with hepatic steatosis (Grinspoon & Carr 2005).

The effects of cART and accompanying obesity causes structural perturbations on the pancreas, kidney, liver and aortic PVAT and more extensive research is needed. The results of the study will provide information on the histological effects of cART combined with a high-calorie diet and be a basis for future research and development into obesity caused by ART. Although ART has changed the health care of HIV infected individuals, the adverse effects of the therapy may cause symptoms affecting various organ systems. Clinicians must concentrate on preventing these adverse drug effects if possible. As ART continues to develop, physicians treating HIV infected patients should remain aware of new and developing syndromes associated with the use of ART.

Stellenbosch University https://scholar.sun.ac.za

3. PROBLEM STATEMENT

HIV/AIDS is associated with disorders such as wasting syndrome and peripheral lipoatrophy. Both of these conditions have decreased with the use of ART, although in some patients on ART both syndromes can still occur (Longenecker *et al*., 2013; Wanke *et al*., 2015). The ART era showed increases in toxicity within organs and leads to some diseases, such as peripheral neuropathy, myopathy, pancreatitis, nephrotoxicity, lactic acidosis, and hepatic steatosis (Cornejo-juárez *et al*. 2003; Elfane *et al*. 2016; Jao & Wyatt 2016; Neuman *et al*. 2012). Kidney lesions associated with HIV-infection has been studied extensively, however HIV-associated nephropathy (HIVAN) with patients on ARV treatment has not been investigated on histological level and knowledge regarding this is still limited (Fabian *et al*. 2013). Studies have suggested that HIV-infected individuals on ART become overweight and/or obese (Pinto Neto *et al*. 2013). Obesity is associated with various diseases, such as hyperlipidaemia, cardiovascular diseases (CVD), coronary heart disease, hypertension, and diabetes (Van Der Merwe & Pepper 2006; Pi-Sunyer 2002). The present study aims to investigate and determine the effects of obesity and ART in the morphological changes of the in the pancreatic islets-, the glomerular and arcuate artery changes in the kidney, and the portal tract changes in the liver.

Stellenbosch University https://scholar.sun.ac.za

4. AIMS AND OBJECTIVES

4.1. Aim

The aim of the study is to compare the histomorphometric effects of antiretroviral treatment (ART) in combination with a high-calorie diet (HCD) on the pancreas, liver, kidneys and leptin expression in aortic perivascular adipose tissue (PVAT) in the rat.

4.2. Hypothesis

Null hypothesis (H_0): There are no significant histomorphometric differences in the pancreas, kidney, liver and leptin expression in aortic PVAT between the four experimental groups.

Hypothesis (H_a): There are significant histomorphometric differences in the pancreas, kidney, liver and leptin expression in aortic PVAT between the four experimental groups.

4.3. Objectives

Histochemical, immunohistochemical morphometric analysis of the four groups will be compared:

1. Surface area (µm²) measurements will be used to compare the size of pancreatic islet area, while the area (µm²) of insulin and glucagon reactive cells will be compared to assess pancreatic histomorphology changes between lean, antiretroviral treated and high-calorie diet groups.
2. The area (µm²), diameter (µm) and perimeter (µm) measurements of the renal corpuscle, glomeruli and renal space, with additional arcuate artery lumen diameter (µm) and artery wall thickness (µm) measurements will be compared to indicate possible glomerular and artery histomorphometry changes between lean, antiretroviral treated and high-calorie diet groups.
4. Leptin stain intensity by unilocular and differentiating adipocytes in aortic PVAT will be compared between lean, antiretroviral treated and high-calorie diet groups.
5. Pancreatic, renal and liver pathology will be compared between lean, antiretroviral treated and high-calorie diet groups in conjunction with a histopathologist and a histologist. This will be done to assess signs of possible toxicity of the organs other than morphometry differences.

Stellenbosch University https://scholar.sun.ac.za

5. STUDY DESIGN

5.1. Ethical Clearance

The Research Ethics Committee: Animal Care and Use of Stellenbosch University permitted ethical clearance for the Medical Physiology Division in the Department of Biomedical Sciences to euthanize and remove the hearts from male Wistar rats for the present study. Furthermore, ethical clearance was obtained for the use of various other organ tissues for histological purposes from the same animals (SU-ACUM13-00025).

5.2. Animals

Male Wistar rats (N=40) (eight weeks of age) were housed and cared for at the animal care facility of Stellenbosch University, Faculty of Medicine and Health Sciences. Animal care throughout the study conformed to the standards for animal use in research as reflected in the South African National Standards document (SANS 10386: 2008, available at www.sun.ac.za/research) of the South African Bureau of Standards (SABS). Animals were housed in cages and subjected to a controlled environment of ±22°C and 40% humidity on a 12 hour artificial day/night cycle. Animals were randomly divided into four groups (n=10/group) as follows in (**Figure 5.1**).

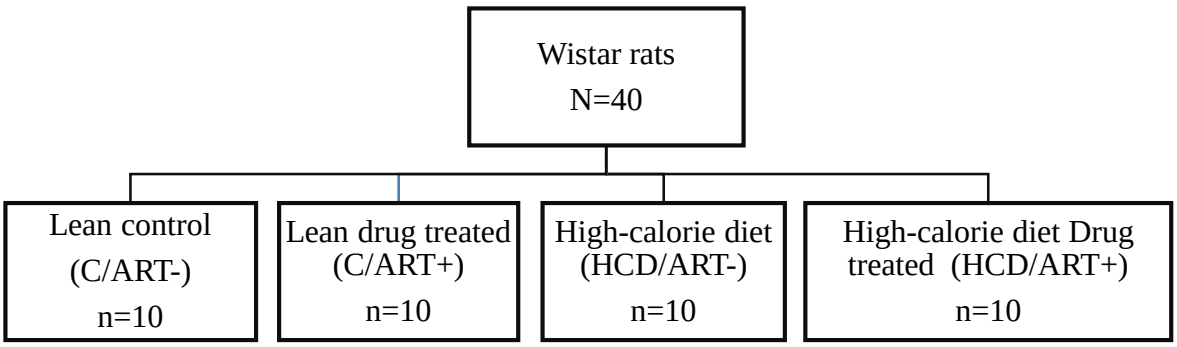

Figure 5.1 Classification of groups and sample sizes. Total Wistar rats (N=40) were divided into four groups (n=10); a lean control, a lean antiretroviral treatment (ART) treated, a high-calorie diet and a high-calorie diet drug treated, each group consisting of 10 Wistar rats.

N: Sample size; C: Lean control; HCD: High-calorie diet; ART-: No antiretroviral drug treatment (untreated); ART+; antiretroviral drug treated.

Stellenbosch University https://scholar.sun.ac.za

5.3. Feeding Programme and Drug Treatment

5.3.1. Feeding Programme

Animals (Initial weight: 224 gram) were placed on a 16-week feeding program, following an *ad* libitum diet (**Appendix A**). The HCD groups (HCD/ART- and HCD/ART+) only had free access to high-calorie food, consisting of 11.5% fat, 8.3% protein, 42% carbohydrates, and 20% sucrose (**Appendix B**). The HCD food was prepared by soaking normal rat chow (600g) in 250 ml mixture of warm water and dissolved sucrose (140g sugar) for 10 min. The soaked rat chow was crushed and melted vegetable fat (4 x 125g Holsum™) and eight cans of full cream, sweetened, condensed milk (8 x 385 g/can, Clover™) were added. The mixture was then well mixed and stored in a refrigerator for use. Each individual animal was weighed and monitored for visible changes in their health. Food and water consumption were monitored daily and total body mass (TBM) of all animals were monitored and recorded weekly.

5.3.2. Antiretroviral treatment (ART)

At week 10 of the feeding programme the ART commenced and continued for the remaining six weeks. The ART groups (C/ART+ and HCD/ART+) received first line ART of South Africa, Odimune, which consists of 200 mg Emtricitabine (FTC), 300 mg Tenofovir Disoproxil fumarate (TDF), and 600 mg Efavirenz (EFV) for an average human (70 kg) (**Appendix C**). The dosage of drugs was calculated according to the average total body mass (TBM) recorded weekly for each group of animals per cage and administered by means of oral gavage, whereas the untreated groups (C/ART- and HCD/ART-) received the same volume of water, relevant to their body weights, by oral gavage.

5.4. Tissue Collection and Processing

Animals were systematically euthanized (two animals per day for four consecutive days, the first at 10:00 and the second at 13:00, until 40 animals were harvested) by intraperitoneal injection of 160 mg/kg sodium pentobarbitone (Bayer (Pty) Ltd. Isando, Gauteng, RSA) after which the hearts were immediately removed by the Medical physiology representative for further studies. After the heart removal, the liver was removed and liver mass was taken.

Stellenbosch University https://scholar.sun.ac.za

Followed by the removal of the distal thoracic aorta with surrounding perivascular adipose tissue (PVAT), splenic region of the pancreas, and right kidney. All organ samples were immediately fixed in 4% paraformaldehyde (PFA) after removal for histological processing. The time lapse between the opening of the thoracic cage and harvesting of the organs for the present study was kept to a minimum as far as practically possible. All tissue samples were stored at 4 °C for 24 hours, after which the samples were transferred to labelled cassettes (**Figure 5.2**), followed by standard histological tissue wax processing procedures (**Appendix D**).

Stellenbosch University https://scholar.sun.ac.za

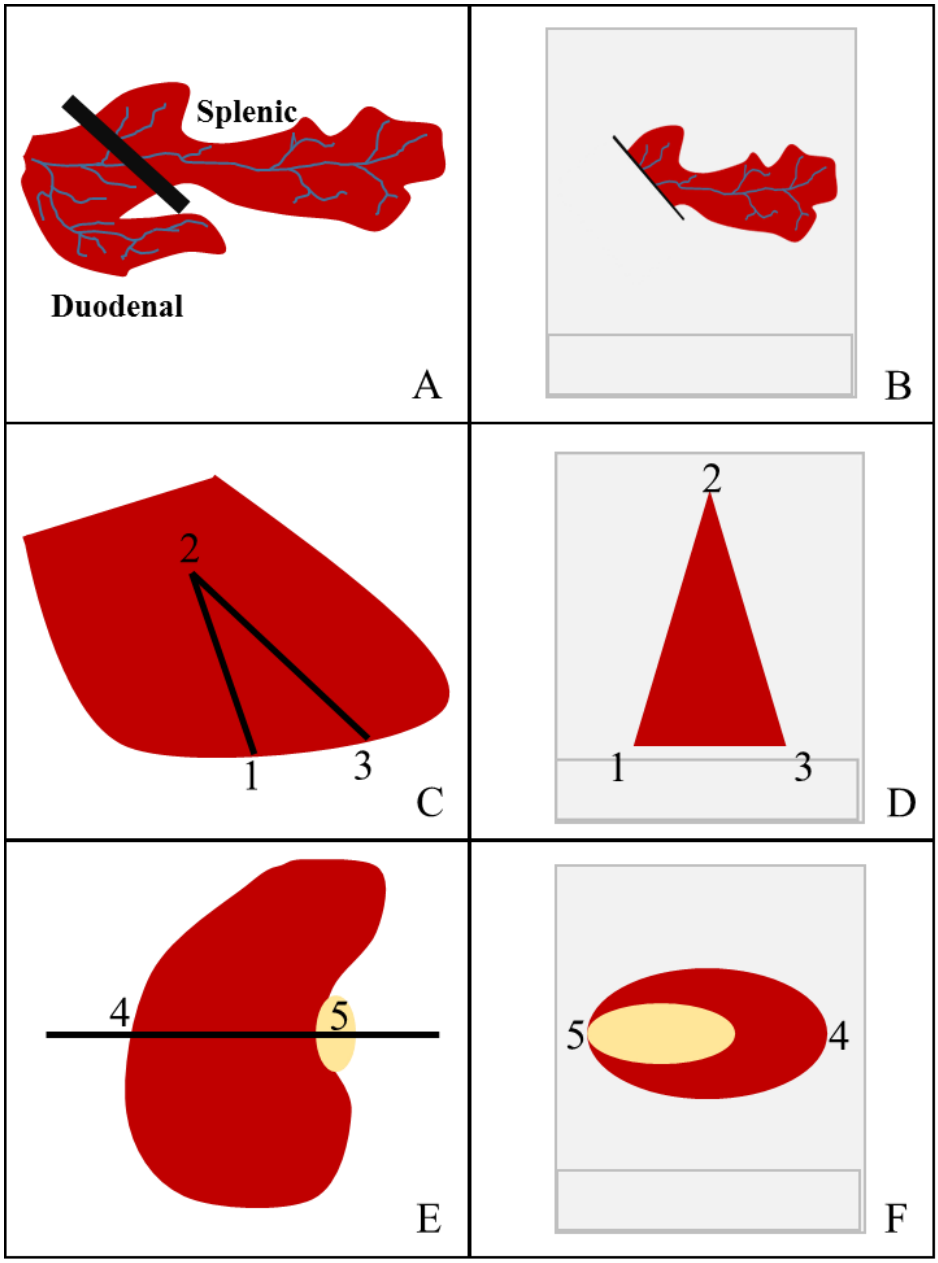

Figure 5.2 Pancreas, liver and kidney tissue cut and positioned for embedding cassettes. A) Pancreas splenic region cut and B) placed in embedding cassette. C) Left liver lobe cut triangular and D) placed on side in embedding cassette. E) Right kidney cut cross-sectional and F) placed cross-sectional in embedding cassette.

After processing, all samples were embedded in metal cassettes, using a Leica EG 1160 embedder, in pre-heated paraffin wax (60 °C). The pancreatic tissue was placed into the cassette, whereas the triangular liver section was placed on the side to show the hepatocytes and portal tracts of the liver. Cross-sections of the kidney and distal thoracic aorta with surrounding PVAT were placed perpendicular to the cassette, allowing cross-sections of the

Stellenbosch University https://scholar.sun.ac.za

glomeruli, arcuate arteries, and the aorta. Tissue blocks obtained were placed on an ice table for approximately two hours before sectioning.

5.5. Pancreas methodology

Two sections of pancreatic tissue were cut using a Leica RM 2125 RT microtome (**Appendix E**). The first section was cut at 3 µm for immunohistochemistry (IHC), floated in a warm waterbath placed on positively charged microscopic slides and used for morphometric analysis. The second section was cut at 5 µm for haematoxylin and eosin (H&E), placed on frosted microscopic slides and used for pathology assessment.

5.5.1. Immunohistochemistry (IHC)

All pancreatic sections on positively charged slides underwent double-labelling for insulin and glucagon of the pancreatic islets (**Figure 5.3**). A standard operating procedure at the Biomedical Research and Innovation Platform at the South African Medical Research Council (SOP ICC\B7-V01, **Appendix G**) for double labelling paraffin sections was used. A polyclonal rabbit anti-glucagon (Dako, North America) which labelled the alpha (α) cells, and monoclonal guinea pig anti-insulin (Dako, North America) which labelled the beta (β) cells was used. After dewaxing the pancreatic tissue sections with xylene and alcohol, sections were blocked for endogenous peroxidase followed by 0.05M Tris buffered saline (TBS) pH 7.2 and 0.1 M Phosphate buffered saline (PBS) pH 7.2. Normal goat serum (NGS, 1:20 dilution) was then added to the slides in a moisture chamber for 20 minutes, to block non-specific binding. Anti-glucagon (100 µl) diluted at 1:100 was added to the sections in the moisture chamber and incubated for 30 minutes where after biotinylated anti-rabbit IgG (1:200 dilution) was added onto the sections in the moisture chamber for 30 minutes to remove cross-reactivity that could interfere with the specific binding, followed by Vectastain® (ABC kit, North America) for one hour, to detect biotinylated molecules. Liquid 3'3-diaminobenzidine (DAB) plus chromogen solution (K3468, Dako, North America) was then added to the sections on a rack over the sink for five minutes. Sections where then placed back into the moisture chamber and normal horse serum (NHS, 1:20 dilution) was added for 20 minutes, for blocking non-specific binding. This was followed by adding the anti-insulin (100 µl) diluted at 1:10 000 to the sections in the moisture chamber and incubated overnight (20-24 hours) at 4 °C. The following day, slides

Stellenbosch University https://scholar.sun.ac.za

were allowed to reach room temperature, followed by the addition of Envision™ kit and a Mayer's haematoxylin counterstain for two to four minutes.

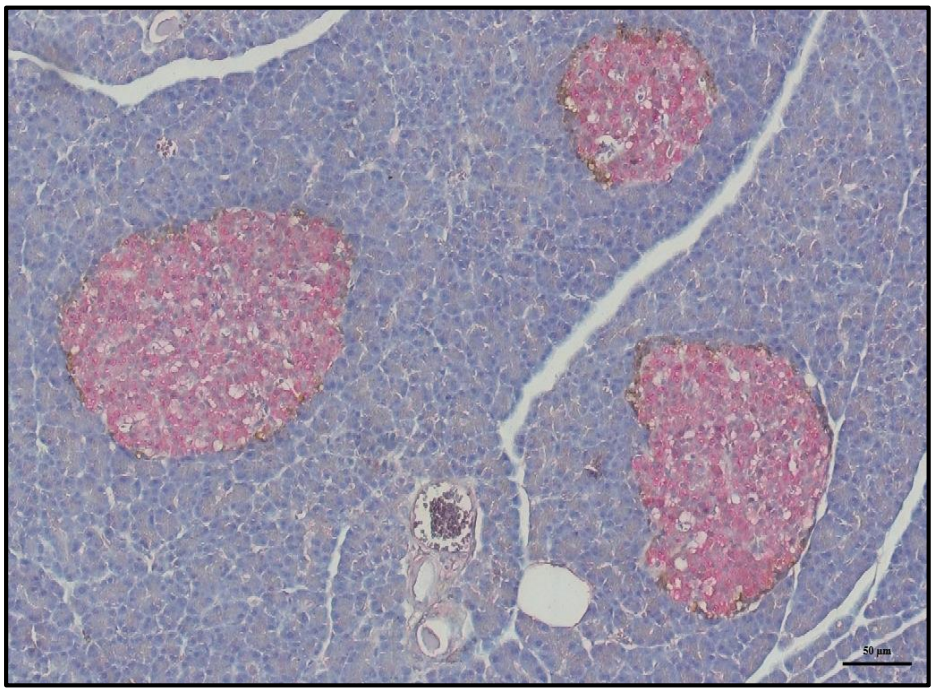

Figure 5.3 A double IHC labelling technique used on pancreatic islets, labelling insulin (β-cells in pink) and glucagon (α-cells in brown). 100x magnification, scale bar = 50µm

5.5.2. Haematoxylin and eosin (H&E)

A haematoxylin and eosin (H&E) stain was performed on all pancreatic sections on the frosted slides using a Leica Auto Stainer XL (SOP, **Appendix F**) with a pre-programmed protocol.

5.5.3. Morphometric analysis

Pancreatic sections were scanned using the Nikon Eclipse Ti-S with PRIOR ProScan III and Nikon automated tissue scanning software (NIS Elements AR4.40) (**Appendix I**) at a 100 x magnification (10 x objective lens). Images were captured with a 10% overlap and were then stitched together forming a composite image of the section. Morphometric analysis was conducted at the South African Medical Research Council (SAMRC) with the use of Leica QWin V3 software (Germany). The total section area was highlighted and the area measured in square micrometres (µm²) per section, this included the pink beta cell, brown alpha cell and blue haematoxylin stained areas. Thereafter, each pancreatic islet is highlighted (**Figure 5.4.A**)

Stellenbosch University https://scholar.sun.ac.za

to measure the total islet area in square micrometres (µm²). A circumference was traced around the islet to ensure that other possible brown and pink stains outside of the islet would be excluded (**Figure 5.4.B).** The brown alpha (glucagon) cell area was highlighted and measured in square micrometres (µm²) to obtain an average alpha cell area per section (**Figure 5.4.C**). The pink beta (insulin) cell area was then highlighted and measured in square micrometres (µm²), obtaining an average beta cell area per section (**Figure 5.4.D**). This was done for all islets per section area and the number of islets per section area was counted and measured in square millimetre (mm²). A total of 1380 islets were measured to obtain significant results, resulting in an average of 300 islets per group (N=10 animals/group) (**Table 18**, **Appendix K**).

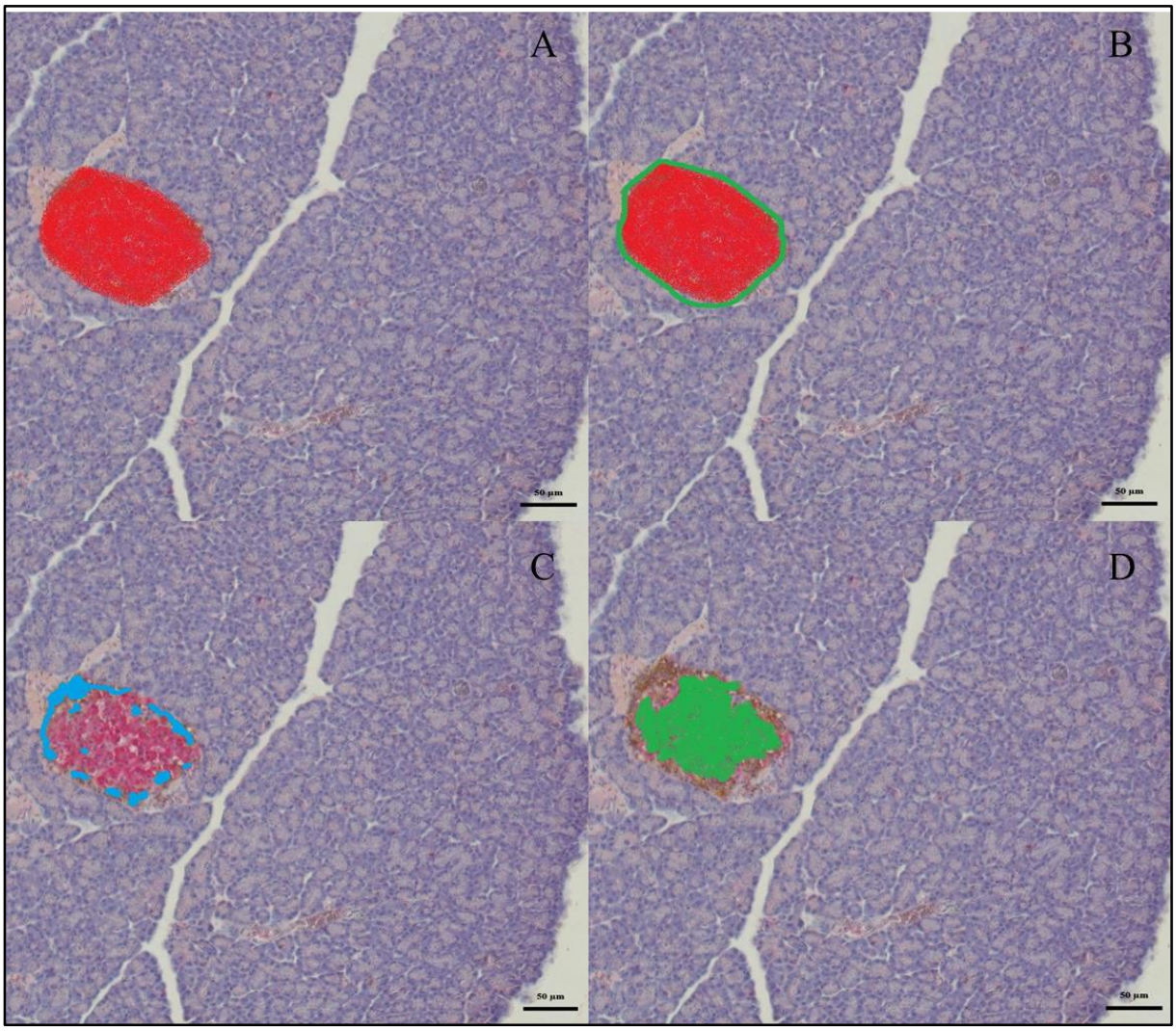

Figure 5.4 Analysis of double labelled IHC pancreatic islets. A) The entire islet is highlighted in red to obtain total islet area, B) a green circumference is traced around the perimeter of the islet, measuring the islet area. C) Brown stained areas are highlighted in blue, measuring alpha cell area and D) pink stained areas are highlighted in green, measuring beta cell area. 100x magnification, scale bar = 50 µm.

Stellenbosch University https://scholar.sun.ac.za

5.5.4. Pathology assessment

The H&E stained sections were assessed for pathology by two histopathologists, a histologist and the researcher. Sections presented with pathology were graded as follows; absent (0), mild (I), moderate (II), severe (III) and expressed as a percentage (%) of the total animal sample (N=40). The grading criteria are defined in **Appendix J**.

5.6. Leptin intensity staining methodology

The aorta with surrounding PVAT was sectioned at 5 µm and placed on positively charged slides for immunohistochemistry (IHC) analysis. The aortic PVAT adipocytes were classified according to their histological characteristics. White (unilocular) adipocytes were defined by one large lipid droplet (leaving a corresponding space in wax sections) and a thin cytoplasmic rim. Brown (multilocular) adipocytes were characterised by multiple small lipid droplets (Cinti 1999; Cousin *et al*. 1992). Adipocytes with a single large lipid droplet surrounded by small droplets were defined as differentiating adipocytes (Cinti 1999).

For IHC, affinity purified polyclonal anti-leptin antibodies (Abcam, ab117751, used for automated and non-automated systems) raised in rabbit were used to label the leptin protein expression within the aortic PVAT adipocytes. A standard *F protocol, used by LEICA Bondmax™ (**Appendix H**), with heat-mediated antigen retrieval using citrate based buffer pH6 (ER1 for 30 minutes) was employed on the Leica Bondmax™ using the Bond Polymer Refine detection kit (DS 9800). The hydrogen peroxide step was modified to 10 minutes to effectively quench endogenous peroxidase in red blood cells. Kidney glomeruli were used as a negative tissue control, whereas placenta samples were used as a positive tissue control to confirm the antigen targeted the relevant tissue cells (**Figure 5.5**). Controls underwent positive and negative reagent reaction, to ensure correct labelling and minimising background staining.

Anti-leptin stained aortic PVAT sections were viewed using the Zeiss Axioskop2 light microscope. Photos were taken of two complete PVAT lobules on 25x magnification (2.5x objective X 10x magnification lens). In order to randomize the analysis, the following procedure was followed in all animals; a grid with set patterns (293.45µm x 293.45µm) was

Stellenbosch University https://scholar.sun.ac.za

placed on the 25x magnification photo of each lobule. Four set patterns were applied according to the placement of the tissue in the photograph (25x magnification). In each pattern five blocks were selected with the use of random numbers. These selected blocks were photographed at 400x magnification, therefore 10 images per slide (5 blocks x 2 lobules) using the AxioVisio software (version 4.7.2.0., Germany). In the case where no unilocular adipocytes were seen in the 10 images, another set of five images per lobule were captured only where the unilocular adipocytes were seen. Leptin expression in unilocular adipocytes and differentiating adipocytes were classified by one researcher, who was blinded to the treatment groups, into four levels of staining intensity similar to methods used in Cinti *et al*. (1997). Classification levels were as follows; leptin negative (0), weak leptin positive (I), leptin positive (II), and intensely leptin positive (III) (**Figure 5.5**). The mode (value appearing the most) intensity level of each experimental group was determined.

Stellenbosch University https://scholar.sun.ac.za

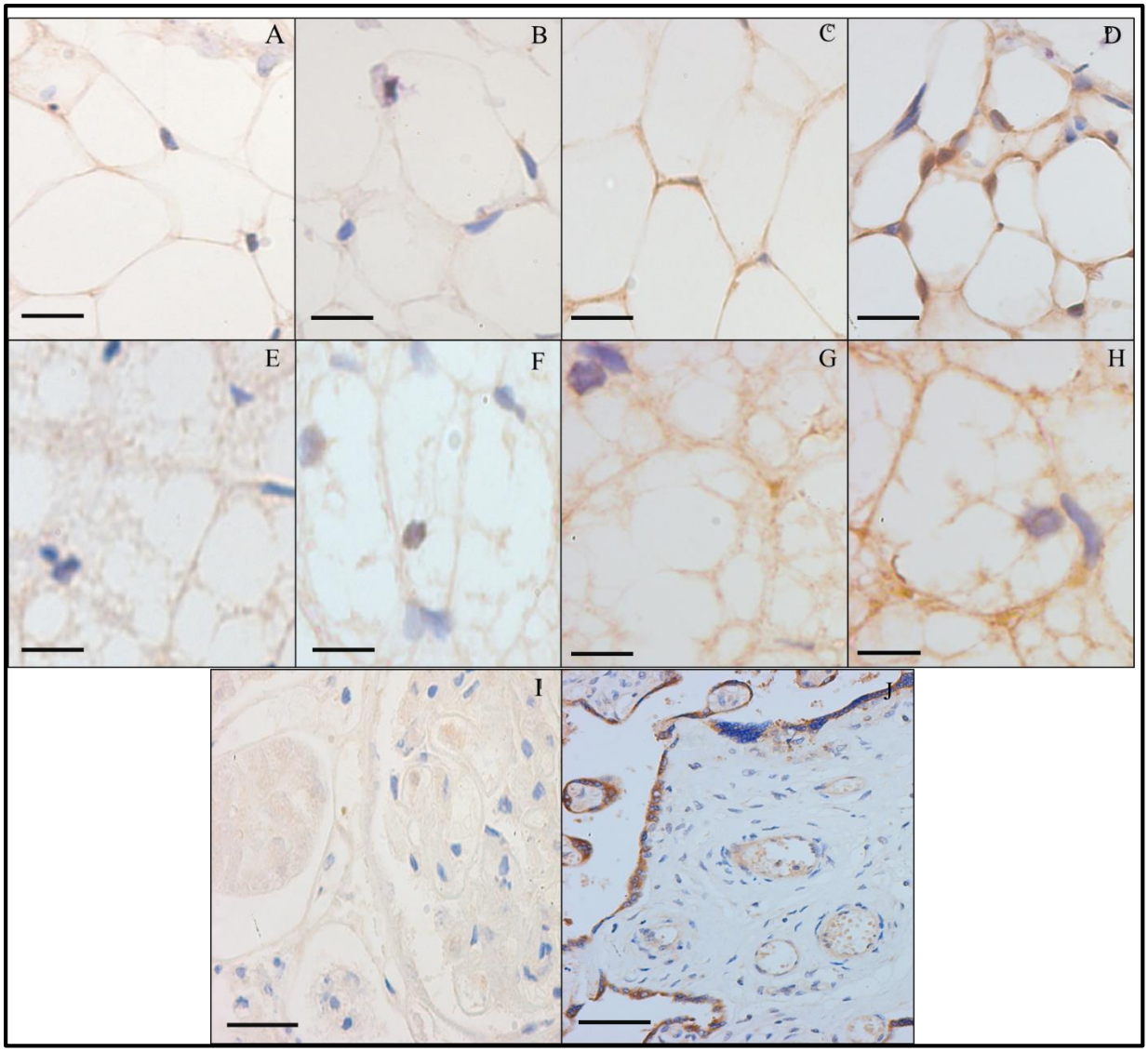

Figure 5.5 Examples of the levels of leptin expression intensity, white adipocytes (A-D) and differentiating adipocytes (E-H). A & E) level 0, leptin negative. B & F) Level I, weak leptin positive. C & G) Level II, leptin positive. D & H) Level III, intense leptin positive, I & J) Negative (kidney glomeruli) and positive (placenta) controls.

5.7. Kidney methodology

Each kidney section was trimmed by 20µm (4 x 5 µm), the first section of the kidney (25µm) was then placed on a frosted microscope slide and stained with H&E for morphometric analysis and pathology assessment. Haematoxylin and eosin (H&E) stain was performed on all kidney sections on frosted slides using a Leica Auto Stainer XL (SOP, **Appendix F**) with a pre-programmed protocol.

Stellenbosch University https://scholar.sun.ac.za

5.7.1. Morphometric analysis

Kidney sections were scanned using the Nikon Eclipse Ti-S with PRIOR ProScan III and Nikon automated tissue scanning software (NIS Elements AR4.40) at a 400 x magnification (40 x objective lens). Images were captured with a 10% overlap and stitched together forming a composite image of the kidney section. Thirty renal corpuscles were analysed per animal. To randomise the analysed renal corpuscles, the scanned kidney was divided into three parts: superior, middle and inferior. In each part, 10 renal corpuscles were measured, to randomise the 10 analysed renal corpuscles every fifth renal corpuscle was selected, thus 30 renal corpuscles per animal (1200 renal corpuscles in total). Similar to techniques used in Sedeek *et al*. (2013), renal corpuscle- and glomeruli –area (µm²), -diameter (µm), and –perimeter (µm) were measured and analysed (**Figure 5.6**). Diameter of the glomeruli were measured as follows; two lines (one horizontal and the other vertical) were placed perpendicular over the glomerulus, obtaining two sets of diameter values (one horizontally and the other vertically). An average of the two perpendicular lines were calculated and used as the diameter value for that specific glomeruli. This was done for each glomeruli measured per animal per group.

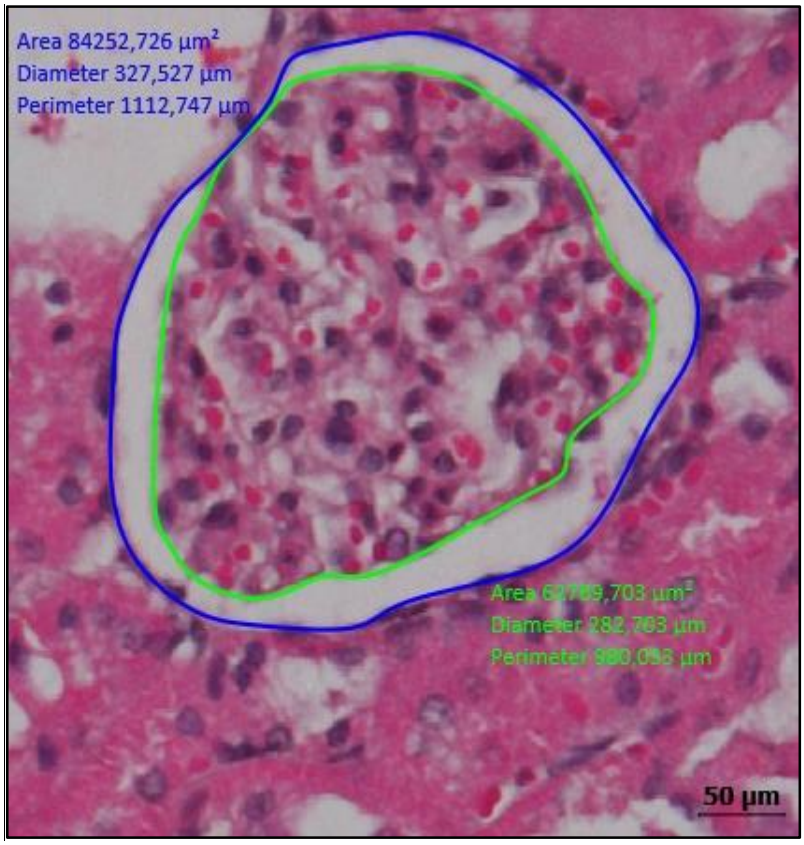

Figure 5.6 Glomerulus with renal corpuscles traced in blue and glomerulus traced in green. The area, diameter and perimeter measurements of the corpuscle and glomerulus are calculated for each of the 1200 renal corpuscles. 400x magnification. Scale bar = 50µm

Stellenbosch University https://scholar.sun.ac.za

Additionally, the kidney arcuate artery tunica media and tunica adventitia thickness and lumen diameter were measured. Measurements of the tunica intima layer was excluded, due to the fact that it was very thin and difficult to measure. The exclusion criteria included arcuate arteries that were slightly or completely longitudinally cut. All arcuate arteries that appeared to be cross-sectioned were measured. The artery wall was measured at four points and the lumen at two lines, to eliminate as much variability as possible, obtaining an average for the wall thickness and an average lumen diameter. Two radial lines perpendicular to each other were placed over the image of the artery, thus crossing the artery wall at four points. Artery wall thickness was measured on these four points (**Figure 5.7**, green and red, 1-4), where an average of the four measurements were calculated to provide the arcuate artery wall thickness. The lumen diameter was measured on these two perpendicular lines, thus obtaining an average lumen diameter for the specific artery (**Figure 5.7**, blue, A-B).

Stellenbosch University https://scholar.sun.ac.za

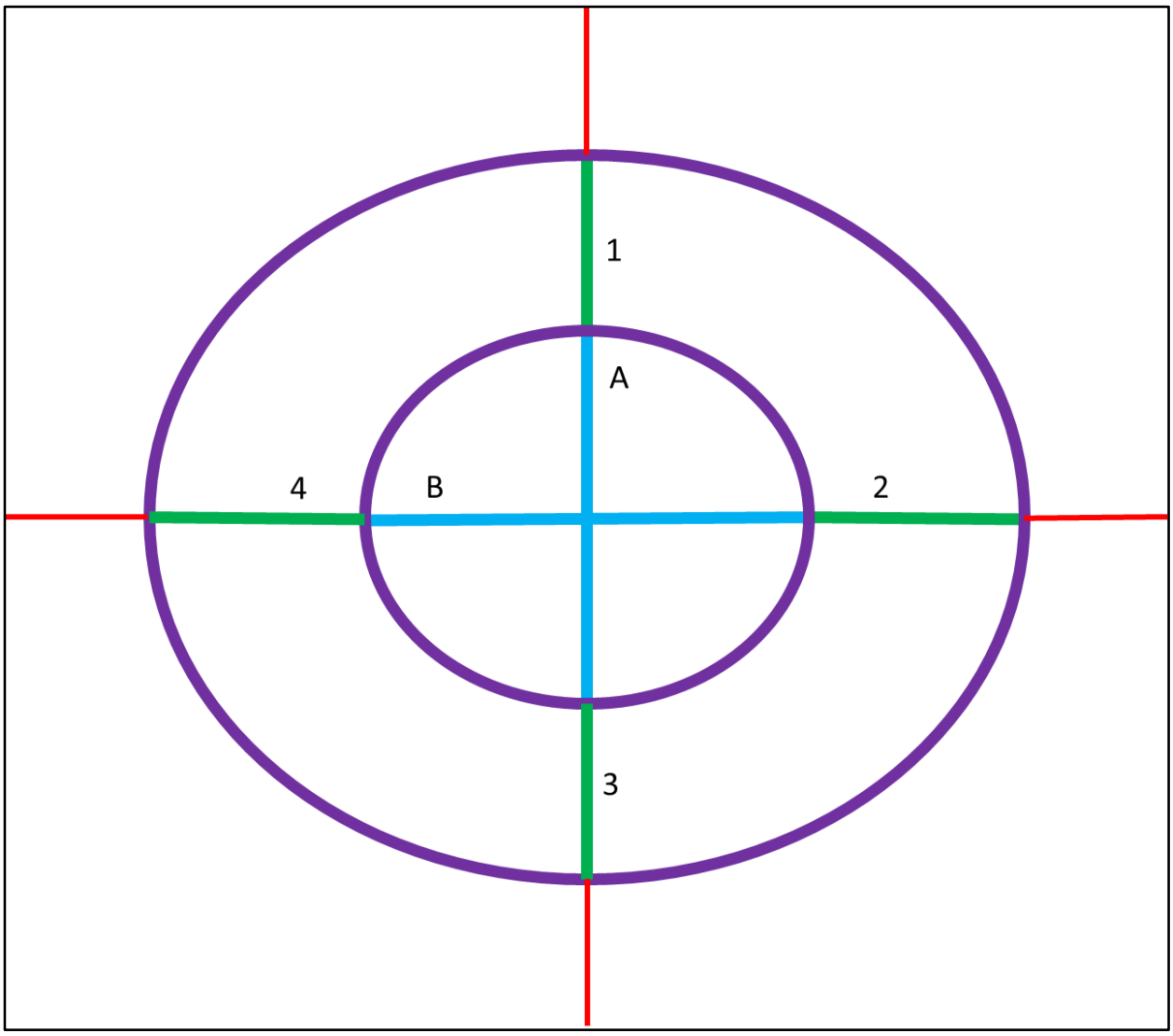

Figure 5.7 Arcuate artery (purple) measurements; tunica media wall thickness (Green), tunica adventitia (red) and two lumen diameters (blue).

5.7.2. Pathology assessment

The H&E stained sections were assessed for pathology in conjunction with two histopathologists, a histologist and the researcher. Pathology on each section was classified with absent (0) and present (1). The sections presented with pathology were graded as follows; mild (I), moderate (II), severe (III) and expressed as a percentage (%) of the total sample size (N=40). The grading criteria are defined in **Appendix J**.

Stellenbosch University https://scholar.sun.ac.za

5.8. Liver methodology

Liver sections were cut at 5 µm using a Leica RM 2125 RT microtome. The sections were placed on frosted microscopic slides to stain for H&E and used for pathology assessment.
A haematoxylin and eosin (H&E) stain was performed on all liver sections on frosted slides using a Leica Auto Stainer XL with a pre-Programmed protocol.

5.8.1. Pathology assessment

The H&E stained sections were assessed for pathology in conjunction with two histopathologists, a histologist and the researcher. Pathology on each section was classified with absent (0) and present (1). The sections presented with pathology were graded as follows; mild (I), moderate (II), severe (III). Possible fatty changes were graded as follows; 0-25% (I), 25-50% (II), 50-75% (III), and 75-100% (III). Data was expressed as a percentage (%) of the total sample size (N=40). The grading criteria are defined in **Appendix J**.

5.9. Statistical Analysis

Data are presented as mean ± standard error (SEM). Statistical analysis of the morphometric data was performed using the Variance Estimation, Precision and Comparison (VEPAC) descriptive statistics followed by (LSD) post hoc test from the Statistica® software (version 12, StatSoft, Southern Africa—Research (Pty.) Ltd.). Statistical analysis of the pathology data was performed using a 2-way summary table with a Chi-square test from the Statistica® software (version 12, StatSoft, Southern Africa—Research (Pty.) Ltd.). Statistical significance was set at a p-value of less than 0.05 ($p<0.05$).

Stellenbosch University https://scholar.sun.ac.za

6. RESULTS

6.1. Body mass

The average initial body mass (grams, g) was in the same range for all four groups. An increase in body mass was seen in all four groups, however no group had more than 50% average body mass increase (**Table 1**). The HCD/ART+ group had a significant increase ($p<0.022$) in body mass compared to the C/ART- at termination (**Table 1** and **Figure 6.1**). The C/ART+ and HCD/ART- groups had a higher body mass compared to the C/ART- group, however the increase was not significant (**Figure 6.1**).

Table 1 Average body mass expressed in grams (g) and percentage (%) increase in each group.

Group	Initial body mass	Body mass at termination	% increase
C/ART-	223.2	376,8	39.7[a]
C/ART+	224.2	399,6	43.1[a b]
HCD/ART-	225.3	409,2	44.4[a b]
HCD/ART+	222.4	442,9	49.4[b]

Stellenbosch University https://scholar.sun.ac.za

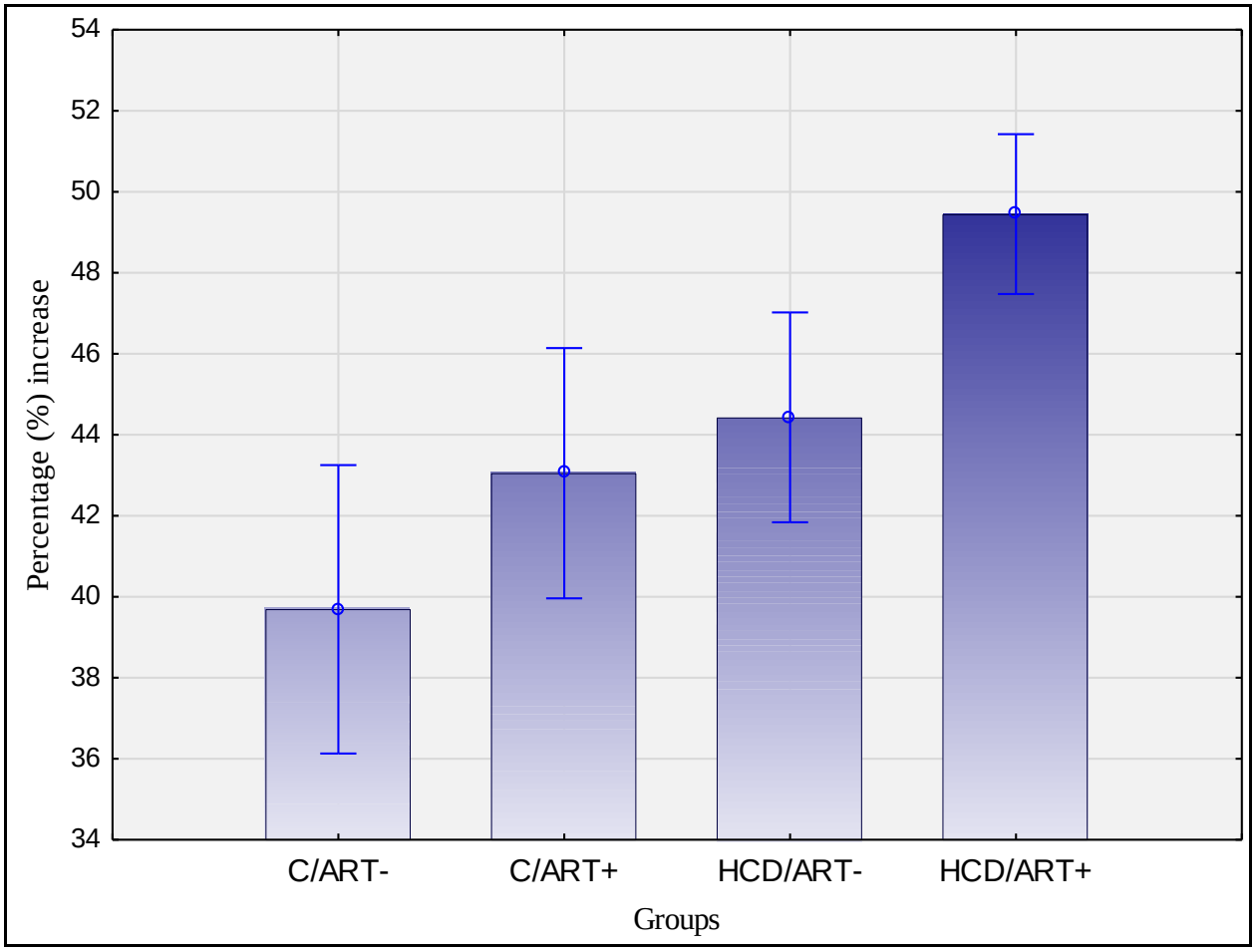

Figure 6.1 Average percentage (%) increase in body mass in each group. A significant increase in the high-calorie diet ART group were seen compared to the lean control.

6.2. Pancreas

With the use of immunohistochemistry, total pancreatic islet area (µm²), alpha (α) and beta (β) cells area (µm²) were measured and analysed. In addition, the number of pancreatic islets per square millimetre (mm²) were analysed, **Table 18 (Appendix K)** indicates the number of islets measured per animal.

6.2.1. Alpha and beta cell analysis

Total pancreatic islet area (µm²) had no significant ($p>0.678$) changes between the four groups (**Table 19**, **Appendix K**). A trend, based on the mean values indicated that the total pancreatic

Stellenbosch University https://scholar.sun.ac.za

islet area in the C/ART+ group had a smaller total area size compared to the control (C/ART-) and HCD groups (HCD/ART- and HCD/ART+) (**Table 2**).

Alpha (α) and beta (β) cell areas were not significantly changed between the four groups (**Figure 6.2**, **Table 20**, **Appendix K**). However, a trend based on the mean values indicated that the average α-cell area in the HCD/ART- group was marginally larger in size compared to the other three groups (**Figure 6.2**). The average β-cell area in the C/ART+, HCD/ART- and HCD/ART+ groups was less compared to the control (C/ART-) group, with the C/ART+ group having the smallest β-cell area compared to the control (C/ART-) group (**Figure 6.2**).

Table 2 Average area of alpha (α)-, beta (β)-cells and total islet area from the pancreatic islets expressed as surface area (µm²) ± SEM.

Average area (µm²±Std.Err.) of islets and cells within pancreatic islets			
	Alpha (α) cells	**Beta (β) cells**	**Total Islet area**
C/ART-	657,99 ± 282,02	3031,3 ± 282,02	4230,55 ± 1053,42
C/ART+	693,37 ± 265,57	2421,52 ± 265,57	3831,39 ± 992,42
HCD/ART-	1014,34 ± 263,62	2981,13 ± 263,62	4752,12 ± 985,57
HCD/ART+	638,39 ± 237,41	2655,71 ± 237,41	4204,47 ± 885,91

Stellenbosch University https://scholar.sun.ac.za

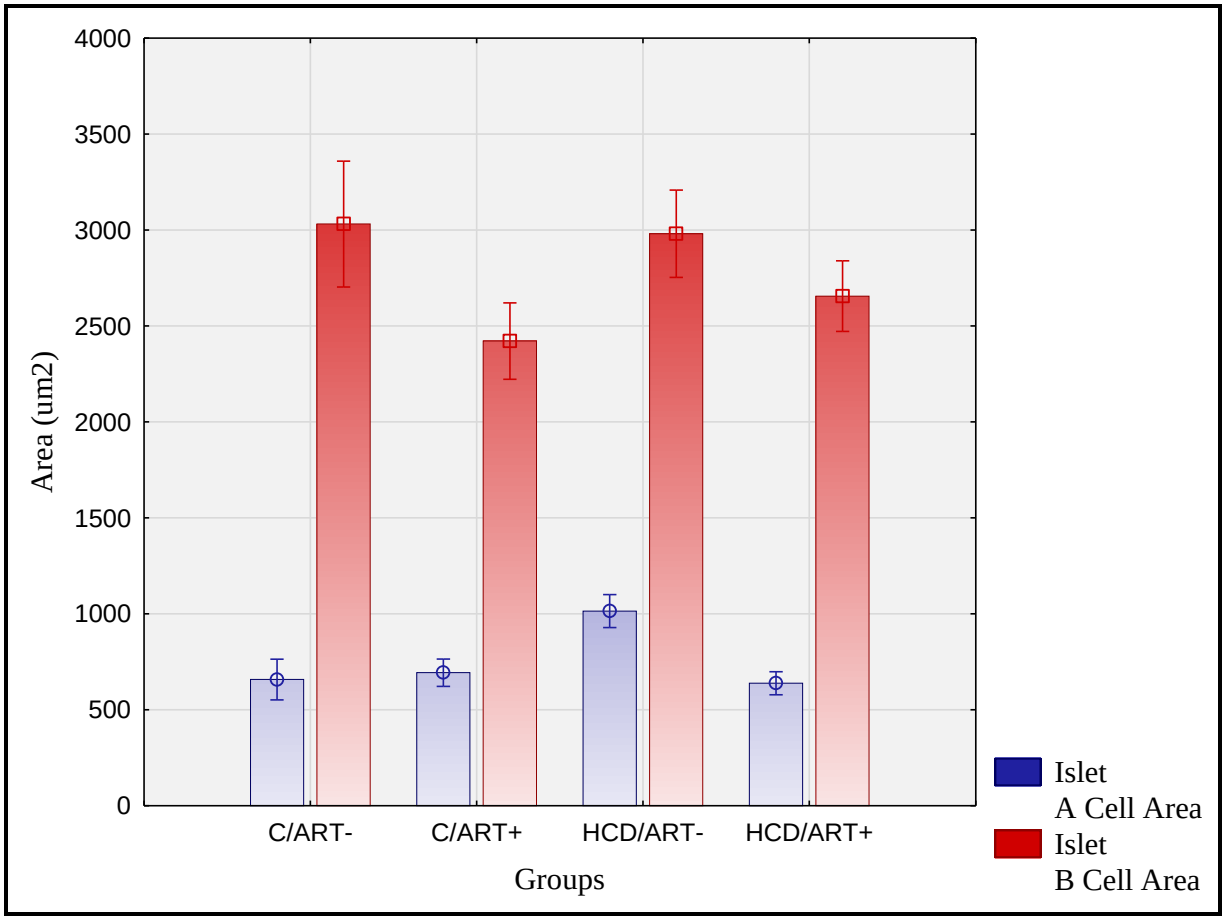

Figure 6.2 Alpha (A)-cell (blue line) and beta (B)-cell (red line) area (µm²) sizes of the pancreatic islets in the four groups. Alpha cells secrete glucagon and beta cells secrete insulin. Alpha- and beta-cell areas showed no statistically significant differences between the four groups.

6.2.2. Pancreatic islet number per square millimetre (mm²)

The number of pancreatic islets per pancreas mm² had no significant difference ($p>0.13$) between the four groups (**Table 21**, **Appendix K**). A trend based on the mean values indicated that both the HCD/ART- and HCD/ART+ groups had more islets per pancreas section area than the C/ART- group (**Figure 6.3**).

Stellenbosch University https://scholar.sun.ac.za

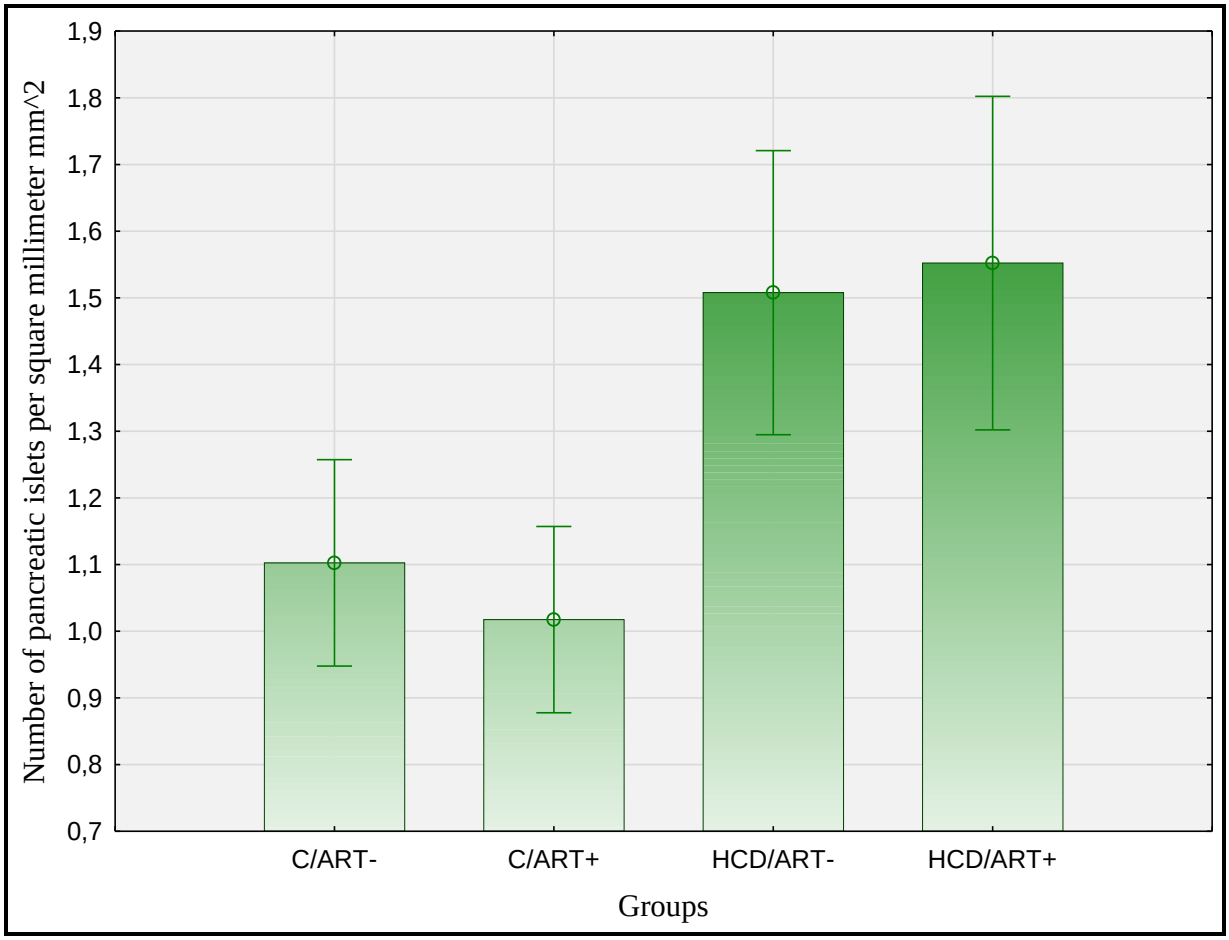

Figure 6.3Average number of pancreatic islets per square millimetre (mm²). No statistically significant increase in number of pancreatic islets per section area were seen between the four groups.

6.2.3. Pathology

Haematoxylin and eosin stain was used to assess pathology each pancreas section. Pathology was graded accordingly; absent (0), mild (I), moderate (II), severe (III), and expressed in percentages (%). No pathology changes were found in the pancreas between the four groups.

6.2.4. Additional findings

When analysing the pancreas sections for pathology changes, additional findings were seen. Eosinophilic proteinaceous casts in collecting ducts were found in 2/40 of the pancreas samples (**Figure 6.4**). One was found in the C/ART+ group, whereas the other one was found in the HCD/ART- group. The HCD/ART+ group had two (5%) reactive lymph nodes (sectioned by

Stellenbosch University https://scholar.sun.ac.za

chance) (**Table 22**, **Appendix K**). These findings are not important for the current study, but are interesting to note.

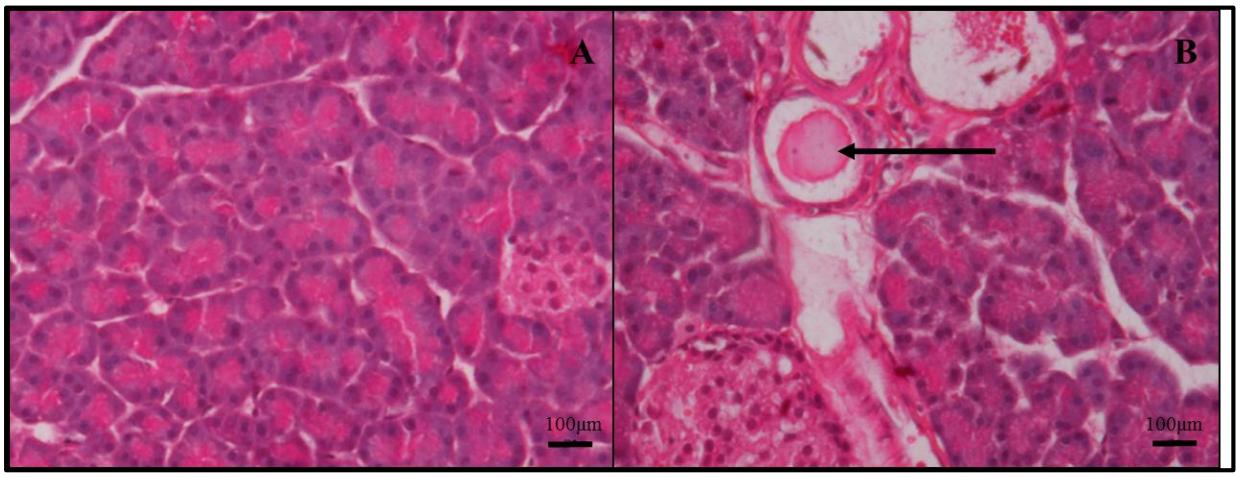

Figure 6.4 Pancreatic tissue with A) no pathology and B) a mildly dilated collecting duct containing eosinophilic proteinaceous material (indicated by the arrow). 200x magnification. Scale bar = 100µm

6.3. Kidney

With the use of haematoxylin and eosin stained kidney sections, the corpuscle, glomeruli, renal space, and arcuate arteries was measured and analysed.

6.3.1. Corpuscle and glomeruli analysis

The corpuscle area ($p>0.392$), corpuscle diameter ($p>0.377$) and corpuscle perimeter ($p>0.351$) showed no significant differences between the four groups (**Appendix L**), all results to follow relates to a trend seen based on the mean values. The glomeruli area ($p>0.371$), glomeruli diameter ($p>0.357$) and glomeruli perimeter ($p>0.494$) showed no significant differences between the four groups (**Appendix L**). No significant differences in renal space area ($p>0.437$) were seen between the four groups (**Appendix L**).

Stellenbosch University https://scholar.sun.ac.za

Table 3 Corpuscle - and glomeruli -area (µm²), -diameter (µm), -perimeter (µm) and renal space (µm²) between the four groups. Area is expressed as square micrometres (µm²) ± SEM. Corpuscle- and glomeruli -diameter and -perimeter are expressed as micrometres (µm) ± SEM.

	Groups			
	C/ART-	**C/ART+**	**HCD/ART-**	**HCD/ART+**
Glomerulus				
Area (µm²)	114436,94 ± 46206,22	121156,44 ± 46206,22	213390,12 ± 46206,22	117263,63 ± 46206,22
Diameter (µm)	372,33 ± 38,69	384,87 ± 38,69	459,22 ± 38,69	377,7 ± 38,69
Perimeter (µm)	1571,53 ± 186,52	1622,71 ± 186,52	1935,01 ± 186,52	1609,73 ± 186,52
Corpuscle				
Area (µm²)	161402,31 ± 72033,55	162217,97 ± 72033,55	307367,41 ± 72033,55	160724,65 ± 72033,55
Diameter (µm)	441,28 ± 49,21	445,85 ± 49,21	544,65 ± 49,21	442,7 ± 49,21
Perimeter (µm)	1536,85 ± 168,15	1557,45 ± 168,15	1901,69 ± 168,15	1541,81 ± 168,15
Renal Space	46965,37 ± 26150,0	41061,52 ± 26150,0	93977,29 ± 26150,0	43461,02 ± 26150,0

Stellenbosch University https://scholar.sun.ac.za

The corpuscle- and glomeruli -area, -diameter and -perimeter in the HCD/ART- group were larger compared to the other three groups, however the changes were not significant. The corpuscle- and glomeruli -area, -diameter and -perimeter between the C/ART-, C/ART+ and HCD/ART+ had similar sizes (**Table 3**). The renal space area in the HCD/ART- group was larger than the other three groups, however the changes were not significant. The renal space area between the C/ART-, C/ART+ and HCD/ART+ had similar areas (**Table 3**).

6.3.2. Arcuate artery analysis

The total lumen diameter ($p>0.417$), total tunica media thickness ($p>0.850$) and total tunica adventitia thickness ($p>0.735$) showed no significant differences between the four groups (**Appendix L**), all results to follow relates to a trend seen based on the mean values. The lumen diameter in the ART groups (C/ART+ and HCD/ART+) was marginally increased compared to the control (C/ART-) and the HCD/ART- groups (**Table 4**). The tunica media and adventitia layer thickness were increased in the ART groups (C/ART+ and HCD/ART+) compared to the control (C/ART-) and the HCD/ART- groups (**Table 4**).

Table 4 Lumen diameter, tunica media and tunica adventitia layer thickness of the arcuate arteries in the kidney between the four treatment groups. Diameter and thickness are expressed as micrometres (µm) ± SEM.

Arcuate artery lumen and layer thickness µm ± SEM			
Groups	**Lumen**	**Tunica Media**	**Tunica Adventitia**
C/ART-	460,87 ± 39,43	125,94 ± 15,25	138,96 ± 16,44
C/ART+	584,2 ± 53,27	174,9 ± 14,21	181,48 ± 16,86
HCD/ART-	474,01 ± 38,10	135,51 ± 23,47	138,18 ± 11,76
HCD/ART+	666,53 ± 72,73	179,98 ± 18,38	175,81 ± 20,42

6.3.3. Pathology

Pathology in haematoxylin and eosin stained each kidney section was graded accordingly; mild (I), moderate (II), severe (III), and expressed in percentages (%) of the total sample size (N=40) (**Table 23**, **Appendix L**).

Vacuolisation of proximal convoluted tubules were seen in all four groups, however no significant differences were seen between the four groups ($p>0.385$). Vacuolisation in all four

Stellenbosch University https://scholar.sun.ac.za

groups had mild to moderate grading, with mild vacuolisation seen in the majority of the samples (**Table 5**). Mild swelling of the proximal convoluted tubules were seen in the HCD/ART- (40%) and HCD/ART+ (10%) groups, indicating significant ($p<0.017$) proximal convoluted tubule swelling differences between the groups (**Table 5**).

Table 5 Kidney vacuolisation and swelling of proximal convoluted tubules and basophilic material pathology expressed in percentages (%) of each group groups.

	Kidney Pathology			
	C/ART-	**C/ART+**	**HCD/ART-**	**HCD/ART+**
Vacuolisation				
Absent	30%	20%	10%	50%
Mild	60%	70%	80%	30%
Moderate	10%	10%	10%	20%
Swelling				
Absent	100%	100%	60%	90%
Mild	0%	0%	40%	10%

6.3.4. Additional findings

When analysing the kidney sections for pathology, additional findings were seen, although these findings are not important for the current study, but are interesting to note. Basophilic material in tubular lumens were seen in 8/40 (20%) of kidney samples, which are found in normal functioning renal tubules (**Figure 6.5**). Three out of the eight samples were found in the C/ART- group, and another three were found in the HCD/ART- and one found in the C/ART+ and HCD/ART+ groups. One sample in the HCD/ART- group had a focus of neutrophilic infiltration.

Stellenbosch University https://scholar.sun.ac.za

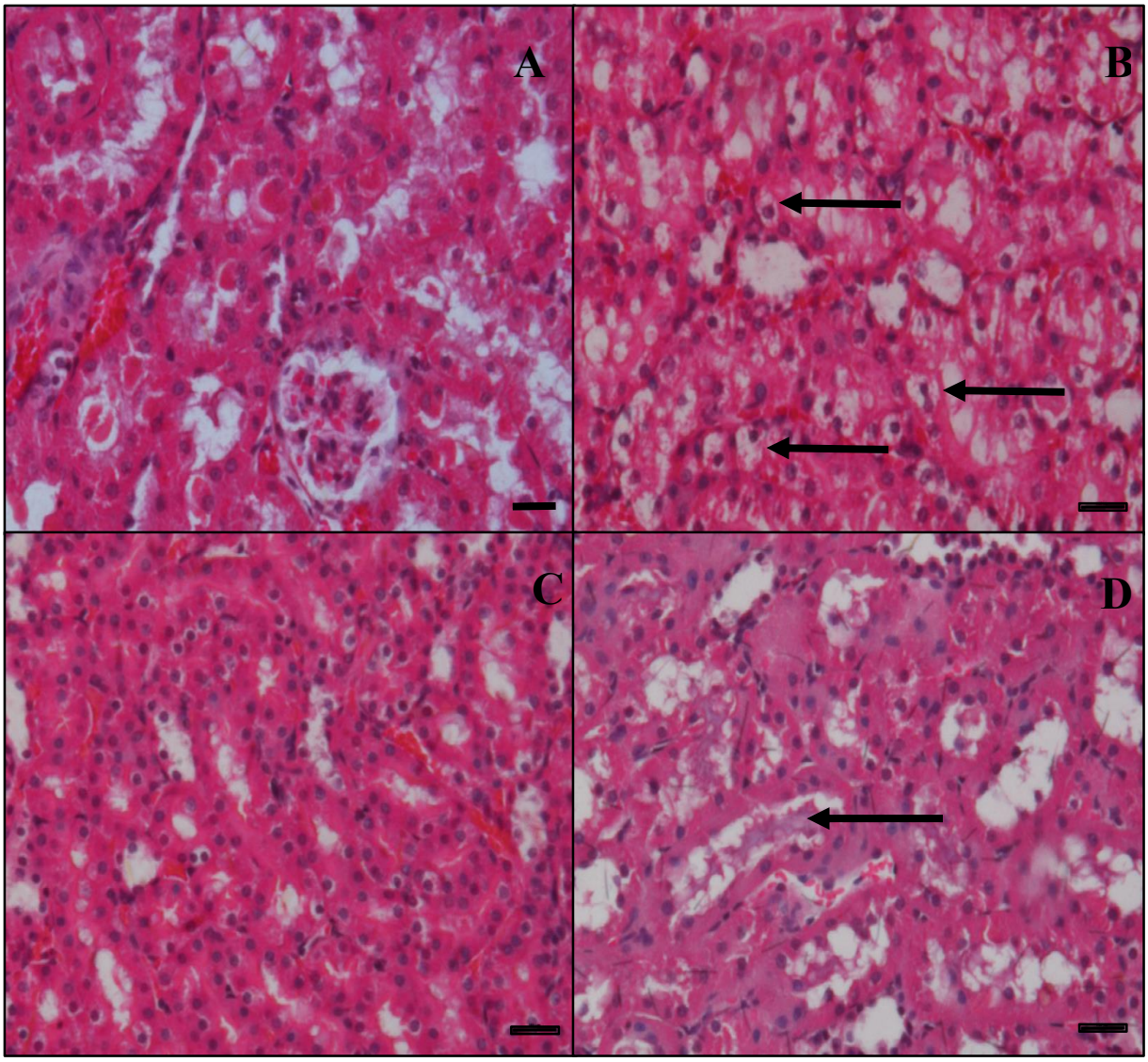

Figure 6.5 Kidney tissue indicating A) no pathology, B) mild vacuolisation (arrows) of the cytoplasm in the proximal convoluted tubular epithelial cells, C) swollen proximal convoluted tubules, and D) basophilic material (arrow) in the lumen of the proximal convoluted tubules. 200x magnification. Scale bar = 50µm

Stellenbosch University https://scholar.sun.ac.za

6.4. Liver

Haematoxylin and eosin stain was used to analyse pathology in the liver sections. Pathology present in each section was graded accordingly; absent (0), mild (I), moderate (II), severe (III), and expressed in percentages (%) of the total sample (N=40). Fatty change was graded as follows; 0-25% (I), 25-50% (II), 50-75% (III), 75-100% (IV) (**Appendix M**).

Mild to moderate granular appearances were seen in all four groups, however no significant ($p>0.445$) granular appearances were seen between the groups (**Figure 6.6**). The C/ART- group had 90% granular appearance, whereas the other three groups had granular appearances ranging from 50% - 80% (**Table 6**).

Vacuolisation of hepatocytes were seen in all four groups, significant vacuolisation ($p>0.5$) was observed between the four groups, however 44% vacuolisation was seen in the lean control (C/ART-) group (**Figure 6.6**). The HCD (HCD/ART- & HCD/ART+) group had 40% and 30% mild vacuolisation, respectively (Table7). Fatty change was seen in all four groups, with 20% (2/10) mild (0-25%) fatty change in the C/ART- and C/ART+ groups. The HCD (HCD/ART- & HCD/ART+) groups each had 10% (1/10) mild (0-25%) fatty change (**Table 6**).

Table 6 Liver hepatocyte vacuolisation and granular appearance in the cytoplasm pathology expressed in percentages (%) between groups.

	Liver Pathology			
	C/ART-	**C/ART+**	**HCD/ART-**	**HCD/ART+**
Granular appearance				
Absent	10%	50%	20%	30%
Mild	60%	40%	70%	60%
Moderate	30%	10%	10%	10%
Vacuolisation				
Absent	56%	100%	60%	70%
Mild	44%	0%	40%	30%
Fatty Change (micro- and macrovesicular)				
Absent	80%	80%	90%	90%
Mild (0-25%)	20%	20%	10%	10%

Stellenbosch University https://scholar.sun.ac.za

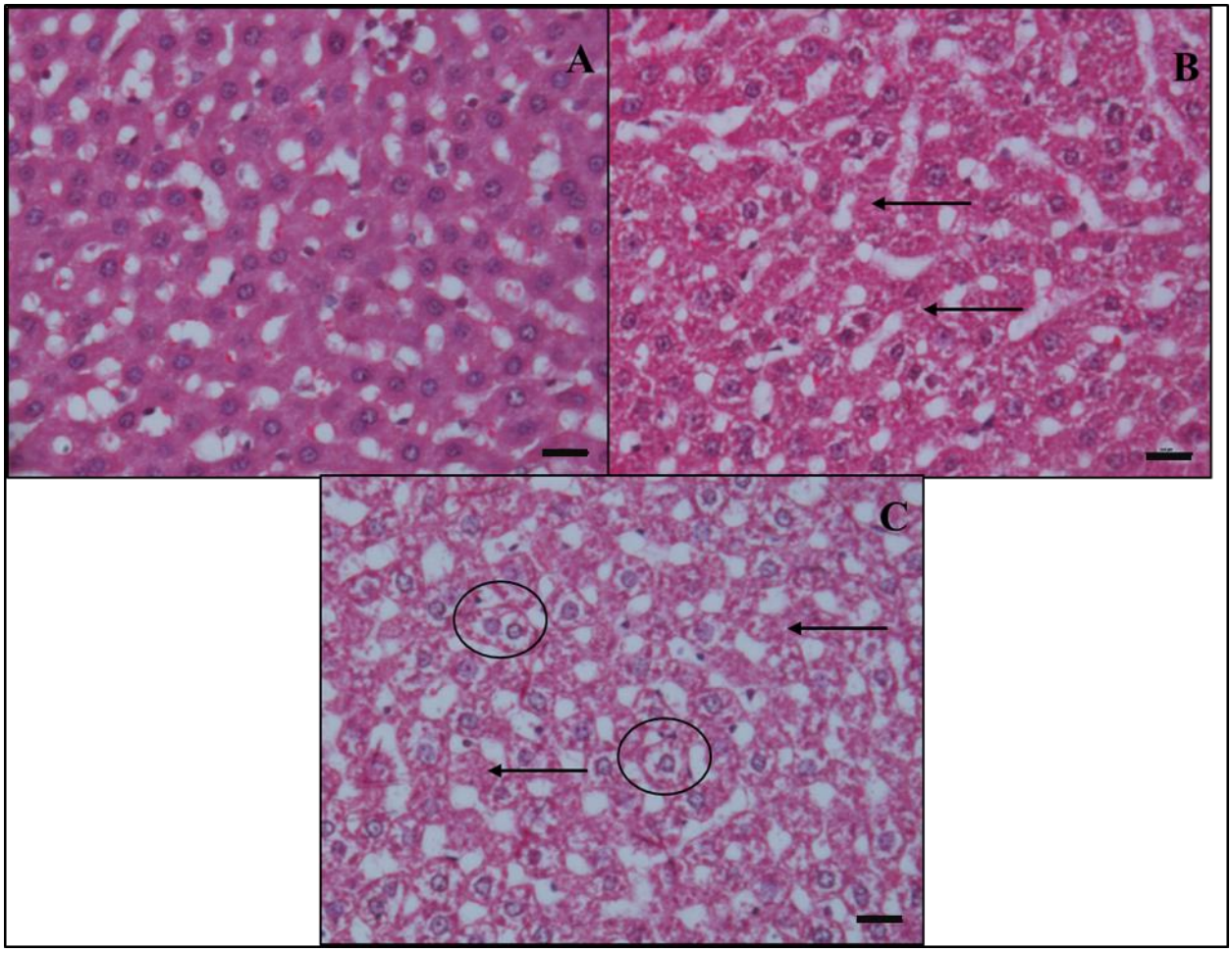

Figure 6.6 Liver tissue indicating A) no pathology, B) mild granularity (arrows) of the cytoplasm of hepatocytes, and C) moderate vacuolisation (circles) and granular appearance (arrows). 200x magnification. Scale bar = 100µm

6.5. Aortic PVAT leptin intensity

Both unilocular and differentiating adipocytes in group C/ART- were classified as level II, showing a leptin positive cytoplasmic rim (**Figure 5.5C & G**). Both unilocular adipocytes and differentiating adipocytes were classified as level III in the C/ART+ group showing an intense leptin positive cytoplasmic rim (**Figure 5.5D & H**). Unilocular adipocytes in the HCD/ART- group had a level II classification, indicating a leptin positive cytoplasmic rim (**Figure 5.5C**). The differentiating adipocytes had a level I classification, showing a weak leptin positive cytoplasmic rim (**Figure 5.5F**). In the HCD/ART+ group the unilocular adipocytes had a classification of level I, showing a weak leptin positive cytoplasmic rim (**Figure 5.5B**). The differentiating adipocytes in this group was classified as level 0, indicative of leptin negative staining (**Figure 5.5E**).

Stellenbosch University https://scholar.sun.ac.za

Table 7 Leptin staining intensity of differentiating and unilocular adipocytes in the aortic PVAT between groups.

	Aortic PVAT adipocyte Leptin intensity level	
Groups	**Differentiating adipocytes**	**Unilocular adipocytes**
C/ART-	II	II
C/ART+	III	III
HF/ART-	I	II
HF/ART+	0	I

Stellenbosch University https://scholar.sun.ac.za

7. DISCUSSION

Both obesity and antiretroviral treatment (ART) have been associated with diseases such as hypertension, lipodystrophy, metabolic syndrome and type 2 diabetes (Sutinen & Yki-Järvinen 2007; Shah, Alio, *et al*. 2012). Antiretroviral treatment has been associated with lipodystrophy, either in the form of fat loss, known as lipoatrophy, or by fat accumulation, known as lipohypertrophy (Parakh *et al*. 2009). A study by Ogunmola *et al*. (2014) indicated that the body mass index (BMI) and obesity had no significant changes between HIV-positive individuals receiving no antiretroviral treatment and HIV-positive individuals receiving ART. The diet used to induce obesity in the present study was a high-calorie diet, which is commonly a risk factor for type 2 diabetes (Everitt *et al*. 2006). The present study showed no significant increase in body mass in the high-calorie diet (HCD/ART-) group compared to the lean control (C/ART-) group, suggested that a 16 week high-calorie diet on its own had no significant effect on body mass. However, a significant increase (10%) in the high-calorie diet drug treated group (HCD/ART+) compared to the lean control group suggested that oxidative stress played a role in the increase of body weight in this group. Obesity caused by oxidative stress stimulates white adipose tissue changes, causing adipocyte differentiation and increased size, whereas obesity inducing oxidative stress has contributing factors, such as chronic inflammation, tissue dysfunction and hyperleptinemia (increased circulating leptin hormone) (Savini *et al*. 2013). A study on body mass and the leptin hormone in HIV-infected patients by Nagy *et al*. (2003) reported that individuals showing signs of lipohypertrophy had high circulating leptin levels (hyperleptinemia), whereas individuals with signs of lipoatrophy had lower leptin levels (hypoleptinemia).

Perivascular adipose tissue (PVAT) is metabolically active by secreting various adipocytokines, such as leptin which is important in regulating appetite (Szasz *et al*. 2013; Mandal 2014). Antiretroviral treatment causes adipose tissue changes, which in turn may cause leptin expression alterations (Jan *et al*. 2004; Lagathu *et al*. 2004). Perivascular adipose tissue in lean animals contributes to the regulation of vascular homeostasis; however, in obesity, PVAT secretes increased amounts of pro-inflammatory adipocytokines such as leptin accompanied by decreased expression of anti-inflammatory adipocytokines, such as adiponectin (Lehman *et al*. 2010; Raucci *et al*. 2013).

Stellenbosch University https://scholar.sun.ac.za

Increased calorie intake causes adipose tissue mass to increase which alters adipocytokine secretion from adipocytes in adipose tissue (Halberg *et al*. 2009; Weisberg *et al*. 2003). Increased leptin levels have been associated with elevated blood pressure suggesting that leptin play a role in obesity-related hypertension (Bravo *et al*. 2006; Martin *et al*. 2008). Previous studies have suggested that the leptin (*ob*) gene is only expressed in mature white adipocytes (Masuzaki *et al*. 1995), whereas other researchers have suggested that the leptin (*ob*) gene is expressed in both brown adipose tissue (BAT) and white adipose tissue (WAT) (Moinat *et al*. 1995). Cinti *et al*. (1997) reported that leptin expression was detected in adipocytes at the multilocular stage of differentiation, suggesting that leptin is expressed by all lipid containing adipocytes within white adipose tissue depots. Therefore, the present study, using an immunohistochemical labelling technique, focused specifically on unilocular adipocytes found in the WAT clusters of the aortic PVAT and the differentiating adipocytes found near or within these WAT clusters. Results show that ART alone was associated with a more intense leptin expression in unilocular adipocytes compared to the other experimental groups, whereas the untreated groups (C/ART- and HCD/ART-) showed a more positive leptin expression compared to the weak leptin expression in the high-calorie diet combined with ART (HCD/ART+) group. The difference in leptin expression between the ART group and a high-calorie diet combined with ART may be due to leptin deficiency in the adipocytes in the latter as leptin deficiency can be caused by either a lack of leptin secreting adipocytes (Oral & Simha 2002) or by the mutation of the leptin (*ob*) gene, which is seen in severe obesity (Farooqi *et al*. 2002). Additional results on the size of the adipocytes in the aortic PVAT indicated that the HCD/ART- and HCD/ART+ groups had smaller unilocular adipocytes compared to the lean control group, suggesting that the weak to no leptin intensity may possibly be due to the lack of leptin secreting adipocytes. Further analysis on the number of adipocytes and leptin gene expression in the aortic PVAT would provide sufficient results on the effect of this cART (FTC, TDF and EFV) and HCD used in the present study.

The differentiating adipocytes in the C/ART+ group were seen to have a more intense leptin expression compared to the other three experimental groups. These observations suggests that ART on its own may cause hyperleptinemia (Nagy *et al*. 2003), which in turn may lead to leptin resistance (Knight *et al*. 2010). Leptin resistance is associated with hyperinsulinemia, insulin resistance and diabetes, causing decreased insulin secretion in the pancreatic beta (β)-cells. Therefore, a link is established between obesity and diabetes (Martin *et al*. 2008).

Stellenbosch University https://scholar.sun.ac.za

Pancreatic islets maintain blood glucose homeostasis with the secretion of peptide hormones such as insulin from beta (β)-cells and glucagon from alpha (α)-cells (Matschinsky & Ellerman 1967). A study on morpometric analysis of the pancreatic islets in obese mice by Slavin *et al*. (2010) showed that islet number and insulin secreteion increased with obesity. Pancreatic toxicity is a side effect of ART which may lead to pancreatitis (Neuman *et al*. 2012). In a study done on mice by Oliveira *et al.* (2014) the pancreatic islet morphology (characterised as round to oval shape, surrounded by a very thin capsule of reticular fibres) in mice on a high-fat diet showed no significant changes compared to the control mice fed a regular chow diet. Pancreatic islets in the present study had no irregular shaped islets, suggesting that the cART and the HCD used in the present study had no effect on the shape of pancreatic islets. The present study showed no significant differences in total pancreatic islet area between the lean control group and the ART and HCD groups, suggesting the cART and a high-calorie diet used in the study caused no significant increase in total pancreatic islet area. However, the high-fat diet group in the study by Oliveira *et al*. (2014) showed a significant increase in islet and β-cell mass, and increase in the number of islets per section. The diet used for the HCD groups in the present study had lower percentages fat, carbohydrates and protein values compared to the high-fat diet used by Oliveira *et al*. (2014). The different nutritional values of the HCD used in the present study could possibly be the cause for the lack in significant changes seen in islet area and number. Results by Slavin *et al*. (2010) on the morphological analysis of pancreatic islets in obese mice indicates that obese mice had increased numbers of islets and increased islet sizes compared to lean mice. A study by Barbosa *et al*. (2013) indicated that HIV infected patients receiving ART had increased number of islets compared to HIV infected patients that did not receive ART. Based on a trend in the present study, the total islet area and number of islets in the present study were increased in the high-calorie diet untreated group compared to the lean control group. This suggests that potentially a longer administration of the high-calorie diet and ART would lead to significant increases in islet size and number of islets, therefore have similar characteristics to obesity in rats seen in previous studies.

With type-2 diabetes mellitus (T2DM), beta (β-) cells remain unchanged, however the cells fail to produce suffucient insulin to maintain normal blood glucose levels. A trend, based on the average values, indicated that insulin secreting β-cells in the ART and HCD groups (C/ART+, HCD/ART- & HCD/ART+) were smaller in area compared to the lean control (C/ART-) group. This suggested that longer exposure to ART in combination with a high-calorie diet could lead to decreased insulin secreting β-cells, leading to decreased insulin secretion which are

Stellenbosch University https://scholar.sun.ac.za

associated with T2DM, and is one of the metabloic disorders asssociated with obesity (Adeyemi *et al*. 2010). In addition to impaired β-cells production with T2DM, glucagon secreted from alpha (α-) cells are also disrupted, with and increase in glucagon secreting cells (Brereton *et al*. 2014). However, based on the average glucagon secreting α-cell area, the high-calorie diet untreated group (HCD/ART-) and ART group (C/ART+) were larger in area compared to the lean control (C/ART-). The increase in glucagon secreting α-cells in the present study correlated with findings by Brereton *et al*. (2014), which indicated a decrease in insulin staining cells and an increase in glucagon staining cells with the onset of chronic hyperglycaemia which is associated with T2DM (Brereton *et al*. 2014). The increased glucagon secreting α-cells in the present study could have more significance with longer treatment and additional blood glucose measurments to confirm hyperglycaemia. In the study by Slavin *et al*. (2010) a decrease in glucagon stained cells in obese mice were noted compared to the lean mice. The insulin stained cells in the same study were increased in the obese mice compared to the lean mice, suggesting β-cell hyperplasia, which could be due to pancreatic homeodomain protein PDX-1 or islet neogenesis associated protein or mitogenic growth factor (Slavin *et al*. 2010).

In the exocrine pancreas, pathological changes in HIV-infected patients before the use of ART included intense acinar or parenchymal atrophy and decreased zymogen granules (Barbosa *et al*., 2013). Whereas in the endocrine pancreas, alterations seen in HIV-infected patients receiving ART has led to hypotheses that the endocrine portion of the pancreas is affected by combination ART (cART) (Dragovic, 2013). In a study by Barbosa *et al*. (2013), the exocrine pancreas showed that decreased dysplasia like alterations, increased pancreatic atrophy, increased apoptosis and parenchymal steatosis maintenance were more evident in HAART group. Another study by Manfredi & Calza (2008) showed that nucleoside reverse transcriptase inhibitor (NRTI) drugs causes an increase in serum pancreatic enzymes, which leads to acute pancreatitis. In the present study no pathology was present in any of the groups studied, suggesting that the six week cART (of FTC, TDF and EFV) and a 16-week HCD caused no pathological changes. The lack of pathology in the ART and HCD groups could be due to the short-term of ART and high-calorie diet or the combination ART used in the study. Several human studies on indicate pancreatic toxicity in individuals diagnosed with HIV and receiving ART, therefore it could be suggested that the HIV combined with ART may possibly cause the severe pancreatic toxicity (Elfane *et al*. 2016; Dragovic 2013).

Stellenbosch University https://scholar.sun.ac.za

Long term exposure to ART is associated with significant renal toxicity which causes kidney injury (Jao & Wyatt 2016). A study done by Fabian *et al*. (2013) showed mild glomerular enlargement within seven months of ART in humans, while morbidly obese patients showed an increase in glomeruli size (Goumenos *et al*., 2009) . The renal corpuscle- and glomeruli -area (μm²), -diameter (μm) and -perimeter (μm) in the present study had no significant differences between the lean control, ART and HCD groups. However, the ART (C/ART+) had smaller renal corpuscle- and glomeruli -area, -diameter and -perimeter compared to the lean control group, suggesting that the cART (of FTC, TDF and EFV) used in the present study will have decreased glomerular filtration rate, possibly due to the Tenofovir which effects the tubular function therefore causes decreased glomerular filtration rate (Post *et al*. 2010). The renal space area (μm²) also had no significant differences between the lean control, ART and HCD groups, however based on the average values the ART group was smaller compared to the lean control group, suggesting that the glomeruli shrunk. This suggested that a six week administration of the specific cART (of FTC, TDF and EFV) used in the present study had no significant histological effect on the renal corpuscle, the glomeruli and renal space.

Antiretroviral therapy has been implicated in atherogenesis (adhesion of monocytes and lymphocytes to the endothelial cell surface) in blood vessels (Grinspoon & Carr 2005), which in turn leads to arterial stiffness, migration of vascular smooth muscle cells from the tunica media to the tunica intima and therefore increased blood pressure and hypertension (Eira *et al*. 2012; Lo and Plutzky, 2012). Arteries undergo hypertrophic remodelling with hypertension, causing the arterial wall to thicken (Jacobsen & Holstein-Rathlou, 2010). In obese individuals, adipose tissue encapsulates the kidneys, which penetrates the medulla causing compression, increased arterial pressures and renal-pressure natriuresis, which could explain the relationship between abdominal obesity and hypertension (Hall 2003). Changes occurring in the kidney due to obesity may cause compensatory mechanisms which leads to increased glomerular wall tension and glomerular hypertrophy. These glomerular changes reduces the filtration surface area which leads to increased blood pressure (Hall *et al.* 2014). The present study showed no significant differences in the arcuate artery lumen diameter, tunica media thickness and tunica adventitia thickness. However, the ART groups (C/ART+ and HCD/ART+) showed larger lumen diameter, thicker tunica media and adventitia compared to the lean control and high-calorie diet untreated group. Although not significant, the trend seen of increased tunica media

Stellenbosch University https://scholar.sun.ac.za

and adventitia suggests that the cART used in the study could initiate hypertrophic remodelling in the arcuate arteries.

Nephrotoxicity has been seen with specific antiretroviral agents (Jao & Wyatt 2016). High doses of Tenofovir (TDF) had pathological effects such as renal failure and/or tubular dysfunction (Karras *et al*. 2003). Emtricitabine (FTC) caused no nephrotoxicity, whereas Efavirenz caused minimal acute renal failure (decline in renal filtration function) (Jao & Wyatt 2016). In the present study mild to moderate vacuolisation of the proximal convoluted tubules were present in all four groups, with the highest percentage (90%) in the high-calorie diet untreated group. Swelling of the proximal convoluted tubules were only present in the HCD groups (HCD/ART- and HCD/ART+), with 40% swelling in the high-calorie diet untreated group. The vacuolisation and swelling of the proximal convoluted tubules lesions were very mild and interpretation was thus difficult, and could be due to possible fixation problems. However, lesions associated with vacuolisation and swelling may arise due to the variety of causes involving hypoxia or disruption of ATP production, mitochondrial injury, free radical formation, peroxidation, or perturbed cell signalling (Schiffer & Friederich-Persson 2017). These conditions mentioned associated with vacuolisation and swelling often affects the proximal convoluted tubules first (Schiffer & Friederich-Persson 2017). Vacuolisation may precede degeneration and necrosis and it is a very non-specific lesion that may also occur in normal animals (Padanilam 2003).

The most common liver diseases with the onset of obesity and ART include; chronic hepatitis, liver steatosis and the development of liver cirrhosis (Yamauchi & Michitaka 1998; Neuman *et al*. 2012). In the present study, granular appearance in the hepatocytes of the liver were present in all groups, with the lean control group having the highest percentage (90%) of mild to moderate granular appearance. Mild to moderate granular appearance is indicative of active cytoplasmic organelles such as the mitochondria, smooth endoplasmic reticulum or peroxisomes. Granular appearance is not usually considered as a distinct pathological lesion, however together with other degenerative lesions such as vacuolar changes, it could indicate mild cell damage/induction (Lemasters & Nieminen 1997). Mild vacuolisation was present in the lean control and HCD (HCD/ART- and HCD/ART+) groups, these changes might be due to fluid or glycogen accumulation in the cytoplasm (Odze & Goldblum 2009). As granular

Stellenbosch University https://scholar.sun.ac.za

appearance and vacuolisation were mostly present in the lean control group (C/ART-), it indicated possible tissue fixation problems in the present study.

The liver plays an important role in lipid metabolism, it is therefore possible that lipids may accumulate in the liver, specifically in hepatocytes, when there is an imbalance between the fat delivery into and out of the liver (Goodman 2016). In conditions such as metabolic imbalances, stress, and cellular injury; lipid droplets increase in size in the cytoplasm of the hepatocytes (Goodman 2016). Hepatic steatosis are signs of severe toxicity in long-term antiretroviral therapy (Brinkman *et al*. 1998). However, in the present study the hepatocytes had mild microvesicular (small intracytoplasmic fat vacuoles, accumulating in the cell) (0-25%) in all the groups, with 20% (2/10) in the lean control and ART groups and 10% (1/10) in the HCD (HCD/ART- and HCD/ART+) groups. Although Nucleoside reverse transcriptase inhibitors (NRTIs) is associated with hepatic steatosis (Grinspoon & Carr 2005), the NRTIs and NNRTIs used in the present study caused no severe hepatic steatosis. The microvesicular changes may possibly be hepatocellular vacuolar changes which may be of metabolic or toxic origin. The liver stores triglycerides and fatty acids in a response to feeding and fasting, where dietary fatty acids are absorbed from the small intestines. Therefore, the microvesicular accumulation in the two lean control animals may possibly be due to metabolic origins (Kawano & Cohen 2013). The ART interferes with the mitochondrial metabolism, which may cause accumulation of lipid droplets in the liver, because of the fatty acids that are being oxidized. Therefore, the observation of hepatic steatosis in patients receiving ARTs, can be a sign of early mitochondrial dysfunction (Cornejo-juárez *et al*. 2003). However, the mild microvesicular changes seen in the present study in all groups are still reversible and it is thus suggested that the six week cART and the 16-week high-calorie diet used in the study caused no severe macrovesicular changes or hepatic steatosis.

Stellenbosch University https://scholar.sun.ac.za

8. CONCLUSION

The results in the present study had very little to no significant differences between the lean control, ART and HCD groups. Emtricitabine undergoes limited metabolism and is excreted by the kidneys, whereas Tenofovir is eliminated by the glomerular filtration and active tubular secretion. Both Emtricitabine (200mg) and Tenofovir (300mg) are eliminated at half-life (15.5 and 17.6 hours, respectively) in healthy human individuals. When both of these drugs were co-administered with other antiretroviral drugs such as Stavudine, Zidovudine, Abacavir, Adefovir Dipivoxil, Efavirenz, Indinavir, Lamivudine, Lopinavir/Ritonavir, no interactions between the drug were observed (Dando & Wagstaff 2004). This suggests that the specific cART used (FTC, TDF, and EFV) for six a week period caused no significant morphometric changes within the pancreas, kidney, liver, apart from the intense leptin stain in the ART positive group.

The diet used for the HCD groups in the present study had lower percentages fat, carbohydrates and protein values compared to the high-fat diet used by Oliveira *et al*. (2014) and Murphy (2013). This difference in nutritional values could be a possible cause for the lack of significant changes seen in islet area and number. In the present study, the high-calorie diet alone and combined with the cART had only minor histological observational changes, although not significant compared to the lean control group. Further studies on the effects of this specific cART should be conducted with several administration periods, due to possible regeneration of the kidney on a longer period as seen by Fabian *et al*. (2013). These time periods in combination with a HCD could possibly lead to histomorphometric changes in various organs. As cART continue to develop, physicians treating HIV infected patients should remain aware of new and developing syndromes associated with the use of ART.

Stellenbosch University https://scholar.sun.ac.za

9. LIMITATIONS

The harvesting time had a possible influence on the autolysis. Multiple researcher were collecting samples from the same animals, therefore waiting periods influenced the harvesting of tissue samples. Harvesting of the organs occurred as quickly as practically possible after the heart of the animal was removed. The organs were then immediately fixed in 4% PFA. Although the organs were harvested as quickly as possible, autolysis still occurred, as seen in some control animals showing pathology relating to autolysis. Formaldehyde products such as 4% PFA is effective in preserving tissue for histological examination (Hassel & Hand 1974).

Fixation problems occurs when conditions were not optimal, which can permanently damage the tissue. The fixative used can influence the degree to which particles within the tissue will stain (Boenisch *et al*. 2001). With formaldehyde solutions, formic acid forms to produce an acidic solution. This acidic solution reacts with haemoglobin which produces an artefact pigment. With formaldehyde fixation the hydrophobicity is increased in the tissue, which leads to increased general background staining (Boenisch *et al*. 2001). Tissues that are prone to increased hydrophobicity include; connective tissue, squamous epithelium and adipocytes (Boenisch *et al*. 2001), this is a possible reason for the intense background staining in the PVAT tissue samples with the leptin antibody. Other reasons for background staining is due to the attachment of the primary antibody to highly charged groups in the connective tissue. Whereas non-specific positive staining is the cause of the primary antibody attaching to the connective tissue. This can be prevented with an innocuous protein solution (bovine serum albumin), which is applied before the primary antibody is applied.

Stellenbosch University https://scholar.sun.ac.za

REFERENCES

Achike, F.I. et al., 2011. Obesity, Metabolic syndrome, adipocytes and vascular function: A holistic viewpoint. *Journal of Clinical Investigation*, 101(5), pp.2273–2282. Available at: http://dx.doi.org/10.1038/hr.2010.11.

Adeyemi, D.O. et al., 2010. Histomorphological and morphometric studies of the pancreatic islet cells of diabetic rats treated with extracts of Annona muricata. *Folia Morphologica*, 69(2), pp.92–100.

Adler, G. et al., 1987. Effect of pancreatic atrophy and hypertrophy small intestine. *Gut*, (Table 1), pp.193–195.

Adler, M. & Schaffner, F., 1979. Fatty liver hepatitis and cirrhosis in obese patients. *American journal of medicine*, 67, pp.811–816.

Akiyoshi, H. & Inoue, A.M., 2012. Comparative histological study of hepatic architecture in the three orders amphibian livers. *Comparative Hepatology*, 11(2), pp.1–8. Available at: Comparative Hepatology.

Amorosa, V. et al., 2005. A Tale of 2 Epidemics The Intersection Between Obesity and HIV Infection in Philadelphia. *Clinical Science*, 39(5), pp.557–561.

Anon, 2017. *UNAIDS Data 2017*, Geneva. Available at: http://www.unaids.org/sites/default/files/media_asset/20170720_Data_book_2017_en.pdf.

Arita, Y. et al., 1999. Paradoxical decrease of an adipose-specific protein, Adiponectin, in obesity. *Biochemical and Biophysical Research Communications*, (257), pp.79–83. Available at: http://www.idealibrary.com.

Arts, E.J. et al., 2012. HIV-1 Antiretroviral Drug Therapy. *Cold Spring Harb Perspect tives in Medicine*, 2, pp.1–23.

Balistreri, C.R., Caruso, C. & Candore, G., 2010. The Role of Adipose Tissue and Adipokines in Obesity-Related Inflammatory Diseases. *Mediators of Inflammation*, 2010, p.19.

Barbosa, A.G. et al., 2013. AIDS and the pancreas in the HAART era : a cross sectional study. *International Archives of Medicine*, 6, p.28. Available at: http://www.intarchmed.com/content/6/1/28.

Boenisch, T. et al., 2001. *Immunochemical staining method* 3rd ed., California: DAKO Corporation.

Bosco, D. et al., 2010. Unique Arrangement of Alpha - and Beta -Cells in Human Islets of Langerhans. *Biabetes*, 59(May), pp.1202–1210.

Bravo, P.E. et al., 2006. Leptin and Hypertension in Obesity. *Vascular health and risk management*, 2(2), pp.163–169.

Brereton, M.F. et al., 2014. Reversible changes in pancreatic islet structure and function produced by elevated blood glucose. *Nature communications*, 5, p.4639. Available at: http://www.nature.com/ncomms/2014/140822/ncomms5639/full/ncomms5639.html.

Stellenbosch University https://scholar.sun.ac.za

Brinkman, K. et al., 1998. Adverse effects of reverse transcriptase inhibitors: mitochondrial toxicity as common pathway. *AIDS, London*, 12(14), pp.1735–1744. Available at: http://www.ncbi.nlm.nih.gov/pubmed/9792373.

Bryan, S. et al., 2013. Redox-inflammatory synergy in the metabolic syndrome. *Canadian journal of physiology and pharmacology*, 91, pp.22–30.

Cancello, R. et al., 1998. Leptin and UCP1 genes are reciprocally regulated in brown adipose tissue. *Endocrinology*, 139(11), pp.4747–4750.

Cannon, B. & Nedergaard, J.A.N., 2004. Brown Adipose Tissue : Function and Physiological Significance. *Physiology Review*, 84, pp.277–359. Available at: www.prv.prg.

Cappell, M., 1997. The pancreas in AIDS. *Gastroenterology clinical North America*, 26, pp.337–365.

Carr, A. et al., 2000. A syndrome of lipoatrophy, lactic acidaemia and liver dysfunction associated with HIV nucleoside analogue therapy: contribution to protease inhibitor-related lipodystrophy syndrome. *Aids*, 14(3), pp.F25–F32.

Cinti, S. et al., 1997. Immunohistochemical Localization of Leptin and Uncoupling Protein in White and Brown Adipose Tissue *. *Endocrinology*, 138(2), pp.797–804.

Cinti, S., 1999. The Adipose Organ. In *Nutrition and Health: Adipose Tissue and Adipokines in Health and Disease*. pp. 3–19.

Cinti, S., 2009. Transdifferentiation properties of adipocytes in the adipose organ. *American journal of physiology. Endocrinology and metabolism*, 297, pp.977–986. Available at: http://www.ajpendo.org.

Cornejo-juárez, P., Sierra-madero, J. & Volkow-fernández, P., 2003. Metabolic Acidosis and Hepatic Steatosis in Two HIV-Infected Patients on Stavudine (d4T) Treatment. *Archives of Medical Research*, 34, pp.64–69.

Cousin, B. et al., 1992. Occurrence of brown adipocytes in rat white adipose tissue : molecular and morphological characterization. *Journal of Cell Science*, 103, pp.931–942.

Crum-cianflone, N. et al., 2008. Obesity among HIV Patients : The Latest Epidemic. *AIDS Patient Care STDS*, 22(12), pp.925–930.

Dando, T.M. & Wagstaff, A.J., 2004. Emtricitabine / Tenofovir Disoproxil Fumarate. *Drugs*, 64(18), pp.2075–2082.

Day, C.., 2002. Pathogenesis of steatohepatitis. *Best Practice and Research clinical Gastroenterology*, 16, pp.663–678.

Dolensek, J., Rupnik, M.S. & Stozer, A., 2015. Structural similarities and differences between the human and the mouse pancreas. *Islets*, 7(1), pp.2–9.

Donath, M.Y. et al., 1999. Hyperglycemia- induced beta-cell apoptosis in pancreatic islets of Psammomys obesus during development of diabetes. *Diabetes*, 48, pp.738–744.

Donath, M.Y. et al., 2013. Inflammation in obesity and diabetes: Islet dysfunction and therapeutic opportunity. *Cell Metabolism*, 17(6), pp.860–872.

Dragovic, G., 2013. A cute pancreatitis in HIV / AIDS patients : an issue of concern. *Asian*

Stellenbosch University https://scholar.sun.ac.za

pacific journal of tropical biomedicine, 3(6), pp.422–425.

Eira, M. et al., 2012. Potent Antiretroviral Therapy for Human Immunodeficiency Virus Infection Increases Aortic Stiffness. *Arquivos Brasileiros de Cardiologia*, 99(6), pp.1100–1107.

Elfane, M. et al., 2016. AIDS & Clinical Research Acute Pancreatitis in Patients Living with HIV. *Journal of AIDS and Clinical Research*, 7(8), pp.8–11.

Everitt, A. V et al., 2006. Dietary approaches that delay age-related diseases. *Clinical interventions in aging*, 1, pp.11–31.

Fabian, J. et al., 2013. The clinical and histological response of HIV-associated kidney disease to antiretroviral therapy in South Africans. *Nephrology dialysis transplant*, 28(February), pp.1543–1554.

Fain, J.N. et al., 2015. Comparison of the Release of Adipokines by Adipose Tissue , Adipose Tissue Matrix , and Adipocytes from Visceral and Subcutaneous Abdominal Adipose Tissues of Obese Humans. *Endocrinology*, 145(5), pp.2273–2282.

Farooqi, I.S. et al., 2002. Beneficial effects of leptin on obesity , T cell hyporesponsiveness , and neuroendocrine / metabolic dysfunction of human congenital leptin deficiency. *Journal of Clinical Investigation*, 110(8), pp.1093–1103.

Ferreira, F.M. et al., 2015. HIV and Pancreas : Endocrinological Patterns of Pancreatic Morphology. *Journal of the Pancreas*, 16(4), pp.369–372.

Frampton, J.E. & Croom, K.F., 2006. Efavirenz / Emtricitabine / Tenofovir. *Drugs*, 66(11), pp.1501–1512.

Giovannucci, E. & Michaud, D., 2007. The Role of Obesity and Related Metabolic Disturbances in Cancers of the Colon, Prostate, and Pancreas. *Gastroenterology*, 132, pp.2208–2225.

Goodman, Z.D., 2016. The Impact of Obesity on Liver Histology. *Clinical liver disease*, 18(2014), pp.33–40.

Goumenos, D.S. et al., 2009. Early histological changes in the kidney of people with morbid obesity. *Nephrology dialysis transplant*, 24(July), pp.3732–3738.

Grinspoon, S. & Carr, A., 2005. Cardiovascular Risk and Body-Fat Abnormalities in HIV-Infected Adults. *The New England Journal of Medicine*, (352), pp.48–62.

Guzik, T.J., Mangalat, D. & Korbut, R., 2006. Adipocytokines - Novel link between inflammation and vascular function? *Journal of Physiology and Pharmacology*, 57, pp.505–528.

Halberg, N., Wernsted, I. & Scherer, P., 2009. The adipocyte as an endcrine cell. *Endocrinology And Metabolism Clinic North Americamerica*, 37(3), pp.1–15.

Hall, J.E., 2003. The kidney, hypertension, and obesity. *Hypertension*, 41, pp.625–633.

Hall, M.E. et al., 2014. Obesity, hypertension, and chronic kidney disease. *International Journal of Nephrology and Renovascular Disease*, 7, pp.75–88.

Haschek, W.M., Wallig, Matthew, A. & Rousseaux, 2010. *Fundamentals of toxicologic pathology* 2nd, ed., Elsevier.

Stellenbosch University https://scholar.sun.ac.za

Hassel, J. & Hand, A.R., 1974. Tissue fixation with diimidoesters as an alternative to aldehydes. II. Cytochemical and biochemical studies of rat liver fixed with dimethylsuberimidate. *Journal of Histochemistry & Cytochemistry*, 22, pp.229–239.

Hawkins, T., 2010. Understanding and managing the adverse effects of antiretroviral therapy. *Antiviral Research*, 85, pp.201–209.

Hellman, B., 1959. Actual distribution of the number and volume of the islets of Langerhans in different size classes in non-diabetic humans of varying ages. *Nature*, 184, pp.1498–1499.

Hostetter, T.H., Troy, J.L. & Brenner, B.M., 1981. Glomerular hemodynamic in experimental diabetes mellitus. *Kidney International*, 19, pp.410–415.

Intengan, H.D. & Schiffrin, E.L., 1993. Vascular remodeling in hypertension. *Scanning microscopy*, 7, p.137–142; discussion 143.

Jacobsen, J. & Holstein-Rathlou, N., 2010. The role of eutrophic remodeling in the hypertensive reduction of vascular reserve. *Acta Physiologica*, 198, p.Supplement 677 :P-MON-32.

Jain, R.G. et al., 2001. Metabolic complications associated with antiretroviral therapy. *Antiviral Research*, 51, pp.151–177.

Jan, V. et al., 2004. Altered fat differentiation and adipocytokine expression are inter-related and linked to morphological changes and insulin resistance in HIV-1-infected lipodystrophic patients. *Antiviral Therapy*, 9, pp.555–564.

Jao, J. & Wyatt, C.M., 2016. Antiretroviral Medications : Adverse Effects on the Kidney. *Advances in Chronic Kidney Disease*, 17(1), pp.72–82. Available at: http://dx.doi.org/10.1053/j.ackd.2009.07.009.

John, M., Nolan, D. & Mallal, S., 1998. Antiretroviral therapy and the lipodystrophy syndrome. *Antiviral Therapy*, 6, pp.9–20.

Karalis, K.. et al., 2009. Mechanisms of obesity and related pathology: linking immune responses to metabolic stress. *Federation of European Biochemical Societies*, 276(20), pp.5747–5754.

Karras, A. et al., 2003. Tenofovir-related nephrotoxicity in human immunodeficiency virus-infected patients: three cases of renal failure, Fanconi syndrome, and nephrogenic diabetes insipidus. *Clinical infectious diseases : an official publication of the Infectious Diseases Society of America*, 36, pp.1070–1073.

Kasiske, B.L. & Napier, J., 1985. Glomerular sclerosis in patients with massive obesity. *American journal of nephrology*, 5(1), pp.45–50. Available at: https://www.ncbi.nlm.nih.gov/pubmed/3970078.

Kawano, Y. & Cohen, D.E., 2013. Mechanisms of hepatic triglyceride accumulation in non-alcoholic fatty liver disease. *Journal of Gastroenterology*, 48(4), pp.434–441.

Kierszenbaum, A.., 2007. *Histology and Cell Biology An Introduction to Pathology* 2nd ed., Philadelphia: Mosby Elsevier.

Knight, Z.. et al., 2010. Hyperleptinemia is required for the development of leptin resistance. *Plos One*, 5(6), pp.1–8.

Stellenbosch University https://scholar.sun.ac.za

Lagathu, C. et al., 2004. Antiretroviral drugs with adverse effects on adipocyte lipid metabolism and survival alter the expression and secretion of proinflammatory cytokines and adiponectin in vitro. *Antiviral Therapy*, 9(6), pp.911–920.

Lagathu, C. et al., 2005. HIV antiretroviral treatment alters adipokine expression and insulin sensitivity of adipose tissue in vitro and in vivo. *Biochimie*, 87(1 SPEC. ISS.), pp.65–71.

Lago, F. et al., 2009. Adipokines as novel modulators of lipid metabolism. *Trends in Biochemical Sciences*, 34(10), pp.500–510.

Lehman, S.J. et al., 2010. Peri-aortic fat, cardiovascular disease risk factors, and aortic calcification: The Framingham Heart Study. *Atherosclerosis*, 210(2), pp.656–661. Available at: http://dx.doi.org/10.1016/j.atherosclerosis.2010.01.007.

Lemasters, J.J. & Nieminen, A.L., 1997. Mitochondrial oxygen radical formation during reductive and oxidative stress to intact hepatocytes. *Bioscience Reports*, 17(3), pp.281–291.

Lo, J. & Plutzky, J., 2012. The Biology of Atherosclerosis : General Paradigms and Distinct Pathogenic Mechanisms Among HIV-Infected Patients. *Journal of Infectious Diseases*, 205, pp.S368-374. Available at: http://jid.oxfordjournals.org.

Longenecker, C.. et al., 2013. Adipokines and vascular health in treated HIV infection: an obesity paradox? *AIDS*, 27(8), pp.1353–1356.

Longnecker, D., 2014. Anatomy and Histology of the Pancreas. *American Pancreatic Association*, 1, pp.1–26.

Lu, C. et al., 2011. Alterations in perivascular adipose tissue structure and function in hypertension. *European Journal of Pharmacology*, 656(1–3), pp.68–73. Available at: http://dx.doi.org/10.1016/j.ejphar.2011.01.023.

Maffei, M. et al., 1995. Increased expression in adipocytes of ob RNA in mice with lesions of the hypothalamus and with mutations at the db locus. *Proceedings of the National Academy of Sciences of the United States of America*, 92(15), pp.6957–6960.

Mandal, A., 2014. Leptin Resistance and Obesity. *Leptin Resistance and Obesity*, p.1. Available at: http://www.news-medical.net/health/Leptin-Resistance-and-Obesity.aspx [Accessed October 18, 2015].

Manfredi, R. & Calza, L., 2008. HIV infection and the pancreas: risk factors and potential managemant guidelines. *International journal of STD and AIDS*, 19(2), pp.99–105.

Marieb, E.N. & Hoehn, K., 2006. *Human Anatomy & Physiology* Seventh., Pearson Prentice Hall.

Martin, S.S., Qasim, A. & Reilly, M.P., 2008. Leptin Resistance. *Journal of the American College of Cardiology*, 52(15).

Masuzaki, H. et al., 1995. Human Obes Gene Expression. *Diabetes*, 44, pp.855–858.

Matschinsky, F.M. & Ellerman, J.., 1967. Metabolism of glucose in the islet of Langerhans. *The journal of Biology Chemistry*, 243(10), pp.2730–2736.

Menezes, A.M. et al., 2011. Prevalence and risk factors associated to chronic kidney disease in HIV-infected patients on HAART and undetectable viral load in Brazil. *PLoS ONE*, 6(10), pp.6–10.

Stellenbosch University https://scholar.sun.ac.za

Van der Merwe, M. & Pepper, M.S., 2006. National Prevalence of Obesity Obesity in South Africa. *Obesity Reviews*, 7, pp.315–322.

Van Der Merwe, M.T. & Pepper, M.S., 2006. Obesity in South Africa. *Obesity Reviews*, 7, pp.315–322.

Moinat, M. et al., 1995. Modulation of obese gene expression in rat brown and white adipose tissues. *Federation of European Biochemical Societies*, 373, pp.131–134.

Montani, J.-P. et al., 2004. Ectopic fat storage in heart, blood vessels and kidneys in the pathogenesis of cardiovascular diseases. *International journal of obesity and related metabolic disorders : journal of the International Association for the Study of Obesity*, 28 Suppl 4, pp.S58–S65.

Montessori, V. et al., 2004. Adverse effects of antiretroviral therapy for HIV infection. *CMAJ : Canadian Medical Association journal = journal de l'Association medicale canadienne*, 170(2), pp.229–238.

Motta, P.M. et al., 1997. Histology of the exocrine pancreas. *Microscopy Research and Technique*, 37(5–6), pp.384–398.

Mulvany, M. et al., 1996. Vascular remodeling. *Hypertension*, 28, pp.505–506.

Murphy, D.A., 2013. *Effects of short term high fat diet on obesity and perivascular adipose structure and function in mice : role of aldose reductase , and aldehyde metabolizing enzyme . By*. University of Louisville's Institutional Repository.

Nagy, G.S. et al., 2003. Human Immunodeficiency Virus Type 1-Related Lipoatrophy and Lipohypertrophy Are Associated with Serum Concentrations of Leptin. *Clinical Infectious Diseases*, 36(6), pp.795–802. Available at: http://cid.oxfordjournals.org/content/36/6/795.abstract.

Nakagawa, K. et al., 2002. Leptin causes vasodilation in humans. *Hypertension research : official journal of the Japanese Society of Hypertension*, 25, pp.161–165.

Neuman, M.G. et al., 2012. HIV-Antiretroviral Therapy Induced Liver , Gastrointestinal , and Pancreatic Injury. *International Journal of Hepatology*.

Nolan, C.J., Damm, P. & Prentki, M., 2011. Type 2 diabetes across generations: From pathophysiology to prevention and management. *The Lancet*, 378(9786), pp.169–181. Available at: http://dx.doi.org/10.1016/S0140-6736(11)60614-4.

Odze, R.D. & Goldblum, J.R., 2009. *Surgical pathology of the GI tract, liver, biliary tract, and pancreas* 2nd ed., Philadelphia: Elsevier.

Ogden, C.L. et al., 2007. The Epidemiology of Obesity. , pp.2087–2102.

Ogunmola, O.J., Oladosu, O.Y. & Olamoyegun, A.M., 2014. Association of hypertension and obesity with HIV and antiretroviral therapy in a rural tertiary health center in Nigeria: A cross-sectional cohort study. *Vascular Health and Risk Management*, 10, pp.129–137.

Oliveira, R.. et al., 2014. Impaired compensatory beta-cell function and growth in response to high-fat diet in LDL receptor knockout mice Impaired compensatory beta-cell function and growth in response to high-fat diet in LDL receptor knockout mice. *International Journal of Experimental pathology*.

Oliveira, R.B.D. et al., 2014. Impaired compensatory beta-cell function and growth in

Stellenbosch University https://scholar.sun.ac.za

response to high-fat diet in LDL receptor knockout mice. *International Journal of Experimental Pathology*, 95(4), pp.296–308.

Oral, E.. & Simha, V., 2002. Leptin-Replacement Therapy for Lipodystrophy. *The New England Journal of Medicine*, 346(8), pp.570–578.

Padanilam, B.J., 2003. Cell death induced by acute renal injury: a perspective on the contributions of apoptosis and necrosis. *American journal of physiology. Renal physiology*, 284(4), pp.F608-27. Available at: http://www.ncbi.nlm.nih.gov/pubmed/12620919.

Palella, F.J. et al., 1998. Declining Morbidity and mortality among patients with advanced human immunodeficiency virus infection. *The New England Journal of Medicine*, 338(13), pp.853–860.

Parakh, A. et al., 2009. Lipodystrophy and Metabolic Complications of Highly Active Antiretroviral Therapy. , 76, pp.1017–1021.

Payne, G. a. et al., 2010. Epicardial perivascular adipose-derived leptin exacerbates coronary endothelial dysfunction in metabolic syndrome via a protein kinase C-β pathway. *Arteriosclerosis, Thrombosis, and Vascular Biology*, 30, pp.1711–1717.

Pi-Sunyer, F.X., 2002. The obesity epidemic: pathophysiology and consequences of obesity. *Obesity research*, 10 Suppl 2, p.97S–104S.

Pinto Neto, L.F.D.S. et al., 2013. Dyslipidemia and fasting glucose impairment among HIV patients three years after the first antiretroviral regimen in a Brazilian AIDS outpatient clinic. *Brazilian Journal of Infectious Diseases*, 17(4), pp.438–443. Available at: http://dx.doi.org/10.1016/j.bjid.2012.12.006.

Post, F. et al., 2010. Randomized comparison of renal effects, efficacy, and safety with once-daily abacavir/lamivudine versus tenofovir/emtricitabine, administered with efavirenz, in antiretroviral-naive, HIV-1-infected adults: 48-week results from the ASSERT study. *Journal of acquired immune deficiency syndromes*, 55(1), pp.49–57.

Ratziu, V. et al., 2000. Liver fibrosis in overweight patients. *Gastroenterology*, 118(6), pp.1117–23. Available at: http://www.ncbi.nlm.nih.gov/pubmed/10833486.

Raucci, R. et al., 2013. Functional and structural features of adipokine family. *Cytokine*, 61, pp.1–14. Available at: http://dx.doi.org/10.1016/j.cyto.2012.08.036.

Rea, D.J. et al., 2006. Glomerular volume and renal histology in obese and non-obese living kidney donors. *Kidney International*, 70(9), pp.1636–1641. Available at: http://dx.doi.org/10.1038/sj.ki.5001799.

Safar, M. et al., 1998. Recent advances on large arteries in hypertension. *Hypertension*, 32, pp.156–161.

Savini, I. et al., 2013. Obesity-Associated Oxidative Stress : Strategies Finalized to Improve Redox State. *International journal of molecular sciences*, 14, pp.10497–10538.

Schiffer, T.A. & Friederich-Persson, M., 2017. Mitochondrial reactive oxygen species and kidney hypoxia in the development of diabetic nephropathy. *Frontiers in Physiology*, 8(APR), pp.1–12.

Schlett, C.L. et al., 2009. Novel measurements of periaortic adipose tissue in comparison to

Stellenbosch University https://scholar.sun.ac.za

anthropometric measures of obesity, and abdominal adipose tissue. *International journal of obesity (2005)*, 33, pp.226–232.

Shah, K., Alio, A.P., et al., 2012. AIDS & Clinical The Physiological Effects of Obesity in HIV-Infected Patients. , 3(4).

Shah, K., P. Alio, A. & J. Hall, W., 2012. The Physiological Effects of Obesity in HIV-Infected Patients. *Journal of AIDS & Clinical Research*, 3(4).

Shek, E.W., Brands, W. & Hall, J.E., 1998. Chronic Leptin Infusion Increases Arterial Pressure. *Hypertension*, 31(2), pp.409–414.

Sherwood, L., 2010. The peripheral endocrine glands. In M. Arbogast & L. Oliveira, eds. *Human Physiology: From Cells to Systems*. Canada: Brooks Cole Cengage Learning, pp. 710–726.

Shimabukuro, M. et al., 1998. Fatty acid-induced beta cell apoptosis: a link between obesity and diabetes. *Proceedings of the National Academy of Sciences of the United States of America*, 95(5), pp.2498–502. Available at: http://www.pubmedcentral.nih.gov/articlerender.fcgi?artid=19389&tool=pmcentrez&rendertype=abstract.

Silverthorn, D.U., 2013. *Human physiology; An integrated approach* 6th ed., Pearson.

Slavin, B.G. et al., 2010. Histological, immunocytochemical, and morphometrical analyses of pancreatic islets in the BSB mouse model of obesity. *Anatomical Record*, 293(1), pp.108–116.

South African National Department of Health, 2015. *National Consolidated Guidelines for the Prevention of Mother-To-Child Transmission of HIV (PMTCT) and the Managment of HIV in Children, Adolescents and Adults*, Pretoria. Available at: www.doh.gov.za.

Steiner, D.J. et al., 2010. Pancreatic islet plasticity: Interspecies comparison of islet architecture and composition. *Islets*, 2(3).

Sutinen, J. & Yki-Järvinen, H., 2007. Increased resting energy expenditure, fat oxidation, and food intake in patients with highly active antiretroviral therapy-associated lipodystrophy. *American journal of physiology. Endocrinology and metabolism*, 292, pp.E687–E692.

Szasz, T., Bomfim, G.F. & Webb, R.C., 2013. The influence of perivascular adipose tissue on vascular homeostasis. *Vascular health and risk management*, 9, pp.105–116.

Tsiodras, S. & Mantzoros, C., 2006. Leptin and Adiponectin in the HIV Associated Metabolic Syndrome: Physiologic and Therapeutic Implications. *American journal of infectious diseases*, 2(3), pp.141–152. Available at: http://www.pubmedcentral.nih.gov/articlerender.fcgi?artid=1712675&tool=pmcentrez&rendertype=abstract.

Tushuizen, M.E. et al., 2007. Pancreatic Fat Content and Beta-Cell Function in Men With and Without Type 2 Diabetes. *Diabetes care*, 30(11), pp.2916–2921.

Vlasova, M. et al., 2010. Role of adipokines in obesity-associated hypertension. *Acta Physiologica*, 200, pp.107–127.

De Vriese, A.S. et al., 2001. Diabetes-induced microvascular dysfunction in the hydronephrotic kidney: Role of nitric oxide. *Kidney International*, 60(1), pp.202–210.

Stellenbosch University https://scholar.sun.ac.za

Wanke, C.A. et al., 2015. HIV / AIDS. *Oxford Journals*, 31(3), pp.803–805.

Weisberg, S.P. et al., 2003. Obesity is associated with macrophage accumulation in adipose tissue. *Journal of Clinical Investigation*, 112(12), pp.1796–1808.

Yamauchi, Y. & Michitaka, K., 1998. Morphometric Analysis of Lymphatic and Blood Vessels in Human Chronic Viral Liver Diseases. *American Journal of Pathology*, 153(4), pp.1131–1137.

Young, B. et al., 2006. *Wheater's Functional Histology: A Text and Colour Atlas* 5th ed., Philadelphia: Elsevier.

Zimmerman, H.J., 1978. *Drug-induced liver disease," in Hepato- toxicity: The Adverse Effects of Drugs and Other Chemicals on the Liver* 1st ed., New-York: Appleton-Century-Crofts.

Stellenbosch University https://scholar.sun.ac.za

APPENDICES

Appendix A: Standard rat chow

- Oval pellet, 10 mm x 25mm length

Table 8: Nutritional Values of the Lean (Chow) Diet

	Lean Diet (%)
Fat	4.8
Protein	17.1
Carbohydrates	34.6
Sucrose	5.2

Appendix B: High-calorie diet

- Normal rat chow (600g) was soaked in a 250ml warm water and dissolved sucrose mixture for 30 minutes
- Dissolved sucrose consisted of 140g standard household sugar
- The soaked mixture was crushed and melted vegetable fat (4 x 125g Holsum™) and eight cans of full cream sweetened condensed milk (8 x 385g Clover™) was added
- The mixture was mixed and stored in a refrigerator

Table 9: Nutritional Value of Holsum™ Vegetable fat

	Per 100g
Energy (KJ)	3700
Protein (g)	0
Glycaemic Carbohydrates (g)	0
Of which total sugar (g)	0
Total fat (g)	100
Of which saturated fay (g)	67.8
Trans fat (g)	<1
Monosaturated fat (g)	26.4
Dietary fibre (g)	0

Stellenbosch University https://scholar.sun.ac.za

Total Sodium (g)	0
Vitamin A (µg)	1380
Vitamin D (µg)	15

Table 10: Nutritional Value of Condensed Milk (Clover™)

	Per 100g
Energy (KJ)	1381
Protein (g)	6.5
Glycaemic Carbohydrates (g)	54
Of which total sugar (g)	54
Total fat (g)	8.7
Of which saturated fay (g)	5.5
Dietary fibre (g)	0
Total Sodium (g)	127
Calcium (mg)	284

Table 11: Nutritional Value of the HCD

	High-Calorie Diet (%)
Fat	11.5
Protein	8.3
Carbohydrates	42
Sucrose	20

Appendix C: Antiretroviral treatment administration

- Drugs administered was South Africa's first line ARV FDC, Odimune (1100mg, *Cipla MedPro (Pty) Ltd.* Bellville, Western Cape, RSA)
- The FDC contained 600mg Efavirenz (EFV), 200mg Emtricitabine (FTC) and 300mg Tenofovir Disoproxil Furmarate (TDF)
- The FDC was initially suspended in jelly cubes, but the animals stopped eating the jelly cubes containing the FDC
- The FDC purchased contained human recommended daily dosage of the active ingredients

Stellenbosch University https://scholar.sun.ac.za

- Tablets were grinded into a fine powder and the proper mass of powder for each group weekly were calculated and weighed according to the average total mass body (TMB) of each group
- The dosage were adjusted weekly according to TMB changes
- Daily FDC dosages were administered, starting with 3 ml water and later adjusted to 2 ml and finally to 1 ml

Appendix D: Standard histological processing – materials and methods

Materials

- 70%, 805, 95% and 99% Ethanol
- Shandon Elliot Duplex Tissue processor
- Embedding moulds
- Paraffin wax (Paraplast, melting point 58°C
- Xylene (Kimix, chemicals, Cape Town, South Africa)

Methods:

- Tissue samples were fixed in 5% PFA for 24 hours at 4°C
- Tissue samples were then processed in the Duplex tissue processor following the procedure in Table 9

Table 12: Tissue processing procedure

Step	Solution	Time (minutes)	Temperature (°C)
1	70% Ethanol	30	40
2	80% Ethanol	30	40
3	95% Ethanol	45	40
4	95% Ethanol	45	40
5	100% Ethanol	45	40
6	100% Ethanol	45	40
7	100% Xylene	45	40
8	100% Xylene	45	40
9	Paraffin	30	58
10	Paraffin	30	58
11	Paraffin	30	58

Stellenbosch University https://scholar.sun.ac.za

12	Paraffin	30	58

Appendix E: Standard histology materials

- Acid alcohol (1%)
- Alternate for Eosin-Phloxine B solution: Eosin Y solution
- Ammonia (0.2%)
- Bio-Scan Microscope Slides Frosted (Trifal Imaging, Chatsworth, USA)
- Bio-Scan Microscope Slides Positive Charge (Trifal Imaging, Chatsworth, USA)
- Bond Polymer Refine Detection kit (SMM Instruments (PTY) Ltd, Midrand, South Africa)
- Bond™ Software ©Version 4.0 (Leica Biosystems, Melbourne, Australia)
- Coplin staining jar
- Cover Slide Box
- Cover Slips
- Distilled water
- DPX Mountant (Kimix, chemicals, Cape Town, South Africa)
- Duplex Tissue Processor
- Embedding Cassette (SPL Life Sciences, Pocheon, Korea)
- Eosin Yellowish (Kimix Chemicals, Cape Town, South Africa)
- Eppendorf tubes (2.0ml)
- Ethanol (99% & 96%)
- Harris's Haematoxylin
- IKAMA® Magnetic Stirrer and Hotplate
- Incubator (IH-150)
- Leica Auto Stainer XL (Leica ST 5010, serial number 1732/07,2007)
- Leica Bond Max immune-autostainer (SMM Instruments (PTY) Ltd, Midrand, South Africa)
- Leica EG 1160 Embedder
- Leica RM 2125RT microtome (SMM Instruments, Cat.)
- M53C Drying Oven
- Mayer's Haematoxylin (Kimix Chemicals, Cape Town, South Africa)
- Paraffin Wax (Paraplast, melting point 58°C)
- Paraformaldehyde

Stellenbosch University https://scholar.sun.ac.za

- Pariodic Acid
- Plastic rack
- Schiff's solution
- Staining rack
- Surgical blade, forceps
- Tap water
- Thermostat
- Water Bath
- Xylene (Kimix, chemicals, Cape Town, South Africa)

Appendix F: Haematoxylin and Eosin (H&E) stain protocol

- Slides were placed into a plastic rack in the autostainer. Slides were stained according to the pre-programmed procedure as tabulated in Table 10

Table 13: H&E stain protocol procedure

Step	Solution	Time	Repetition
1	Xylene	10 min	2
2	Ethanol (99%)	5 min	2
3	Ethanol (96%)	2 min	1
4	Ethanol (70%)	2 min	1
5	Distilled water	5 sec	1
6	Haematoxylin	8 min	1
7	Running water	5 min	1
8	Ethanol (1% acid alcohol)	30 sec	1
9	Running water	1 min	1
10	Ammonia (0.2%)	45 sec	1
11	Running water	5 min	2
12	Ethanol (96%)	10 dips	1
13	Eosin	45 sec	1
14	Ethanol (96%)	5 min	2
15	Xylene	5 min	2

- Cover slides were mounted on completed slides with PDX.
- Outcome:
    - Nuclei: Blue
    - Cytoplasm: Pink to red

Stellenbosch University https://scholar.sun.ac.za

Appendix G: Immunohistochemistry standard protocol – Pancreas

List of referred SOPs used in the SOP for pancreas double staining:

- ICC\B8-V01 Vectastain Kit
- ICC\B14-V01 0.05M Tris Buffered Saline pH7.2
- ICC\B9-V01 Biotinylated Mouse Anti-IgG
- ICC\B16-V01 Normal Goat Serum
- ICC\B17-V01 Normal Horse Serum
- ICC\B18-V01 0.1M Phosphate Buffered Saline pH7.2
- ICC\B20-V01 Polyclonal Anti-Glucagon
- ICC\B17-V01 Monoclonal Anti-Insulin
- ICC\B27-V01 Liquid DAB+ Substrate Chromagen System
- ICC\B26-V01 Envision G/2 System/AP, Rabbit/Mouse Kit

Table 14 Antibody information

Antibody	Source	Clonality	Raised	Dilution	Country
Anti-Glucagon	Dako	Polyclonal	Rabbit	1:100	North America
Anti-Insulin	Dako	Monoclonal	Guinea pig	1:10 000	North America

Materials:

- Moisture Chamber
- Staining Rack
- Staining jar
- 1-10 µl, 1-100 µl, 20-200 µl, 1000 µl pipettes & tips
- Magnetic Stirrer
- Coverslips
- Gloves
- Magnetic stirrer
- 250ml measuring cylinder
- Distilled Water

Stellenbosch University https://scholar.sun.ac.za

- Hydrogen Peroxide
- 0.05M Tris Buffered Saline (TBS) pH7.2
- 0.1M Phosphate Buffered Saline (PBS) pH7.2
- Normal Goat Serum
- Normal Horse Serum
- Polyclonal Anti-Glucagon
- Monoclonal Anti-Insulin
- Biotinylated Rabbit Anti-IgG
- Biotinylated Mouse Anti-IgG
- Vectastain
- EnvisionG/2 System/AP Kit
- Liquid DAB+ Substrate Chromagen Solution
- Haematoxylin
- DPX Mounting Media

Methods:

• Dewax sections through xylene and alcohol.

• Rinse slides in staining jar in distilled water.

• Block for endogenous peroxidase with 3% hydrogen peroxide (H_2O_2) for five (5) minutes in staining jar. (6ml H_2O_2/194ml distilled water – left fridge).

• Rinse slides with 0.05M TBS pH7.2 for five (5) minutes in staining jar.

• Dry around section and add normal goat serum (NGS) 1:20 to slides in a moisture chamber (Completely cover the section) for twenty (20) minutes at room temperature (18˚C- 20˚C).

• Blot excess serum. (Do not rinse).

• Add approximately 100µl anti-glucagon (P) (primary antibody) 1:100 to sections in moisture chamber and incubate at room temperature (18˚C- 20˚C) for thirty (30) minutes.

• Jet wash with 0.05M TBS pH7.2 and rinse in staining jar in 0.05M TBS pH7.2 for five (5) minutes. (N.B. Make up Biotinylated Anti-Rabbit IgG and Vectastain)

• Dry around sections and add Biotinylated Anti-Rabbit IgG 1:200 to slides in moisture chamber for (30) minutes at room temperature (18˚C- 20˚C).

• Jet wash with 0.05M TBS pH7.2 and rinse in staining jar in 0.05M TBS pH7.2 for ten (10) minutes.

Stellenbosch University https://scholar.sun.ac.za

• Dry around sections and add Vectastain to slides in moisture chamber for one (1) hour at room temperature (18°C- 20°C).

• Jet wash slides with 0.05M TBS pH 7.2 and rinse for ten (10) minutes in 0.05M TBS pH7.2 in staining jar.

• Dry around sections and add Liquid DAB+ Chromagen solution to slides on a rack over the sink for five (5) minutes. (Check progress under microscope).

• Jet wash slides with distilled water and rinse with distilled water in a staining jar for five (5) minutes.

• Rinse slides in 0.05M TBS pH7.2 in staining jar for five (5) minutes.

• Dry around section and add normal horse serum (NHS) 1:20 to slides in a moisture chamber (completely cover the section) for twenty (20) minutes at room temperature (R.T.) (18°C- 20°C).

• Blot excess serum. (Do not rinse).

• Add approximately 100µl anti-insulin (M) 1:10 000 to sections in moisture chamber and incubate at 4ºC overnight.

• Allow slides to reach room temperature.

• Jet wash with 0.05M TBS pH7.2 and rinse in staining jar in 0.05M TBS pH7.2 for five (5) minutes.

• Dry around sections and add 100µl Rabbit/Mouse (LINK) to slides in moisture chamber for thirty (30) minutes at room temperature (R.T.) (18°C- 20°C).

• Jet wash with 0.05M TBS pH7.2 and rinse in staining jar in 0.05M TBS pH7.2 for ten (10) minutes.

• Dry around sections and add 100ul AP Enzyme (ENHANCER) to slides in moisture chamber thirty (30) minutes at room temperature (R.T.) (18°C- 20°C).

• Jet wash slides with 0.05M TBS pH 7.2 and rinse for ten (10) minutes in 0.05M TBS PH7.2 in staining jar.

• Dry around sections and add Substrate Working Solution to slides on a rack for three - five (3-5)

Minutes at room temperature (R.T.) (18°C- 20°C). (Check progress under microscope).

• Jet wash slides with distilled water and rinse in distilled water in staining jar for five (5) minutes.

• Counterstain with haematoxylin for 2-4 minutes.

• Rinse well in tap water.

• Leave to “blue” in tap water for thirty (30) minutes.

• Dry completely on paper towel (sections facing upwards).

Stellenbosch University https://scholar.sun.ac.za

• Mount slides in DPX.

Quality control:

- Method Control slides are included to monitor any non-specific staining.
- Pipettes are serviced annually or more often as required.

Appendix H: Immunohistochemistry protocol – Leptin

Table 15 IHC stain protocol procedure, LEICA Bond Max protocol F

Step	Type	Incubation Time	Temperature	Dispense Type
1	Peroxide Block	5 min	Ambient	selected vol.
2	Bond Wash Solution	0 min	Ambient	selected vol.
3	Bond Wash Solution	0 min	Ambient	open
4	Bond Wash Solution	0 min	Ambient	selected vol.
5	Primary Antibody	15 min	Ambient	selected vol.
6	Bond Wash Solution	0 min	Ambient	selected vol.
7	Bond Wash Solution	0 min	Ambient	selected vol.
8	Bond Wash Solution	0 min	Ambient	selected vol.
9	Post Primary	8 min	Ambient	selected vol.
10	Bond Wash Solution	2 min	Ambient	selected vol.
11	Bond Wash Solution	2 min	Ambient	selected vol.
12	Bond Wash Solution	2 min	Ambient	selected vol.
13	Polymer	8 min	Ambient	selected vol.
14	Bond Wash Solution	2 min	Ambient	selected vol.
15	Bond Wash Solution	2 min	Ambient	selected vol.
16	Deionized Water	0 min	Ambient	selected vol.
17	Deionized Water	0 min	Ambient	selected vol.
18	Mixed DAB Refine	10 min	Ambient	selected vol.
19	Deionized Water	0 min	Ambient	selected vol.
20	Deionized Water	0 min	Ambient	selected vol.
21	Deionized Water	0 min	Ambient	selected vol.
22	Haematoxylin	5min	Ambient	selected vol.

Stellenbosch University https://scholar.sun.ac.za

23	Deionized Water	0 min	Ambient	selected vol.
24	Deionized Water	0 min	Ambient	selected vol.
25	Deionized Water	0 min	Ambient	selected vol.

Table 16: Manual rehydration procedure

Step	Solution	Time	Repetitions
1	Ethanol (70%)	5 dips	1
2	Ethanol (96%)	5 dips	1
3	Ethanol (99%)	5 dips	1
4	Xylene	1 min	2

Table 17: Antibody information

Antibody	Source	Antibody ID	Clonality	Raised	Dilution
Anti-Leptin	Abcam	Ab117751	Polyclonal	Rabbit	1:50

Appendix I: Morphometric analysis equipment

- Nikon Eclipse Ti-S with PRIOR ProScan III. NIS Elements AR4.40 ©1991-2015
- Leica QWin V3 software (Germany)
- Zeiss Axioskop2, serial number 801452 (Carl Zeiss, AG, Oberkochen, Germany)
- AxioVisio, version 4.7.2.0 (Carl Zeiss, AG, Oberkochen, Germany)
- ZEN Lite 2012 (blue edition, version 1.1.2.0 (Carl Zeiss Microscopy GmbH)

Appendix J Pathology grading criteria

Grade 0 (absent): No pathological changes seen on the entire tissue section

Grade I (mild): Present in <25% of tissue section

Grade II (moderate): Present in 25-50% of tissue sections

Grade III (severe): Present in >50% of tissue section

Appendix K: Pancreas data

Table 18 Number of islets per animal

Stellenbosch University https://scholar.sun.ac.za

Rot	Treatment	Islet Number
256/15	C/ART-	4
276/15	C/ART-	34
285/14	C/ART-	8
331/15	C/ART-	15
372/15	C/ART-	20
402/15	C/ART-	23
419/15	C/ART-	32
433/15	C/ART-	27
474/14	C/ART-	32
492/14	C/ART-	30
266/15	C/ART+	20
267/14	C/ART+	14
281/15	C/ART+	42
303/14	C/ART+	26
339/14	C/ART+	68
361/15	C/ART+	63
409/15	C/ART+	12
429/15	C/ART+	13
444/15	C/ART+	25
474/15	C/ART+	23
261/15	HCD/ART-	18
276/14	HCD/ART-	52
312/14	HCD/ART-	61
336/15	HCD/ART-	54
382/15	HCD/ART-	11
397/15	HCD/ART-	42
424/15	HCD/ART-	78
438/15	HCD/ART-	9
479/15	HCD/ART-	11
483/14	HCD/ART-	9
258/14	HCD/ART+	63
271/15	HCD/ART+	62
286/15	HCD/ART+	65
294/14	HCD/ART+	36
366/15	HCD/ART+	38
377/15	HCD/ART+	26
402/14	HCD/ART+	41
414/15	HCD/ART+	20
484/15	HCD/ART+	32
644/15	HCD/ART+	71

Table 19 LSD post-hoc test of pancreatic islets area compared between the four groups. P-value, mean and standard error of islet area are indicated between the four groups.

Stellenbosch University https://scholar.sun.ac.za

Comparisons Cell {#1}-{#2}	LSD test; variable Area (Spreadsheet in Surface and islet area.stw) Simultaneous confidence intervals Effect: Treatment Include condition: Islet="Islet Area"				
	1st Mean	2nd Mean	Mean Differ.	Standard Error	p
{1}-{2}	C/ART-	C/ART+	743,25	1447,27	0,61
{1}-{3}	C/ART-	HCD/ART-	-717,60	1442,58	0,62
{1}-{4}	C/ART-	HCD/ART+	-696,51	1376,42	0,62
{2}-{3}	C/ART+	HCD/ART-	-1460,85	1398,66	0,30
{2}-{4}	C/ART+	HCD/ART+	-1439,76	1330,31	0,29
{3}-{4}	HCD/ART-	HCD/ART+	21,09	1325,21	0,99

Table 20 LSD post-hoc test of alpha- and beta-cell area p-values compared between the four groups. Values in red indicates all significant differences (p<0.05).

Comparisons Cell {#1}-{#2}	LSD test; variable Area (Spreadsheet in Surface and islet area.stw) Simultaneous confidence intervals Effect: Treatment*Islet				
	1st Mean	2nd Mean	Mean Differ.	Standard Error	p
{1}-{2}	C/ART-*A Cell Area	C/ART-*B Cell Area	-2315,61	361,66	0,00
{1}-{3}	C/ART-*A Cell Area	C/ART+*A Cell Area	20,88	387,37	0,96
{1}-{4}	C/ART-*A Cell Area	C/ART+*B Cell Area	-1627,57	387,37	0,00
{1}-{5}	C/ART-*A Cell Area	HCD/ART-*A Cell Area	-253,70	386,04	0,52
{1}-{6}	C/ART-*A Cell Area	HCD/ART-*B Cell Area	-2112,16	386,04	0,00
{1}-{7}	C/ART-*A Cell Area	HCD/ART+*A Cell Area	14,25	368,64	0,97
{1}-{8}	C/ART-*A Cell Area	HCD/ART+*B Cell Area	-2032,71	368,64	0,00
{2}-{3}	C/ART-*B Cell Area	C/ART+*A Cell Area	2336,48	387,37	0,00
{2}-{4}	C/ART-*B Cell Area	C/ART+*B Cell Area	688,04	387,37	0,08
{2}-{5}	C/ART-*B Cell Area	HCD/ART-*A Cell Area	2061,91	386,04	0,00
{2}-{6}	C/ART-*B Cell Area	HCD/ART-*B Cell Area	203,45	386,04	0,60
{2}-{7}	C/ART-*B Cell Area	HCD/ART+*A Cell Area	2329,85	368,64	0,00
{2}-{8}	C/ART-*B Cell Area	HCD/ART+*B Cell Area	282,90	368,64	0,45
{3}-{4}	C/ART+*A Cell Area	C/ART+*B Cell Area	-1648,44	336,30	0,00
{3}-{5}	C/ART+*A Cell Area	HCD/ART-*A Cell Area	-274,58	374,19	0,47
{3}-{6}	C/ART+*A Cell Area	HCD/ART-*B Cell Area	-2133,04	374,19	0,00
{3}-{7}	C/ART+*A Cell Area	HCD/ART+*A Cell Area	-6,63	356,22	0,99
{3}-{8}	C/ART+*A Cell Area	HCD/ART+*B Cell Area	-2053,58	356,22	0,00
{4}-{5}	C/ART+*B Cell Area	HCD/ART-*A Cell Area	1373,87	374,19	0,00
{4}-{6}	C/ART+*B Cell Area	HCD/ART-*B Cell Area	-484,59	374,19	0,20
{4}-{7}	C/ART+*B Cell Area	HCD/ART+*A Cell Area	1641,81	356,22	0,00
{4}-{8}	C/ART+*B Cell Area	HCD/ART+*B Cell Area	-405,14	356,22	0,26
{5}-{6}	HCD/ART-*A Cell Area	HCD/ART-*B Cell Area	-1858,46	330,71	0,00
{5}-{7}	HCD/ART-*A Cell Area	HCD/ART+*A Cell Area	267,95	354,77	0,46
{5}-{8}	HCD/ART-*A Cell Area	HCD/ART+*B Cell Area	-1779,01	354,77	0,00
{6}-{7}	HCD/ART-*B Cell Area	HCD/ART+*A Cell Area	2126,41	354,77	0,00
{6}-{8}	HCD/ART-*B Cell Area	HCD/ART+*B Cell Area	79,45	354,77	0,82
{7}-{8}	HCD/ART+*A Cell Area	HCD/ART+*B Cell Area	-2046,95	293,99	0,00

Stellenbosch University https://scholar.sun.ac.za

Table 21 LSD post-hoc test of the number of islets per section area compared between the four groups. Significant differences between groups will be indicated in red. If no significant differences are seen between the four groups no red values will appear.

Cell No.	LSD test; variable #isletspermm^2 (Spreadsheet in Surface and islet area.stw) Probabilities for Post Hoc Tests Error: Between MS = .37844, df = 36.000				
	Treatment	{1} 1.1025	{2} 1.0175	{3} 1.5078	{4} 1.5521
1	C/ART-		0,759090	0,149358	0,110877
2	C/ART+	0,759090		0,083132	0,059807
3	HCD/ART-	0,149358	0,083132		0,872870
4	HCD/ART+	0,110877	0,059807	0,872870	

Stellenbosch University https://scholar.sun.ac.za

Table 22 Pathology changes seen within each pancreas sample. Pathology was classified as follows; absent (0), mild (1), moderate (2) and severe (3).

Rat	Treatment	Absent/Present	Pathology	Comments
			Eosinophilic duct	
258/14	HCD/ART+	0	0	
429/14	C/ART-	0	0	
474/14	C/ART-	0	0	
267/14	C/ART+	0	0	
339/14	C/ART+	1	1	Some collecting ducts contain eosinophilic proteinaceous material and are mildly dilated
276/14	HCD/ART-	0	0	
312/14	HCD/ART-	0	0	
483/14	HCD/ART-	0	0	
402/14	HCD/ART+	0	0	Microvesicular space
294/14	HCD/ART+	0	0	Microvesicular space
258/15	C/ART-	0	0	Microvesicular space
256/15	C/ART-	0	0	
281/15	C/ART+	0	0	Microvesicular space
377/15	HCD/ART+	0	0	
366/15	HCD/ART+	0	0	
414/15	HCD/ART+	0	0	
438/15	HCD/ART-	0	0	Some fat cells outside of pancreas tissue
419/15	C/ART-	0	0	One islet had a built up of nuclei
433/15	C/ART-	0	0	
429/15	C/ART+	0	0	
474/15	C/ART+	0	0	
479/15	HCD/ART-	0	0	

Stellenbosch University https://scholar.sun.ac.za

261/15	HCD/ART-	0		0	
303/14	C/ART+	0		0	
331/15	C/ART-	0		0	
276/15	C/ART-	0		0	
372/15	C/ART-	0		0	
402/15	C/ART-	0		0	
444/15	C/ART+	0		0	
361/15	C/ART+	0		0	
266/15	C/ART+	0		0	
409/15	C/ART+	0		0	
336/15	HCD/ART-	0		0	
424/15	HCD/ART-	1		1	Some collecting ducts contain eosinophilic proteinaceous material and are mildly dilated.
397/15	HCD/ART-	0		0	
382/15	HCD/ART-	0		0	
644/15	HCD/ART+	0		0	
484/15	HCD/ART+	0		0	
271/15	HCD/ART+	0		0	
286/15	HCD/ART+	0	0		

Stellenbosch University https://scholar.sun.ac.za

Appendix L: Kidney data

Corpuscle:

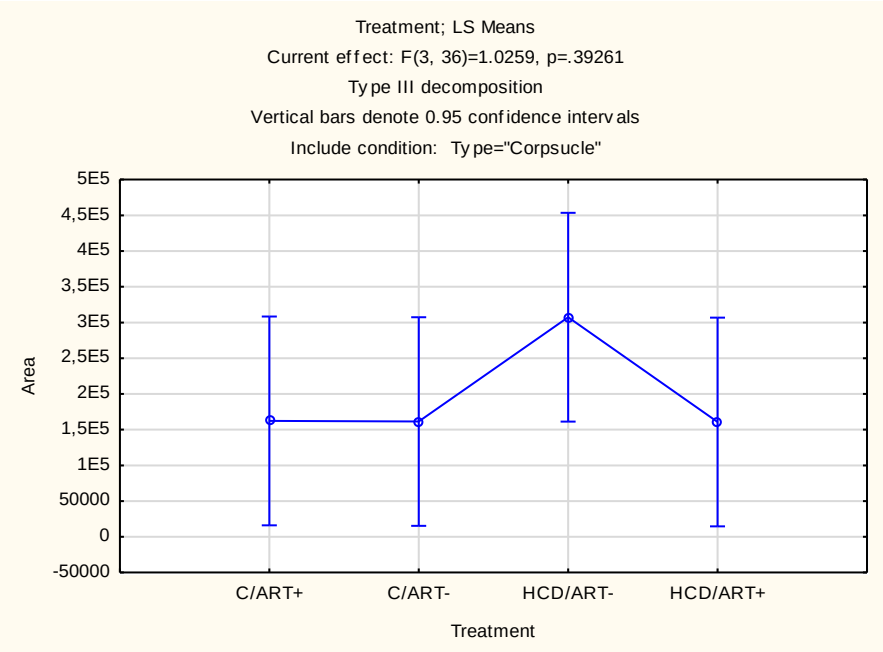

Figure 0.1 Average corpuscle area (µm²) between the four groups. No significant differences were seen between the four groups (p>0.392).

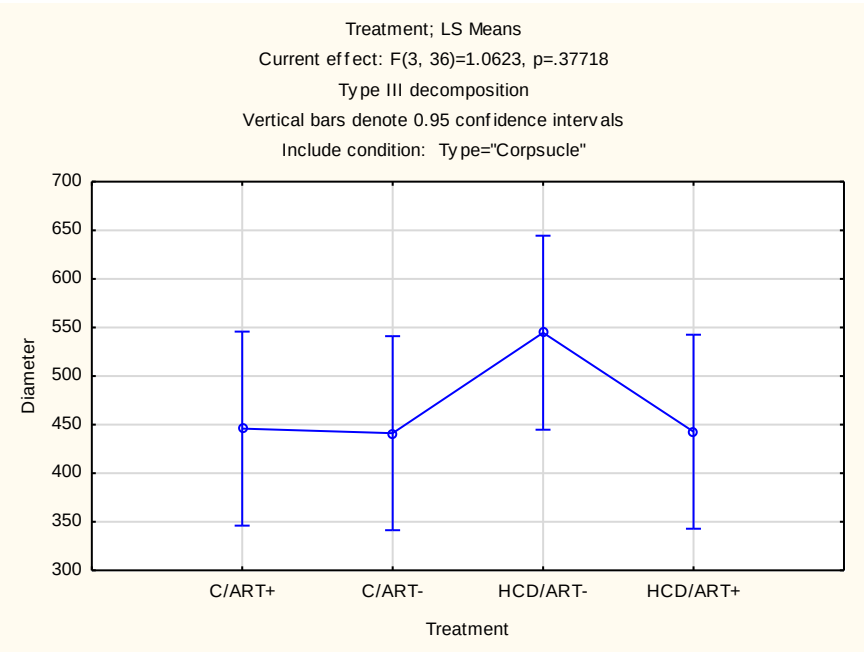

Figure 0.2 Average corpuscle diameter (µm) between the four groups. No significant differences were seen between the four groups (p>0.377)

Stellenbosch University https://scholar.sun.ac.za

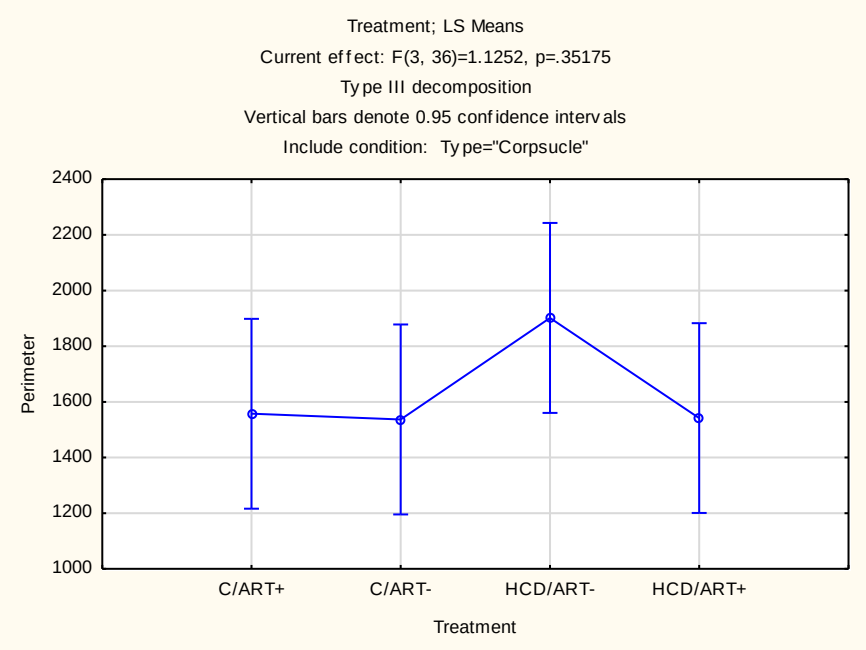

Figure 0.3 Average corpuscle perimeter (µm) between the four groups. No significant differences were seen between the four groups (p>0.351).

Glomeruli:

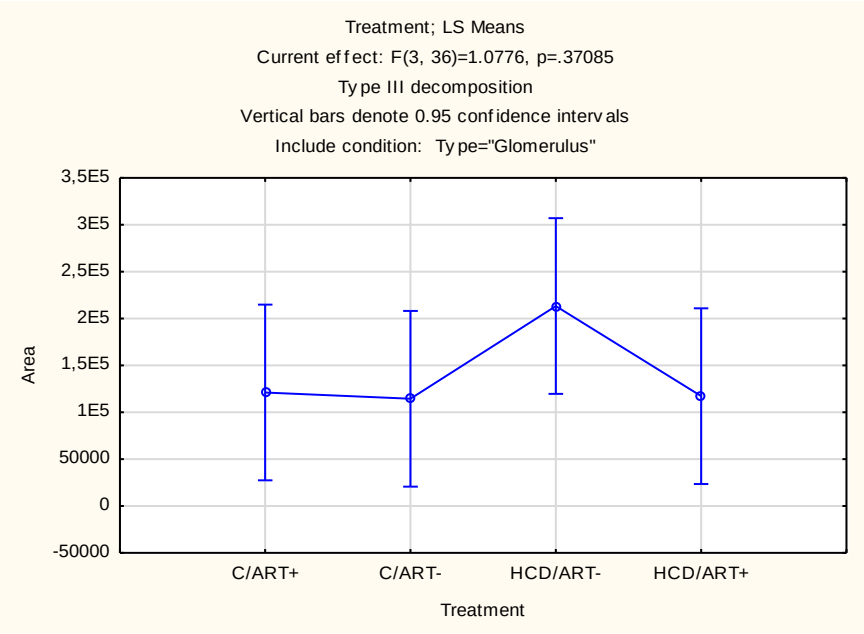

Figure 0.4 Average glomeruli area (µm²) between the four treatment groups. No significant differences were seen between the four groups (p>0.371).

Stellenbosch University https://scholar.sun.ac.za

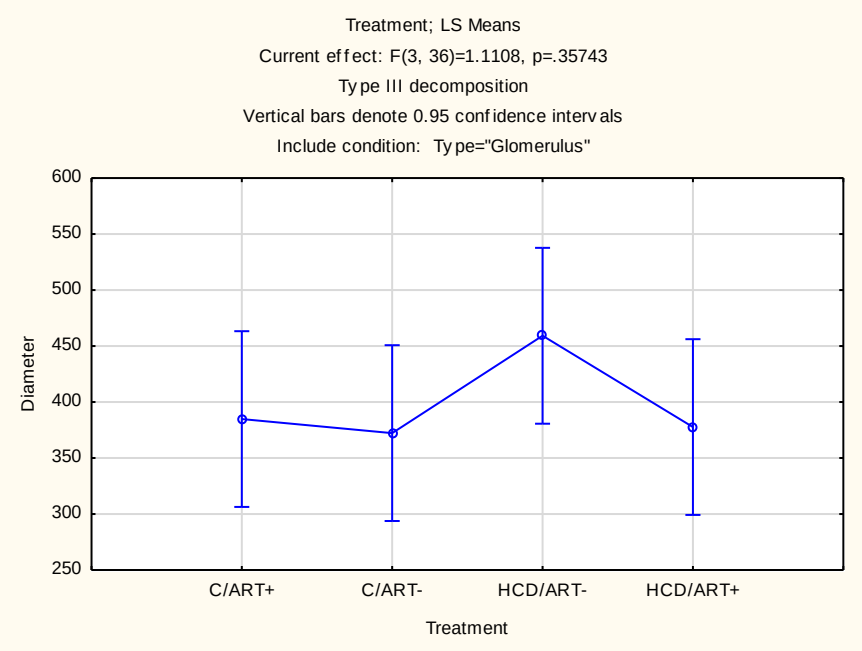

Figure 0.5 Average glomeruli diameter (µm) between the four treatment groups. No significant differences were seen between the four groups (p>0.357).

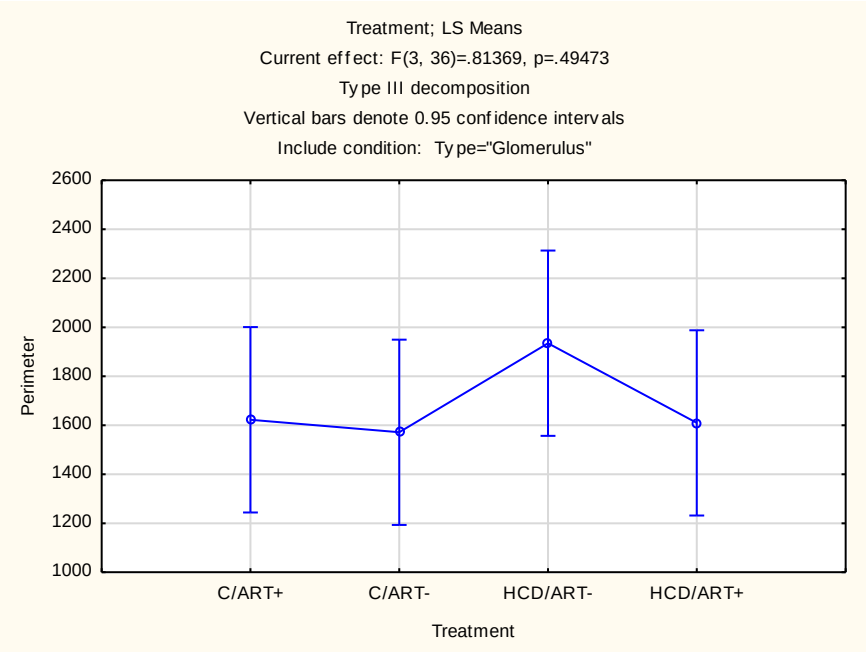

Figure 0.6 Average glomeruli perimeter (µm) between the four treatment groups. No significant differences were seen between the four groups (p>0.494).

Stellenbosch University https://scholar.sun.ac.za

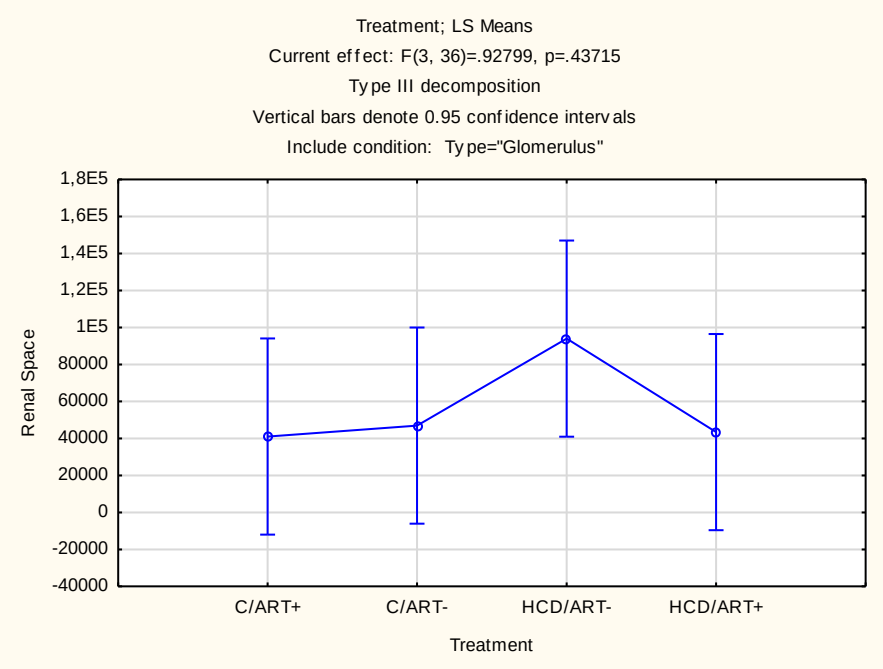

Figure 0.7 Average renal space area (µm²) between the four treatment groups. No significant differences were seen between the four groups (p>0.437).

Arcuate arteries:

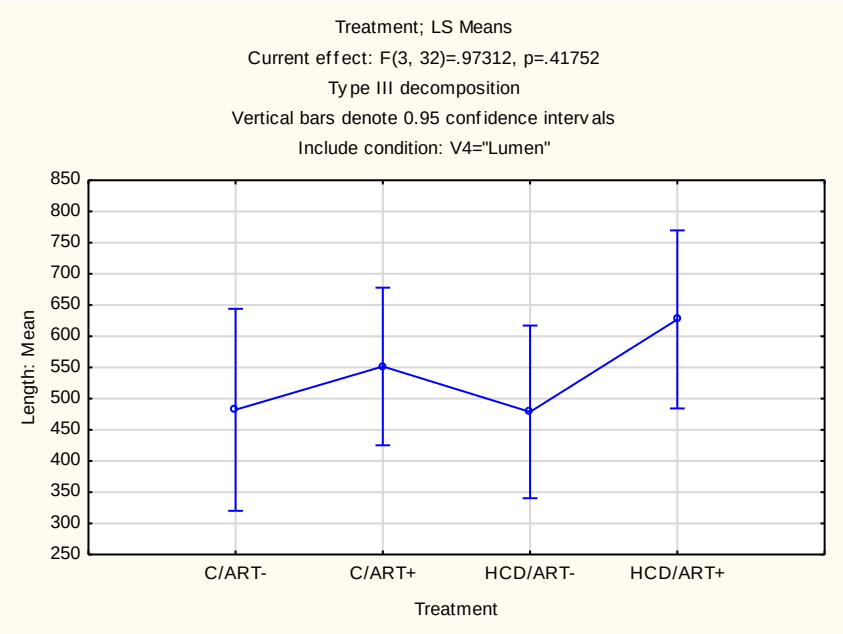

Figure 0.8 Average lumen diameter (µm) between the four treatment groups. No significant differences were seen between the four groups (p>0.417).

Stellenbosch University https://scholar.sun.ac.za

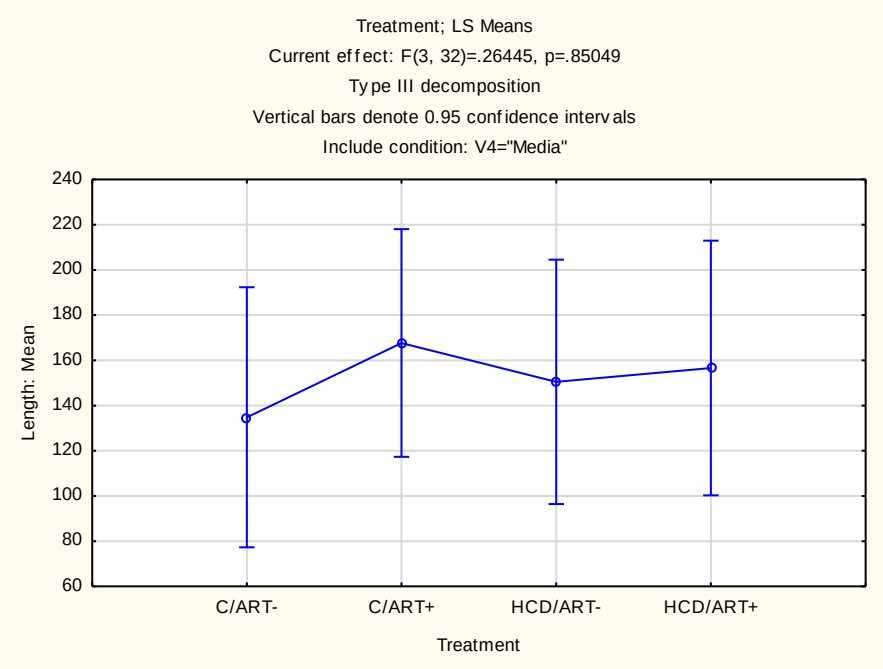

Figure 0.9 Average tunica media thickness (µm) between the four treatment groups. No significant differences were seen between the four groups (p>0.85).

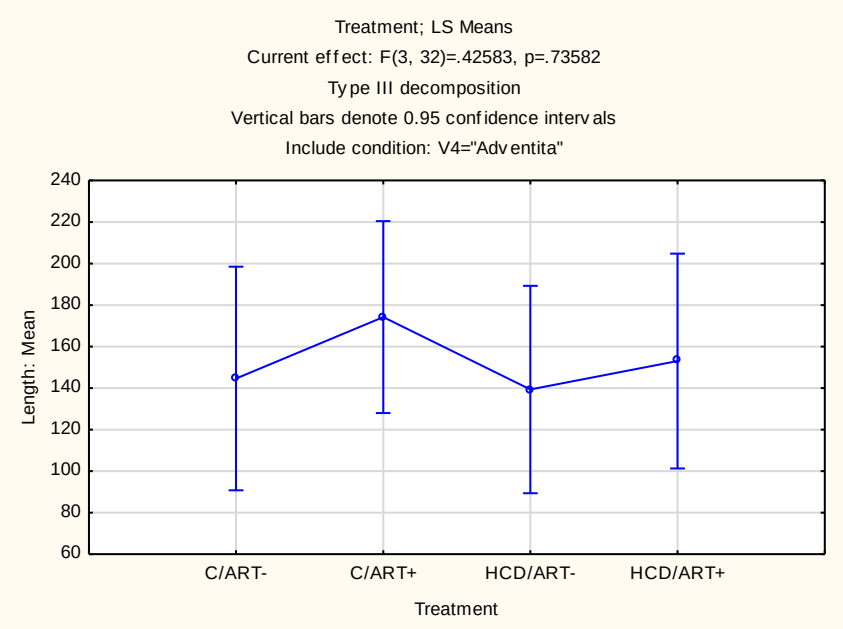

Figure 0.10 Average tunica adventitia thickness (µm) between the four treatment groups. No significant differences were seen between the four groups (p>0.735).

Stellenbosch University https://scholar.sun.ac.za

Table 23 Pathology changes seen within all kidney samples. Pathology was classified as follows; absent (0), mild (1), moderate (2) and severe (3).

Rat	Treatment	Absent/Present	Pathology					
			Vacuolisation	Swelling	Eosinophilia	Basophilic	Dilation of perivascular spaces	
630/15	HCD/ART+	1	2	0	0	0	0	
555/15	C/ART-	0	0	0	0	0	0	
480/15	HCD/ART-	1	1	0	0	0	1	Mild dilation of perivascular spaces associated with t
475/15	C/ART+	1	2	0	0	0	0	
425/15	HCD/ART-	0	0	0	0	0	0	
420/15	C/ART-	1	0	0	0	0	1	Mild dilation of perivascular spaces associated with t
445/15	C/ART+	1	0	0	0	0	1	Mild dilation of perivascular spaces associated with t
440/15	HCD/ART-	1	1	0	0	0	0	
403/15	C/ART-	1	1	0	0	0	0	
470/15	C/ART-	1	1	0	0	1	0	Few proximal convoluted tubular structures contain s
398/15	HCD/ART-	1	2	0	0	0	0	
415/15	HCD/ART+	1	1	0	0	1	0	Few proximal convoluted tubular structures contain s
378/14/15	HCD/ART+	0	0	0	0	0	0	
373/15	C/ART-	1	2	0	0	1	0	Few proximal convoluted tubular structures contain s
367/15	HCD/ART+	1	2	0	0	0	0	
635/15	C/ART+	1	1	0	0	0	0	
362/15	C/ART+	1	1	0	0	0	0	
645/15	HCD/ART+	0	0	0	0	0	0	
640/15	C/ART+	1	1	0	0	0	0	
332/15	C/ART-	1	1	0	0	0	0	Few proximal convoluted tubular epithelial cells sho
684/15	C/ART+	1	1	0	0	0	0	
689/15	HCD/ART+	1	1	0	0	0	0	Few proximal convoluted tubular epithelial cells sho

Stellenbosch University https://scholar.sun.ac.za

708/14	HCD/ART+	1	1	0	0	0	0	
782/14	HCD/ART-	1	1	0	0	1	0	Few proximal convoluted tubular structures contain s
257/15	C/ART-	1	0	0	0	0	1	Mild dilation of perivascular spaces associated with t
277/15	C/ART-	1	1	0	0	1	0	Single cortical tubules show scant basophilic materia
435/15	C/ART-	1	1	0	0	0	0	Mild multifocal vacuolisation of proximal convolute
655/15	C/ART-	1	1	0	0	0	0	Mild multifocal vacuolisation of proximal convolute
430/15	C/ART+	1	1	0	0	0	0	Mild multifocal vacuolisation of proximal convolute
282/15	C/ART+	1	1	0	0	1	0	Few proximal convoluted tubular structures contain s
267/15	C/ART+	1	1	0	0	0	0	
410/15	C/ART+	0	0	0	0	0	0	
337/15	HCD/ART-	1	1	1	0	1	0	Multifocal mild vacuolated appearance of proximal c
262/15	HCD/ART-	1	1	1	0	1	0	Multifocal scattered proximal convoluted tubular epi
650/15	HCD/ART-	1	1	1	0	0	0	Multifocal scattered few (minimal) proximal convolu
383/15	HCD/ART-	1	1	1	0	0	0	Multifocal scattered few (minimal) proximal convolu
703/15	HCD/ART+	0	0	0	0	0	0	
485/15	HCD/ART+	0	0	0	0	0	0	
272/15	HCD/ART+	0	0	0	0	0	0	
287/15	HCD/ART+	1	1	1	1	0	0	Single cells appear slightly swollen with mildly incre

Appendix M: Liver data

Table 24 Pathology changes seen within all liver samples. Pathology was classified as follows; absent (0), mild (1), moderate (2) and severe (3).

Rat	Treatment	Absent/Present	Pathology			
			Granular appearance	Vacuolisation	Fatty change	
379/14	C/ART+	1	0	0	1	More than 1, but less than 2
660/14	HCD/ART+	0	0	0	0	

Stellenbosch University https://scholar.sun.ac.za

620/14	HCD/ART+	1	1	0	0	Autolysis, artifactual changes
690/14	HCD/ART+	1	1	1	0	Mild granular appearance and vacuolisation
361/14	C/ART+	1	1	0	0	
442/14	C/ART+	1	0	2	1	less than 1
469/14	HCD/ART-	1	1	0	0	
433/14	C/ART-	1	2	2	0	
478/14	C/ART-	0	0	0	0	Artifact, eosin crystals, small focus of inflammatory infiltrate, query necrosis
487/14	HCD/ART-	1	2	1	0	Mild Granular appearance
406/14	HCD/ART+	1	1	0	0	Mild Granular appearance
460/14	C/ART+	1	1	1	0	Mild Granular appearance
496/14	C/ART-	1	1	1	1	Mild Granular appearance, with autolysis, mild vac in some areas, less than 1 fc
424/14	HCD/ART-	1	1	1	0	Mild gran app diffuse, vac in some area
540/14	HCD/ART+	1	2	1	0	Moderate granular appearance in some areas, mild vac in some areas
560/14	HCD/ART-	1	1	1	0	Mild gran app, with autolysis, vac
590/14	C/ART+	1	1	0	0	mild gran app, with autolysis
520/14	HCD/ART-	1	1	1	0	Mild gran app (not in central areas)
580/14	HCD/ART+	1	1	0	0	Mild gran app, some connective tissue found
570/14	C/ART-	1	1	1	0	mild gran app, mild vac in some cells
630/14	C/ART+	0	0	0	0	
530/14	C/ART-	1	1	1	1	mild gran appearance, vac, less than 1 fc
343/14	C/ART+	0	0	0	0	Query vac
242/14	HCD/ART-	1	1	1	1	mild gran appearance, vac, less than 1 fatty change
251/14	C/ART-	1	1	0	0	Few areas show centrilobular hepatocytes with mildly increased granular appearance of evident in few of these cells, few are also swollen.
397/14	C/ART-	1	1	0	0	Hepatocytes have a slightly granular cytoplasm diffusely throughout the section.
325/14	C/ART-	1	2	1	0	
289/14	C/ART-	1	2	0	0	Moderate granular appearance of the cytoplasm of hepatocytes in the centrilobular regio adjacent to the centrilobular zones that show the presence of single large fat vacuoles (fa
307/14	C/ART+	1	2	0	0	Moderately granular appearance of the hepatocyte cytoplasm's, appearing more promine
421/14	C/ART+	1	1	0	0	Hepatocytes show mildly granular cytoplasm diffusely

Stellenbosch University https://scholar.sun.ac.za

271/14	C/ART+	1	1	0	0	Slight granularity of hepatocyte cytoplasm diffuse
415/14	C/ART+	0	0	0	0	
280/14	HCD/ART-	1	2	0	0	Moderately granular appearance of the hepatocyte cytoplasm, appearing more prominen
388/14	HCD/ART-	1	1	0	0	Mild granularity of the cytoplasm of hepatocytes diffusely
352/14	HCD/ART-	0	0	0	0	Congested
316/14	HCD/ART-	0	0	0	0	
262/14	HCD/ART+	1	1	0	0	Mild diffuse granularity of the hepatocyte cytoplasm.
298/14	HCD/ART+	1	1	0	0	Hepatocyte cytoplasm are diffusely mildly granular in appearance.
370/14	HCD/ART+	1	0	1	0	Scattered hepatocytes in the centrilobular areas show mild vacuolar change consisting of change. Scattered single Ito cells in these areas are also vacuolated
334/14	HCD/ART+	1	0	0	1	Less than 1 fc

Stellenbosch University https://scholar.sun.ac.za

Appendix N: Leptin Section of thesis published Acta Hitochemica

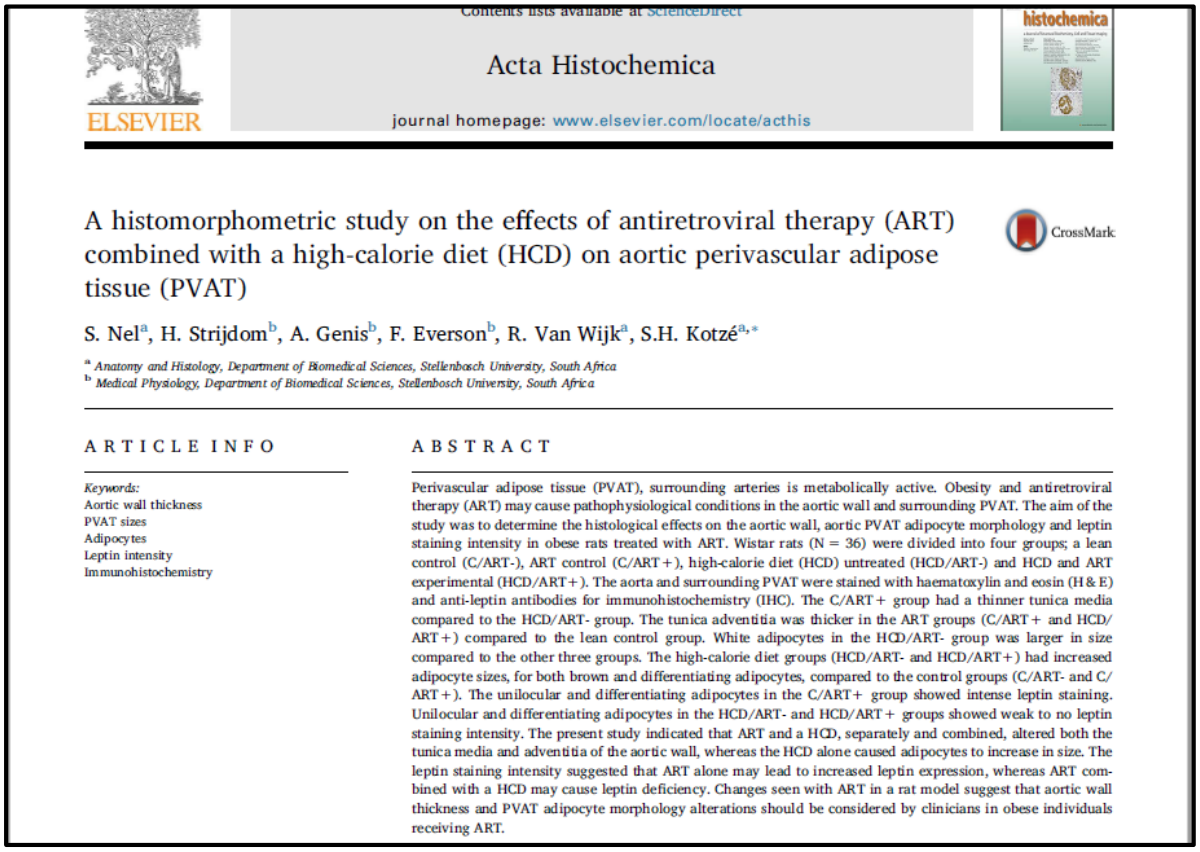

Contents lists available at ScienceDirect

Acta Histochemica

journal homepage: www.elsevier.com/locate/acthis

A histomorphometric study on the effects of antiretroviral therapy (ART) combined with a high-calorie diet (HCD) on aortic perivascular adipose tissue (PVAT)

S. Nel[a], H. Strijdom[b], A. Genis[b], F. Everson[b], R. Van Wijk[a], S.H. Kotzé[a,*]

[a] Anatomy and Histology, Department of Biomedical Sciences, Stellenbosch University, South Africa
[b] Medical Physiology, Department of Biomedical Sciences, Stellenbosch University, South Africa

ARTICLE INFO

Keywords:
Aortic wall thickness
PVAT sizes
Adipocytes
Leptin intensity
Immunohistochemistry

ABSTRACT

Perivascular adipose tissue (PVAT), surrounding arteries is metabolically active. Obesity and antiretroviral therapy (ART) may cause pathophysiological conditions in the aortic wall and surrounding PVAT. The aim of the study was to determine the histological effects on the aortic wall, aortic PVAT adipocyte morphology and leptin staining intensity in obese rats treated with ART. Wistar rats (N = 36) were divided into four groups; a lean control (C/ART-), ART control (C/ART+), high-calorie diet (HCD) untreated (HCD/ART-) and HCD and ART experimental (HCD/ART+). The aorta and surrounding PVAT were stained with haematoxylin and eosin (H & E) and anti-leptin antibodies for immunohistochemistry (IHC). The C/ART+ group had a thinner tunica media compared to the HCD/ART- group. The tunica adventitia was thicker in the ART groups (C/ART+ and HCD/ART+) compared to the lean control group. White adipocytes in the HCD/ART- group was larger in size compared to the other three groups. The high-calorie diet groups (HCD/ART- and HCD/ART+) had increased adipocyte sizes, for both brown and differentiating adipocytes, compared to the control groups (C/ART- and C/ART+). The unilocular and differentiating adipocytes in the C/ART+ group showed intense leptin staining. Unilocular and differentiating adipocytes in the HCD/ART- and HCD/ART+ groups showed weak to no leptin staining intensity. The present study indicated that ART and a HCD, separately and combined, altered both the tunica media and adventitia of the aortic wall, whereas the HCD alone caused adipocytes to increase in size. The leptin staining intensity suggested that ART alone may lead to increased leptin expression, whereas ART combined with a HCD may cause leptin deficiency. Changes seen with ART in a rat model suggest that aortic wall thickness and PVAT adipocyte morphology alterations should be considered by clinicians in obese individuals receiving ART.

Turnitin

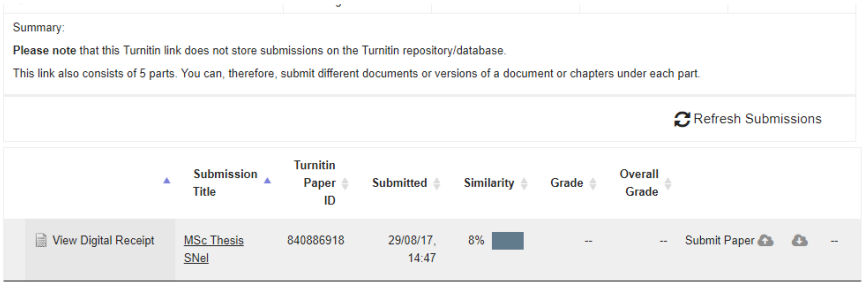

Summary:

Please note that this Turnitin link does not store submissions on the Turnitin repository/database.

This link also consists of 5 parts. You can, therefore, submit different documents or versions of a document or chapters under each part.

Refresh Submissions

	Submission Title	Turnitin Paper ID	Submitted	Similarity	Grade	Overall Grade	
View Digital Receipt	MSc Thesis SNel	840886918	29/08/17, 14:47	8%	--	--	Submit Paper --

Stellenbosch University https://scholar.sun.ac.za